THOMAS M. MASSIE

DYNAMIC BEHAVIOR OF PHYTOPLANKTON POPULATIONS FAR FROM STEADY STATE

Published online at the
Institutional Repository of the University of Potsdam:
URL http://opus.kobv.de/ubp/volltexte/2012/5810/
URN urn:nbn:de:kobv:517-opus-58102
http://nbn-resolving.de/urn:nbn:de:kobv:517-opus-58102

DYNAMIC BEHAVIOR OF PHYTOPLANKTON POPULATIONS FAR FROM STEADY STATE

Chemostat experiments and mathematical modeling

THOMAS M. MASSIE

Doctoral thesis (cummulative)

in partial fulfillment for the award of the degree
doctor rerum naturalium (Dr. rer. nat.)
in the scientific discipline of *Ecology*

Department of Ecology and Ecological Modeling
Institute for Biochemistry and Biology
University of Potsdam

Potsdam, November 2011

DYNAMISCHES VERHALTEN VON PHYTOPLANKTON-POPULATION FERN VOM GLEICHGEWICHT

Chemostatexperimente und mathematische Modellierung

THOMAS M. MASSIE

Dissertation (kumulativ)

zur Erlangung des akademischen Grades
doctor rerum naturalium (Dr. rer. nat.)
in der Wissenschaftsdisziplin *Ökologie*

Professur für Ökologie und Ökosystemmodellierung
Institut für Biochemie und Biologie
Universität Potsdam

Potsdam, November 2011

'To see a world in a grain of sand
And a heaven in a wild flower,
Hold infinity in the palm of your hand
And eternity in an hour.'

— William Blake
(from 'Auguries of Innocence')

For my family...

ABSTRACT

Nature changes continuously and is only seemingly at equilibrium. Environmental parameters like temperature, humidity or insolation may strongly fluctuate on scales ranging from seconds to millions of years. Being part of an ecosystem, species have to cope with these environmental changes. For ecologists, it is of special interest how individual responses to environmental changes affect the dynamics of an entire population – and, if this behavior is predictable. In this context, the demographic structure of a population plays a decisive role since it originates from processes of growth and mortality. These processes are fundamentally influenced by the environment. But, how exactly does the environment influence the behavior of populations? And what does the transient behavior look like?

As a result from environmental influences on demography, so called cohorts form. They are age or size classes that are disproportionally represented in the demographic distribution of a population. For instance, if most old and young individuals die due to a cold spell, the population finally consists of mainly middle-aged individuals. Hence, the population got synchronized. Such a population tends to show regular fluctuations in numbers (denoted as oscillations) since the alternating phases of individual growth and population growth (due to reproduction) are now performed synchronously by the majority of the population.That is, one time the population growths, and the other time it declines due to mortality.

Synchronous behavior is one of the most pervasive phenomena in nature. Gravitational synchrony in the solar system; fireflies flashing in unison; coordinate firing of pacemaker cells in the heart; electrons in a superconductor marching in lockstep. Whatever scale one looks at, in animate as well as inanimate systems, one is likely to encounter synchrony. In experiments with phytoplankton populations, I could show that this principle of synchrony (as used by physicists) could well-explain the oscillations observed in the experiments, too. The size of the fluctuations depended on the strength by which environmental parameters changed as well as on the demographic state of a population prior to this change. That is, two population living in different habitats can be equally influenced by an environmental change, however, the resulting population dynamics may be significantly different when both populations differed in their demographic state before.

Moreover, specific mechanisms relevant for the dynamic behavior of populations, appear only when the environmental conditions change. In my experiments, the population density declined by 50% after ressource supply was doubled. This counter-intuitive behavior can be

explained by increasing ressource consumption. The phytoplankton cells grew larger and enhanced their individual constitution. But at the same time, reproduction was delayed and the population density declined due to the losses by mortality.

Environmental influences can also synchronize two or more populations over large distances, which is denoted as Moran effect. Assume two populations living on two distant islands. Although there is no exchange of individuals between them, both populations show a high similarity when comparing their time series. This is because the globally acting climate synchronizes the regionally acting weather on both island. Since the weather fluctuations influence the population dynamics, the Moran effect states that the synchrony between the environment equals the one between the populations. My experiments support this theory and also explain deviations arising when accounting for differences in the populations and the habitats they are living in. Moreover, model simulations and experiments astonishingly show that the synchrony between the populations can be higher than between the environment, when accounting for differences in the environmental fluctuations (“noise color”).

ZUSAMMENFASSUNG

Die Natur unterliegt ständigen Veränderungen und befindet sich nur vermeintlich in einem Gleichgewicht. Umweltparameter wie Temperatur, Luftfeuchtigkeit oder Sonneneinstrahlung schwanken auf einer Zeitskala von Sekunden bis Jahrmillionen und beinhalten teils beträchtliche Unterschiede. Mit diesen Umweltveränderungen müssen sich Arten als Teil eines Ökosystems auseinandersetzen. Für Ökologen ist interessant, wie sich individuelle Reaktionen auf die Umweltveränderungen im dynamischen Verhalten einer ganzen Population bemerkbar machen und ob deren Verhalten vorhersagbar ist. Der Demografie einer Population kommt hierbei eine entscheidende Rolle zu, da sie das Resultat von Wachstums- und Sterbeprozessen darstellt. Eben jene Prozesse werden von der Umwelt maßgeblich beeinflusst. Doch wie genau beeinflussen Umweltveränderungen das Verhalten ganzer Populationen? Wie sieht das vorübergehende, transiente Verhalten aus?

Als Resultat von Umwelteinflüssen bilden sich in Populationen sogenannte Kohorten, hinsichtlich der Zahl an Individuen überproportional stark vertretene Alters- oder Größenklassen. Sterben z.B. aufgrund eines außergewöhnlich harten Winters, die alten und jungen Individuen einer Population, so besteht diese anschließend hauptsächlich aus Individuen mittleren Alters. Sie wurde sozusagen synchronisiert. Eine solche Populationen neigt zu regelmäßigen Schwankungen (Oszillationen) in ihrer Dichte, da die sich abwechselnden Phasen der individuellen Entwicklung und der Reproduktion nun von einem Großteil der Individuen synchron durchschritten werden. D.h., mal wächst die Population und mal nimmt sie entsprechend der Sterblichkeit ab. In Experimenten mit Phytoplankton-Populationen konnte ich zeigen, dass dieses oszillierende Verhalten mit dem in der Physik gebräuchlichen Konzept der Synchronisation beschrieben werden kann. Synchrones Verhalten ist eines der verbreitetsten Phänomene in der Natur und kann z.B. in synchron schwingenden Brücken, als auch bei der Erzeugung von Lasern oder in Form von rhythmischem Applaus auf einem Konzert beobachtet werden. Wie stark die Schwankungen sind, hängt dabei sowohl von der Stärke der Umweltveränderung als auch vom demografischen Zustand der Population vor der Veränderung ab. Zwei Populationen, die sich in verschiedenen Habitaten aufhalten, können zwar gleich stark von einer Umweltveränderung beeinflusst werden. Die Reaktionen im anschließenden Verhalten können jedoch äußerst unterschiedlich ausfallen, wenn sich die Populationen zuvor in stark unterschiedlichen demografischen Zuständen befanden. Darüber hinaus treten bestimmte, für das Verhalten einer

Population relevante Mechanismen überhaupt erst in Erscheinung, wenn sich die Umweltbedingungen ändern. So fiel in Experimenten beispielsweise die Populationsdichte um rund 50 Prozent ab nachdem sich die Ressourcenverfügbarkeit verdoppelte. Der Grund für dieses gegenintuitive Verhalten konnte mit der erhöhten Aufnahme von Ressourcen erklärt werden. Damit verbessert eine Algenzelle zwar die eigene Konstitution, jedoch verzögert sich dadurch die auch die Reproduktion und die Populationsdichte nimmt gemäß ihrer Verluste bzw. Sterblichkeit ab.

Zwei oder mehr räumlich getrennte Populationen können darüber hinaus durch Umwelteinflüsse synchronisiert werden. Dies wird als Moran-Effekt bezeichnet. Angenommen auf zwei weit voneinander entfernten Inseln lebt jeweils eine Population. Zwischen beiden findet kein Austausch statt – und doch zeigt sich beim Vergleich ihrer Zeitreihen eine große Ähnlichkeit. Das überregionale Klima synchronisiert hierbei die lokalen Umwelteinflüsse. Diese wiederum bestimmen das Verhalten der jeweiligen Population. Der Moran-Effekt besagt nun, dass die Ähnlichkeit zwischen den Populationen jener zwischen den Umwelteinflüssen entspricht, oder geringer ist. Meine Ergebnisse bestätigen dies und zeigen darüber hinaus, dass sich die Populationen sogar ähnlicher sein können als die Umwelteinflüsse, wenn man von unterschiedlich stark schwankenden Einflüssen ausgeht.

ACKNOWLEDGMENTS

An erster Stelle möchte ich Prof. Dr. Ursula Gaedke und Prof. Dr. Bernd Blasius danken. Zum einen, weil sie es mir ermöglichten meine eigenen Forschungsinteressen im Antrag zur Finanzierung dieser Doktorarbeit einzubringen. Und zum anderen, weil sich ihre beiden Persönlichkeiten im Hinblick auf die Planung und Durchführung meiner Doktorarbeit wunderbar ergänzten. Vielen Dank euch beiden!
Eine weitere große Hilfe war PD Dr. Guntram Weithoff. Tipps zur Planung der Experimente, Kontakte zum IGB in Berlin, hilfreicher Diskussionspartner... Guntram Weithoffs Tür stand mir immer offen!
Mein weiterer Dank gilt Prof. Dr. Gregor Fussmann, ohne dessen Einfluss ich womöglich nicht in diesem Forschungsgebiet promoviert hätte. Ich hatte die Kooperationen hinsichtlich meiner Diplomarbeit und dem ersten Manuskript der Doktorarbeit sehr genossen!
Danke auch an Dr. Alexei Ryabov, der einen Teil der mathematischen Modellierung übernahm!
Ein großes Dankeschön möchte ich an die gesamte AG Ökologie & Ökosystemmodellierung richten. Ich habe das Umfeld über die Jahre sehr genossen und bin jedem dankbar, der mir an den Wochenende oder zu anderen 'unmöglichen' Zeiten in der Klimakammer aushalf! Hierbei ist vor allem Edith Denzin hervorzuheben, die mir jahrelang bei den Experimenten unterstützend zur Seite stand.
Außderdem möchte ich mich bei der gesamten AG Mathematische Modellierung am ICBM in Oldenburg bedanken, die mich während meiner Kurzaufenthalte super aufgenommen hat.
Und natürlich möchte ich all meinen Freunden danken, welche meine Studienzeit in Gießen und Potsdam zu einem besonderen Abschnitt in meinem Leben haben werden lassen!

Vor allem aber danke ich meinen Eltern Adolf & Monika. Ohne euch wäre diese Arbeit nur schwer möglich gewesen. Vielen, vielen Dank!

Wie dankbar ich meiner Freundin Britta bin, vermag ich kaum zu sagen. Es ist unglaublich schön mit dir!

Und sollte ich an dieser Stelle noch jemanden vergessen haben, so tut es mir schrecklich leid. Es ist mittlerweile 6:30 Uhr und meine Augen fallen langsam, aber sicher zu. Bitte seht es mir nach...

CONTENTS

Part I

GENERAL INTRODUCTION

1

DYNAMICS FAR FROM STEADY STATE

1.1 ARE POPULATIONS AT STEADY STATE?

A population at steady state implies a stable number of individuals (or any other characterizing variable like its biomass) that does not change over time and in which change in one direction is continually balanced by change in another. That is, the gains from reproduction and immigration into a population equal the losses due to mortality and emigration. This implies that a population's turn-over rate can be high although the population density does not change at all.

At steady state, the gains equal the losses.

Since the term "steady state" is naturally related to time, the question whether a population is at steady state or not is always a matter of scale. For instance, while a bacterium like *Escherichia coli* has fulfilled its life cycle within 30 minutes, the life of an elephant typically has not changed much within this time interval. Thus, the generation time of an organism is a fundamental issue when talking about population dynamics and steady state.

Whether a population is at steady state or not depends on its biotic and abiotic environment that determines the gains and losses. A population is embedded into a trophic network and is part of the complex biotic interactions among the participating species, e.g. predator-prey relationships or competition for resources. This network represents the animate part of an ecosystem and underlies its abiotic environmental influences, e.g. climate fluctuations or geological processes. In this context, it becomes clear that there are infinite ways to drive a population away from a dynamical steady state – each acting on a different temporal scale that determines its influence on a population. E.g., continental drift is of no direct interest to the elephant from above when thinking about his life and the ones of his children and grand children. However, he will surly be concerned about more frequent fire events due to global climate change. In the context of this work, I excluded biotic interactions and focused on two causations that bear great potential to disturb the steady state of populations: demographic structure and environmental variability.

Environmental influences are always a matter of scale.

DEMOGRAPHIC STRUCTURE Any population on this planet has a demographic structure, even the ones that elude the human eye and are therefore readily considered unstructured. The reason for this is the life cycle of an organism: the different life stages interact differently with the environment. This is apparent for organisms of higher order, especially when the developmental stages can be clearly distinguished

Figure 1.1: A matter of scale. Whether organisms are sensitive to environmental variations or not, strongly depends on their size. Here, *E. coli*'s driping tap might be the elephant's thunderstorm. (Photo copyright: Gunnar Assmy, top left; Mark Greenwood, top right; Beverly Joubert, bottom left; Sean Heavey, bottom right)

by morphology, e.g., in holometabolic insects. But also populations of unicellular microorganisms show a stage structure evolving from the distinct phases of the cell cycle (G_1-, S-, G_2-, and M-phase). Their life cycle is structured according to the physiology of the cell.

Demographic structure implies developmental stages that differently interact with the environment.

To describe the demography of a population, individuals are typically classified by a characteristic developmental feature like age or size. At steady state, the stage distribution is balanced and does not change. That is, according to both, the progression velocity describing maturation or somatic growth, and the mortality rate, a stable demographic structure is established being characteristic for the prevailing environmental conditions. From a theoretical, population biological point of view, structured populations bear much more potential to be pushed away from steady state [140, 22]. Whenever the steady state demography is disturbed, the ratio of gains and losses becomes unbalanced. For instance, assume a population whose number of individuals in the stage class with the highest productivity is dramatically decreased. Since reproduction is decreased, the gains cannot

compensate any longer the losses due to mortality and the population density will decrease. This simple, but vivid example illustrates that a population's demographic structure can be easily brought out of balance so that the population dynamics are no longer at steady state. But it also shows that the environment has numerous potential ways of impacting population structure.

ENVIRONMENTAL VARIABILITY Whatever ecosystem one looks at, the prevailing environmental conditions are never absolutely stable, but rather characterized by continuous fluctuations varying in amplitude and frequency. Temperature, insolation, rainfall and all other environmental parameters vary in time and space. Hence, populations underly permanent disturbances making it hard to imagine that they can ever reach a steady state. However, amplitude and frequency of the environmental fluctuations are relative. Whether a population is sensitive to changes or not, depends to a large amount on the size and generation time of a species. In periods of minor fluctuations, populations are able to reach a steady state since their individuals are not sufficiently affected to disturb demography. This changes again when the fluctuations become more intense and the population dynamics change as a response to an altered demographic structure.

Environmental fluctuations are characterized by their amplitude and frequency.

The frequency by which environmental changes occur is important, too. A population might be able to compensate a single perturbation once in a while without any distinct changes in demography. The picture changes, however, when the perturbations become more frequent and start leaving marks in the population structure. The frequency by which perturbations occur is important in relation to the generation time of an organism. Very low frequencies are practically identical to singular events a population might respond to. Very high frequencies in turn, might not be able to change the population structure but may continuously alter the density. Although often acting with small amplitudes, such fluctuations become important when occurring over vast distances since they may synchronize populations that do not interact. And a third possibility is that the frequencies of the perturbations overlap with the frequencies by which organisms reproduce. When such perturbations alter the demography (although only slightly), a population responds to the subsequent perturbations with a different structure. The resulting behavior might not only be complex but chaotic. Here, I will investigate the impacts of long-term changes and high-frequent perturbations, known as environmental stochasticity or noise, respectively.

1.2 COMPLEX BEHAVIOR AND SYNCHRONY

The dynamic behavior in response to environmental changes can be as diverse as the factors provoking it. Traditionally, ecological

research addresses the stability of populations and the future steady states after the occurrence of environmental changes. But in the last years, transient behavior has become a focal point. It turns out that theory of long-term dynamics or steady state theory, respectively, is unable to explain most transient dynamics since it often lacks the essential mechanisms [61, 62]. For example, to describe the 'dynamics' of a population at steady state one does not need to account for demographic structure since the population is stable. However, when the environmental conditions change and do not equally affect all developmental stages (e.g. most juveniles die due to a cold spell), demographic structure is essential to explain the resulting dynamics. Further, only transient behavior reveals the mechanisms that determine population dynamics, e.g. storage of surplus nutrients leading to delays in the growth of phytoplankton populations [27]. Generally, to predict future dynamics one has to study populations far from steady state because only there they will reveal the causes underlying their dynamics.

Transients describe the population dynamics between steady states.

OSCILLATORY DYNAMICS Regular fluctuations or oscillations, respectively, in the number of species are most often reported for predator-prey systems and attracted notice to ecologists ever since Elton (1924) first described the famous Hare-Lynx-cycles from a scientific point of view [42]. But also single species populations are able to exhibit oscillatory behavior that is caused by intrinsic mechanisms related to demography. Taking the example of the population suffering from a cold spell, the loss of juveniles synchronizes the population since all other developmental stages are disproportionally represented in the demographic distribution. As a result, a cohort forms that exists until the demographic structure is in balance again. The cohort can be tracked over time as is 'travels' along the different stages of development. Oscillations arise when the majority of individuals find themselves in a similar stage of development. That is, those individuals progress through their life cycle in lockstep. Their somatic growth and the point in time when they reproduce is synchronized. Hence, the population does not noticeably grow until the cohort starts reproducing. As a result, periods of somatic growth and population growth alternate according to the generation time.

Oscillations arise from the synchronization of individuals within a population.

Populations can be synchronized in many ways. One that is commonly known is the synchronization due to an external factor, denoted as entrainment [117]. Although the term "entrainment" is commonly not used in ecological research, ecologists are familiar with this kind of synchronization since the restriction of population growth due to insufficient resources is ubiquitous.

In the second and the third chapter, I demonstrate how readily oscillations arise as transient behavior in response to environmental changes. Especially in the second chapter, I will explicitly apply the

physical concept of synchronization to single species populations and explain the occurrence of self-sustained, persistent oscillations in the experimental chemostat populations. In the third chapter, I focus more on the strength and direction of the environmental changes. I show that, similar to a memory effect, the demographic structure before the environmental conditions change plays an eminent role for the transient dynamics. Moreover, I explain why the population density can temporarily decrease ($\approx$ 50%!) in response to ameliorated resource concentrations. This counter-intuitive observation represents a prime example of a mechanism having a noticable effect only under nonsteady-state conditions.

SYNCHRONY OVER LARGE DISTANCES In ecology, synchrony plays not only a role in single populations whose individuals are in synchrony, but also in the remarkably synchronous behavior of whole population that are spatially disjunct. Such synchrony might be achieved by three primary mechanisms [86]: (*i*) migration of individuals from one population to another; (*ii*) trophic interactions with populations of mobile species or populations that are themselves in synchrony; and (*iii*) correlated environmental stochasticity (noise) which is known as Moran effect [100, 130].

Correlated environmental fluctuations can synchronize populations over large distances.

Assume two islands that are separated by a vast distance with one population living on each island. Migration between the islands is not possible nor is there a common predator or the like that the populations interact with. And anyway, when comparing the time series of the two populations one would observe a remarkably high correlation between them. The cause for this is the globally acting climate that correlates the regionally acting weather on both islands. Since the correlated environmental fluctuations determine the dynamics of both populations, the correlation coefficient of the populations r_p should be dependent on the one of the environment r. For linear systems, Moran pointed out that both coefficients are identical, $r_p = r$.
In chapter four, the Moran effect was investigated in three comprehensive scenarios. For this purpose, chemostat populations of *C. vulgaris* experienced correlated noise realized as fluctuations of the turn-over rate (dilution rate). I demonstrate that the Moran effect held for identical populations that experienced white noise (first scenario), meaning $r_p = r$. When both populations differed in carrying capacity and average turn-over rate (second scenario), r_p was generally smaller than r, $r_p < r$ (second scenario). Finally, experimental results and model simulations show that $r_p > r$ when two identical populations experience differently autocorrelated environmental noise (third scenario).

1.3 CHEMOSTAT POPULATIONS AND THEIR ENVIRONMENT

All studies in my doctoral thesis combined theory and mathematical modeling with chemostat experiments. In this section I will briefly explain the experimental setup comprising much more than just the chemostat systems. Chemostats are sophisticated experimental tools that require profound experience, especially in this case where they are embedded in a highly technical environment that allows for computer-controlled changes of the dilution rate as well as automatic sampling. This was especially required in the experiments investigating the Moran effect.

It took nearly one year of development until all parts worked properly. Thomas Hintze from the 'Leibniz Institute of Freshwater Ecology and Inland Fisheries' (IGB,Berlin) was the technician responsible for Simulink programming and the development of the light extinction measurement device that allowed for a quasi-continuous, noninvasive estimation of the algal biomass. Assisted by Thomas Hintze and Guntram Weithoff, I installed the 'hardware' that guaranteed proper interaction between the chemostats and the computer. All this together made the planning and performance of these chemostat experiments an acutely time-intense venture.

CHEMOSTAT SETUP A chemostat is a continuous culturing system and a powerful experimental tool not only in ecological research [108, 76]. It allows to test for specific influences on populations under well-defined conditions. In contrast to simple batch cultures, a chemostat is a flow-through system. By continuously supplying the population with fresh medium and removing the chemostat content at the same rate, it allows for the maintenance of populations over a long period of time. Therefore, it fits perfectly to studies investigating transient population dynamics in response to perturbations of the steady state.

Chemostats are continuous-culture devices that allow for the testing of specific mechanisms under well-defined conditions.

The chemostat system as used in chapters two to five, basically consisted of the chemostat vessel containing the algal population and the medium, and three ports enabling supply with fresh medium and air, automatic sampling of light extinction and washout by dilution (Fig. 1.2). To analyze population structure, samples for particle counter measurements were taken from the effluent to be noninvasive, too.

EXPERIMENTAL MODEL ORGANISMS In numerous pre-experiments, I investigated the suitability of the three unicellular phytoplankton species *Monoraphidium minutum*, *Chlamydomonas reinhardtii*, and *Chlorella vulgaris*. Results from chemostat experiments with all species are shown in chapter 2.

Chlorella vulgaris has short generation times and is easy to handle – the perfect model organism.

I decided to use solely *C. vulgaris* for all other experiments whose results are presented in chapters three and four. *C. vulgaris* is a coccal green alga and is found as part of phytoplankton communities, on the

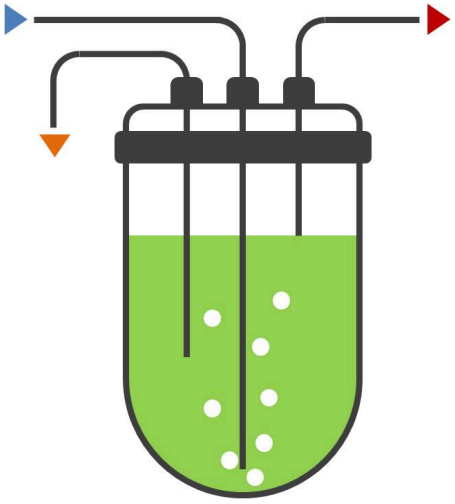

Figure 1.2: Schematic chemostat setup as used in this work. The chemostat vessel contains the phytoplankton population and the medium. Dilution provides a continuous flow through the system equally determining the rate by which fresh medium is supplied (blue triangle) and all chemostat content is washed out of the system (red triangle). Noninvasive samples for light extinction measurements were taken at the third port (orange triangle), samples for particle counter measurements were taken from the effluent. Fresh air entered the vessel together with the supplied medium guaranteeing both, prevention from CO_2-limitation and homogeneous mixing.

bark of trees, and as symbiont in lichens, *Paramecium*, and *Hydra*. Besides that, *C. vulgaris* is a well-known and often used model organism in chemostat studies. Due to the short generation times and the easy handling microorganisms like *C. vulgaris* allow for experiments of general ecological relevance that would not possible to perform with more complex organisms. Possessing a life cycle with four distinct phases, it brings the minimum requirements to study structured populations in continuous culture (Fig. 1.3). That is, nitrogen-dependent cell progression in the G_1-phase results in a demographic structure that is defined by the environmental parameters of the chemostat, namely the nitrogen concentration of the inflowing medium and the dilution rate.

1.4 MATHEMATICAL MODELING

The structured population model as used in chapters two and three, represents an extension of the Kuramoto model [82, 83], adapted to chemostat populations. It describes a structured population of algal cells that interacts with the ambient nitrogen in the system. All cells start as small daughter cells and progress through their life cycle to finally become large mother cells that release new daughter again and so on. The model distinguishes only between a nitrogen-dependent phase

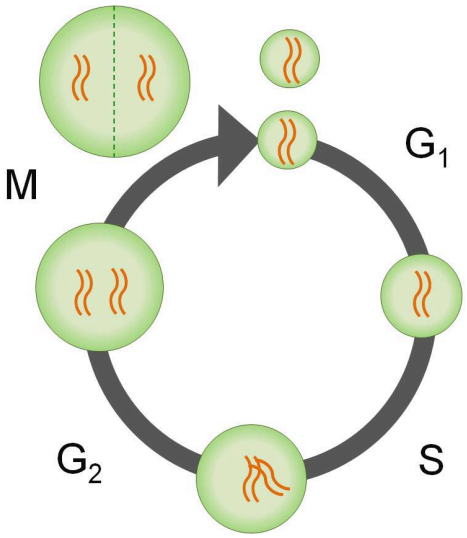

Figure 1.3: Schematic description of the life cycle of *C. vulgaris*. Typically for eukaryotic organisms, the cell cycle consists of four physiologically distinct phases (G_1, S, G_2, and M).

(G_1) and a phase in which progression is constant and independent from the ambient nitrogen concentrations (remaining cycle) (Fig. 1.4). The nitrogen dependency is given by a Monod-wise function with ν being the progression velocity, ν_m the maximum progression velocity, N the ambient nitrogen concentration, and K_N the half-saturation constant. This simple but effective mechanism structures the population according to the availability of nitrogen. In the third chapter, this model is extended by a mechanism allowing for the elongation of the G_1-phase when nitrogen concentrations are high. Although a cell progresses faster through this phase when nitrogen is available in excess, it takes comparably longer in the extended model since the G_1-phase is longer.

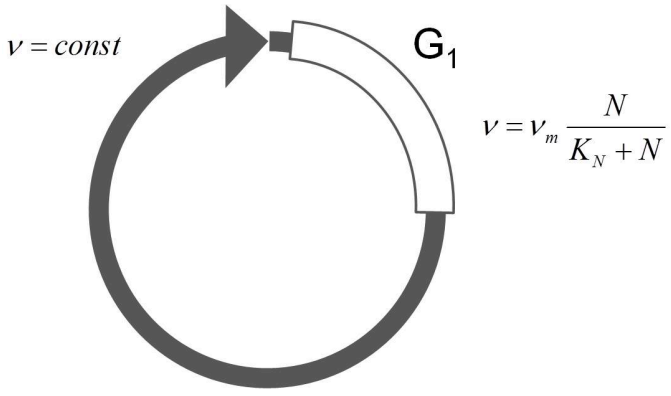

Figure 1.4: Simplified life cycle as used in in the structured population models of chapters two and three. Progression velocity is nitrogen-dependent within the G_1-phase, outside it is constant.

The structured population model as used in chapters two and three, describes a population of algal cells that interacts with the ambient nitrogen in the system. Cells start as small daughter cells and progress through their life cycle to finally become mother cells that release new daughter again and so on. The model distinguishes only between a nitrogen-dependent phase (G_1) and a phase in which progression is constant and independent from the ambient nitrogen concentrations (remaining cycle) (Fig. 1.4). The nitrogen dependency is given by a Monod-wise function with ν being the progression velocity, ν_m the maximum progression velocity, N the ambient nitrogen concentration, and K_N the half-saturation constant. This simple but effective mechanism structures the population according to the availability of nitrogen. In the third chapter, this model is extended by a mechanism allowing for the elongation of the G_1-phase when nitrogen concentrations are high. Although a cell progresses faster through this phase when nitrogen is available in excess, it takes comparably longer in the extended model since the G_1-phase is longer.

In both models, the cells develop rather continuous than in discrete steps. Therefore, the model consists of a set of partial differential equations (PDEs). Numerical modeling and analyses were done in C and Matlab. Since the populations in chapter five did not require any demographic structure to explain their dynamics, the model used here consisted of a set of ordinary differential equations (ODEs). In accordance to the experiments, the populations experienced stochastic variations by changing the values of the dilution rate in discrete time steps. Simulations and analyses were done in Matlab.

Part II

THE MANUSCRIPTS

AUTHOR CONTRIBUTIONS

CYCLES, PHASE SYNCHRONIZATION, AND ENTRAINMENT I designed the research with the helpful advices from Bernd Blasius, Gregor F. Fussmann, Guntram Weithoff and Ursula Gaedke. I performed the chemostat experiments assisted by Guntram Weithoff and performed all lab work. Bernd Blasius realized the numerical modeling. Together with Bernd Blasius and Gregor F. Fussmann, I analyzed the data and wrote the manuscript.

COMPLEX TRANSIENT DYNAMICS I designed the research with the helpful advices from Bernd Blasius and Ursula Gaedke. I performed the chemostat experiments and all lab work. I analyzed the data in close collaboration with Alexei Ryabov and Bernd Blasius. Alexei Ryabov and Bernd Blasius realized the numerical modeling. I wrote the manuscript together with Ursula Gaedke. Guntram Weithoff was a great help discussing the manuscript.

ENHANCED MORAN-EFFECT I designed the research together with Bernd Blasius and Nina Kuckländer. I performed the chemostat experiments and all lab work. Together with Bernd Blasius, I realized the numerical modeling, analyzed the data, and wrote the paper. Ursula Gaedke and Guntram Weithoff assisted the planning of the experiments and help discussing the manuscript.

2

CYCLES, PHASE SYNCHRONIZATION, AND ENTRAINMENT

by Thomas M. Massie, Bernd Blasius, Guntram Weithoff, Ursula Gaedke, and Gregor F. Fussmann

The manuscript was published as

Massie, T.M.[1], B. Blasius[2], G. Weithoff[1], U. Gaedke[1], and G.F. Fussmann[3] (2010) *Cycles, phase synchronization, and entrainment in single-species phytoplankton populations.* Proceedings of the National Academy of Sciences of the United States of America **107** (9) 4236–4241

[1] Institute of Biochemistry & Biology, University of Potsdam, Maulbeeralle 2, 14467 Potsdam, Germany
[2] Institute for Chemistry and Biology of the Marine Environment, Carl von Ossietzky University, 26111 Oldenburg, Germany
[3] Department of Biology, McGill University, Montreal, QC H3A 1B1, Canada

2.1 ABSTRACT

Complex dynamics, such as population cycles, can arise when the individual members of a population become synchronized. However, it is an open question how readily and through which mechanisms synchronization-driven cycles can occur in unstructured microbial populations. In experimental chemostats we studied large populations ($> 10^9$ cells) of unicellular phytoplankton that displayed regular, inducible and reproducible population oscillations. Measurements of cell size distributions revealed that progression through the mitotic cycle was synchronized with the population cycles. A mathematical model that accounts for both the cell cycle and population-level processes suggests that cycles occur because individual cells become synchronized by interacting with one another through their common nutrient pool. An external perturbation by direct manipulation of the nutrient availability resulted in phase resetting, unmasking intrinsic oscillations and producing a transient collective cycle as the individuals gradually drift apart. Our study indicates a strong connection between complex within-cell processes and population dynamics, where synchronized cell cycles of unicellular phytoplankton provide sufficient population structure to cause small-amplitude oscillations at the population level.

2.2 INTRODUCTION

Phase synchronization is an adjustment of the rhythms of oscillating objects that can lead to the emergence of complex synchronized behavior [136, 117, 152], such as periodic color changes of catalytic microparticles [138], the simultaneous flashing of fireflies [17] or the rhythmic clapping of human audiences [107]. Similarly, the densities of many ecological populations oscillate with frequencies that cannot be explained by diurnal, annual or other seasonal variation [37, 79, 98]. Often, such regular oscillations are caused by multi-species interactions [15, 49, 7, 143]. Experiments have shown that also single-species populations can undergo regular sustained or damped oscillations [29, 5]. "Single-generation cycles" and "delayed-feedback cycles" [104] are types of single-species oscillations that are known to occur when vital rates are density-dependent. Here we are concerned with single-species oscillations that occur when individuals synchronize the progression through their life cycles. Synchronization may be caused by locking of individual life cycles to an external force (entrainment), but it may also arise spontaneously through the internal interactions among the individuals [117, 152, 138], and can occur in spatially distant populations [15, 143, 56, 91]. Populations with obvious internal structure can easily become synchronized by environmental triggers; for example, an insect population that loses all adults to a cold spell before eggs are produced and needs to restart growth based on the surviving larval fraction of the population. In contrast, little is known about the potential for synchronized cycles in microbial populations, despite their important role in all ecosystems across the globe.

In this study, we experimentally induced regular oscillations in populations of unicellular algae that lack distinct life stages other than defined by their cell cycle. The oscillations could be maintained in the absence of external periodic rhythms and can be explained through collective synchronization among a large population of interacting phase oscillators, in agreement with a generalized version of the Kuramoto Model [83]. Given the causal link between the cell cycle and the cycling of the population we provide evidence for synchronization of oscillatory dynamics across biological levels of organization. We ran chemostat experiments with three different unicellular freshwater phytoplankton species and compared the dynamics with those predicted by a mathematical model that allows for nitrogen availability and the nitrogen-dependent progression of phytoplankton cells through their cell cycle (see: supporting information (SI)). To track phytoplankton dynamics in the chemostats we used an automated light extinction measurement system (20, SI section 2). This allowed us to collect measurements with a signal sensitivity and temporal resolution (5 min intervals) that is unusually accurate for ecological time-series experiments. In addition, we used a particle counter to

determine cell abundance and size distribution (4 to 12 hour intervals). We used cell volume as a proxy for the phase of the cell cycle in which a phytoplankton cell is located.

2.3 RESULTS

We present results from two experimental scenarios, involving three different phytoplankton species, in which we induced cell cycle synchronization that led to oscillatory population dynamics. We hypothesize that phytoplankton cells can become synchronized by nitrogen depletion and can remain synchronized over several generations of population growth. Basic chemostat theory predicts that single-species populations show sigmoid growth after inoculation and reach a steady state. In the first scenario we tested whether characteristics of the sigmoid growth depend on the potential degree of synchronization among cells and started chemostats with phytoplankton cultures that had a different history of nutrient availability: either nitrogen-limited or not limited by nitrogen. Chemostat cultures inoculated with either type of phytoplankton showed sigmoid growth, but we observed the smoothly increasing curve predicted by theory only when cells had been previously cultured under non-limiting conditions (Fig. 2.1a). When we inoculated from a nitrogen-limited culture, however, cell numbers did not increase monotonously but displayed oscillations towards steady-state (Fig. 2.1a). These results agree with our hypothesis that cells become synchronized when nitrogen depletion arrests cell progression in the nitrogen-sensitive phase in their cell cycle.

In the second, more comprehensive scenario, we tested whether oscillations can be induced in steady-state chemostat populations by directly manipulating nitrogen availability to cells. This set up would, in theory [112, 85, 6](and our model described further down), induce oscillations through synchronization. We grew non-synchronized phytoplankton populations to steady-state and then stopped inflow into and outflow out of the chemostat (dilution rate $\delta = 0$ day^{-1}) for several days. This manipulation potentially synchronizes cells because initially cell numbers increase (no mortality due to outflow) but, as the remaining nutrients are being depleted (no nutrient inflow), the cells accumulate in the nitrogen-sensitive phase of their cell cycles. When the flow through the chemostat vessel resumes cell numbers will decrease to previous steady-state levels. However, cell density will now oscillate because the majority of cells enter the nitrogen-nonsensitive phase of the cell cycle simultaneously and cell divisions occur at approximately the same time.

In our experiments, we observed exactly the dynamical behavior predicted by theory. Small-amplitude oscillations (measured as changes in light extinction or cell densities; Figs. 2.1b-c, 2.2, 2.3) occurred after the "off-on" manipulation of the chemostat in separate cultures of three

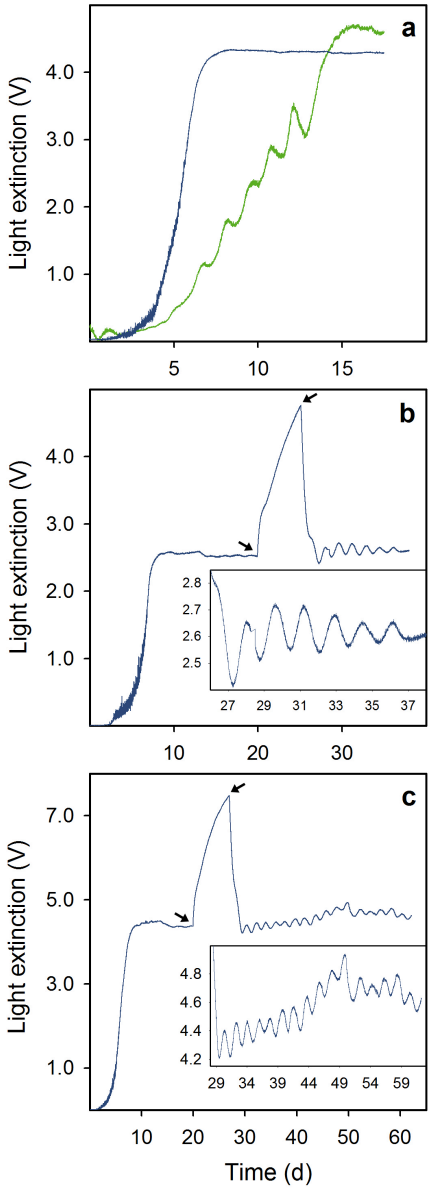

Figure 2.1: Oscillatory dynamics in one-species phytoplankton chemostats. Measurements of light extinction [V] are equivalent to algal biovolume (see SI section 2). (**a**) Smooth and oscillatory increase toward steady state. *Chlorella vulgaris* (blue) from nitrogen-sufficient culture, $\delta = 0.65$ day^{-1}, $N_i = 320$ µmol·L^{-1}; *Monoraphidium minutum* (green) from nitrogen-limited culture, $\delta = 0.51$ day^{-1}, $N_i = 160$ µmol·L^{-1}. (**b**) Induced damped oscillations after pausing of chemostat flow. *C. vulgaris*, $\delta = 0.0$ day^{-1} from day 20 to 25, otherwise $\delta = 0.81$ day^{-1}, $N_i = 160$ µmol·L^{-1}. (**c**) Induced sustained oscillations after pausing of chemostat flow. *C. vulgaris*, $\delta = 0.0$ day^{-1} from day 22 to 29, otherwise $\delta = 0.61$ day^{-1}, $N_i = 320$ µmol·L^{-1}. Arrows indicate when chemostat flow was switched off and back on. Insets show details of the oscillatory part of the dynamics.

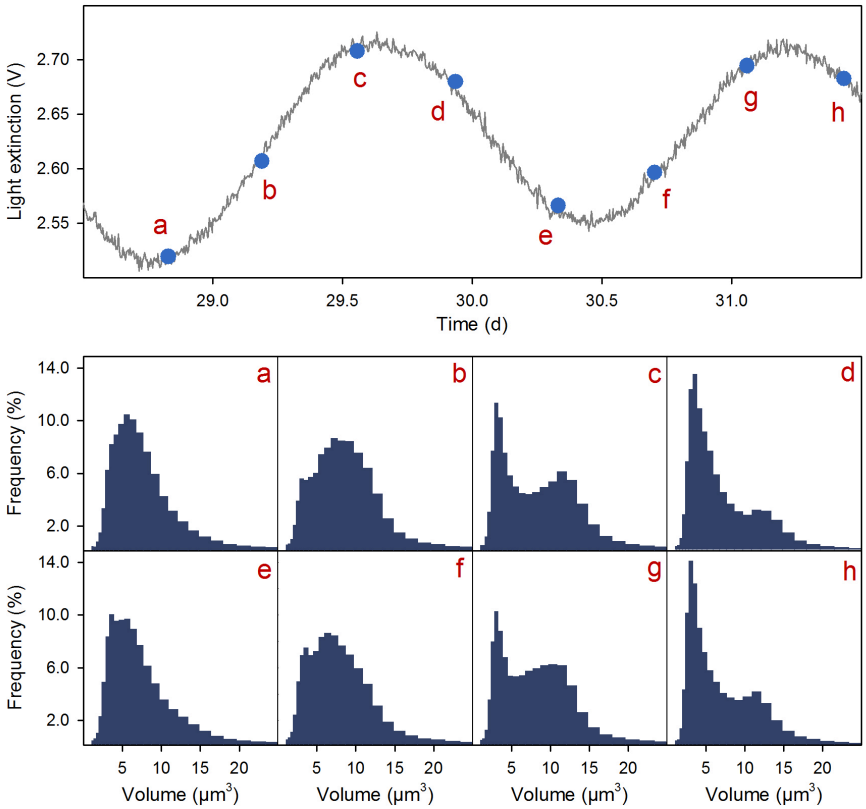

Figure 2.2: Cell size distributions (lower panels) at consecutive phase locations of the population cycle (upper panel; detail from chemostat trial with *C. vulgaris*, Fig. 2.1b). Letters (**a**) - (**h**) indicate locations in the population cycle at which cell size distributions were measured (see text for details).

different phytoplankton species and at a variety of chemostat dilution rates and nitrogen concentrations, N_i, of the inflowing medium (SI section 5). The induced oscillations were damped for small values of external nutrient concentration combined with high dilution rates (Fig. 2.1b), however we observed sustained oscillations (up to 16 cycles) when δ was lower and N_i was high (Fig. 2.1c). The oscillations showed period lengths ranging from 1.03 to 3.5 days, thus ruling out circadian cell culture rhythms [6, 50] as the general cause of the oscillations. Measurements of cell size distributions provide evidence that the phytoplankton populations periodically changed their demographic structure with the periodicity of the population oscillations. We measured cell size distributions at distinct phase locations of the population cycles induced by the "off-on" manipulation and found recurring patterns that can be linked to phases of the cell cycle (Fig. 2.2). The cycle starts with a unimodal distribution of cell-sizes (Fig. 2.2 a, e) around a small volume of 5 μm^3, directly after division of most cells, reminiscent to the cell size distribution in the stationary state (Fig.

S4 SI section 4). From this point cells grow as a cohort from small to large, which is visible as a moving peak in the cell size distribution that shifts to the right (Fig. 2.2 a-d, e-h). As soon as the first cells of the cohort begin to divide a second peak in the cell size distribution at small cell sizes appears, giving rise to a distinct bimodal cell size distribution (Fig. 2.2 c, g). Since progression through the cell cycle is retarded in the nitrogen-dependent, pre-mitotic phase of the cell cycle, cells entering this second peak are temporarily arrested in their progress. Consequently, the left peak does not shift to the right but increases in size as cells continue to divide, whereas the right peak continues to shift and decreases in size (Fig. 2.2 d, h). When all cells of the cohort have finished cell division and the right peak of large cells has disappeared the cycle starts anew if sufficient nitrogen is available (see also Fig. S5 in SI for comparison of experimental with simulated cell size distributions).

Spectral plots of cell size distributions measured over the full length of the chemostat experiment clearly reveal the contribution of cellular level events to the synchronization of the whole population. The steady state population before the "off-on" manipulation was characterized by a rather broad unimodal stationary cell size distribution (see also Fig. S4, SI). Switching off flow through the chemostat led to an extreme accumulation of small cells. After the flow had resumed the collective development of cell cohorts is clearly visible as recurring diagonal stripes in a phase time plot (Fig. 2.3d). These time periodic patterns align with the oscillations of cell counts (Fig. 2.3a) and light extinction and can be quantified by oscillations in the order parameter, as a direct measure of the degree of synchronization among individuals (Fig. 2.3b). The periodicity and intensity of oscillations in light extinction and in cell volume distributions remained directly linked to one another for many generations. Further, the cell size distribution indicates ratios in cell volumes between mother and daughter cells ranging from 3.81 to 4.29 (assuming spherical shapes), which is consistent with Chlorella's typical mode of division by splitting into four daughter cells.

2.4 MODEL PREDICTIONS AND AGREEMENT WITH DATA

A mathematical model can provide further insight into the mechanisms that led to synchronization of population and cell cycles in our experimental cultures. The model is based on the Kuramoto theory [83] describing the collective synchronization among a large population of all-to-all coupled oscillators, i.e. each cell adjusts its cell cycle with that of all other cells. In the model we associate a cell's age to a phase variable $\theta_i \in [0, 2\pi]$, which may be interpreted as the cell's development index. For each cell this phase advances according to

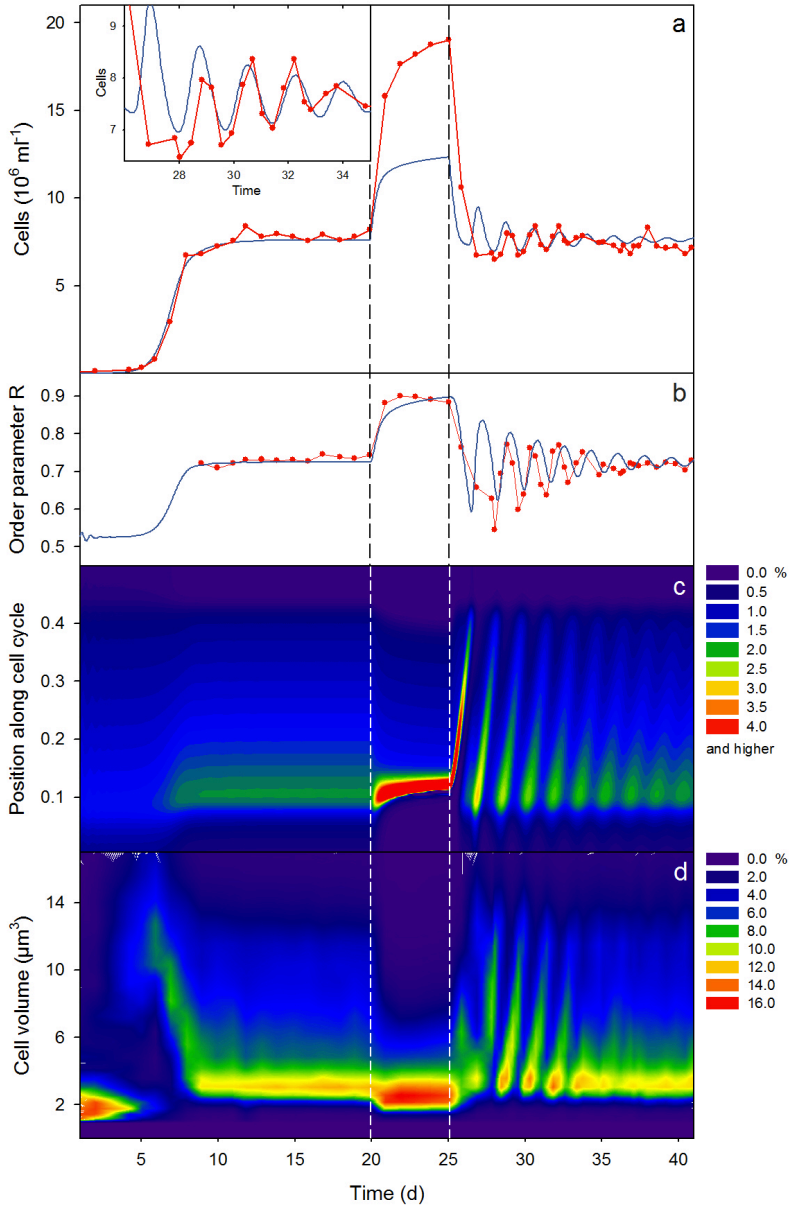

Figure 2.3: Fundamental agreement of oscillatory population behavior and cell cycle phases between experiment and structured model simulation for a chemostat trial with *C. vulgaris* (cf. Fig. 2.1b). (**a**) Observed dynamics (red, cell numbers) and model prediction (blue). Inset shows detail of days 26 - 35. (**b**) Order parameter R as a simple, direct measure of the degree of synchronization among individual oscillators for the experimental populations (red) and the simulations (blue). (**c**) Model prediction of cell phase distributions. For each time step color indicates the fraction of the algal population that occupies a certain position along the cell cycle. (**d**) Observed cell volume distributions as proxy for the cell phase distributions. Color indicates the fraction of the population that has a certain cell volume V (200 bins in 0 m^3 $\leqslant V \leqslant$ 4189 m^3).

its aging velocity $g(N, \theta)$ and is disturbed by independent, identically distributed white noises $\xi_i(t)$ [135, 2]:

$$\dot{\theta}_i = g(N, \theta_i) + \xi_i(t). \tag{2.1}$$

Because individual organisms in the mixed culture cannot sense their phase difference to others, in contrast to the Kuramoto model [83], we propose that the nutrient concentration $N(t)$ acts as a mean field that is able to mediate interactions among the oscillators. Following Pascual and Caswell [112] we assume that the cell progression $g(\theta, N)$ is divided into a nutrient-sensitive and a non-sensitive phase:

$$g = g(\theta, N) = \begin{cases} \omega \frac{N}{K_N + N} & \text{if } \theta \in [\theta_0, \theta_c] \\ \omega & \text{otherwise.} \end{cases} \tag{2.2}$$

In the interval $[\theta_0, \theta_c]$ aging depends on the nutrient concentration in a Monod-wise function, with half-saturation constant K_N. In the absence of nutrients ($N = 0$) progression in this interval becomes zero ($\dot{theta} = 0$) and a cell stops its individual development. For the rest of the cycle, cell phase progression g occurs with the constant maturation velocity ω (taken to be identical for all cells). This gives rise to the following model for the phase distribution $p(\theta, t)$ of oscillators at phase ω (note the similarity to the McKendrick-von Foerster equation; see e.g. ref. [37])

$$\frac{\partial p}{\partial t} + \frac{\partial}{\partial \theta}[gp] = D\frac{\partial^2 p}{\partial \theta^2} - \delta p, \tag{2.3}$$

where the last term takes into account the losses by the chemostat system with dilution rate δ and the term $D > 0$ derives from the noise terms [135, 2].

Synchronization theory describes a fixed number of oscillators, but in our case the number of oscillators is not necessarily conserved. This leads to a system of oscillators, where each oscillator gives birth to new ones when its phase has reached 2π and is subsequently eliminated. Cell division enters the model in form of a boundary condition $p(0, t) = \nu p(2\pi, t)$, where ν is the number of daughter cells after cell division (note that in the model the phase of a cell is only defined in the interval $0 \leqslant \theta \leqslant 2\pi$). Finally, the model is complemented by a dynamic equation for the nutrient concentration

$$\dot{N} = \delta(N_i - N) - \nu_m \frac{N}{K_N + N} P, \text{with} P(t) = \int_0^{2\pi} p(\theta, t) d\theta, \tag{2.4}$$

where N_i is the input nutrient concentration and $P(t)$ the total population density. We fitted model parameters to one data set using maximum likelihood estimation (Fig. 2.3, SI section 3) and used these to independently generate simulations for the remaining data sets. Predictions of the parameterized model are in good agreement with

the observed dynamics (Fig. 2.3). Most notably, across all experiments performed the observed period lengths and the equilibrium cell density agree well with those predicted by our model at different dilution rates (Fig. 2.4). Moreover, all three major model components ("population dynamics", "cell cycle dynamics", and "nutrients as common medium") are essential and necessary to explain the dynamics of the phytoplankton populations. As in standard Monod-type chemostat models, the growth of the population density $P(t)$ depends on the nutrient concentration. But the model also exhibits a synchronized state in which phase-locked cell cohorts rotate and divide with a common frequency and the population density oscillates in time. These synchronized dynamics appear as two dynamic variants. For some parameter combinations the model exhibits a spontaneous transition to the synchronized state where oscillations are self sustained. For other parameters, the internal coupling is not sufficient to maintain sustained oscillations, so that cycles are damped and decay as the oscillators drift apart in phase. This behavior is reminiscent to the Kuramoto theory [83, 2], where a phase transition occurs at a critical coupling strength. When the coupling strength is below the threshold, the system relaxes to an incoherent state ($p(\theta, t) = 1/2\pi$). However, for coupling above the threshold collective synchronization sets in spontaneously among a fraction of oscillators which are locked in phase.

Note that even below the synchronization threshold individual oscillators are rotating along their cycle, but since the oscillators are desynchronized there is no rhythm in the macroscopic average. In this situation it is possible to unmask the intrinsic dynamics by manually resetting the oscillators' phase. Such an external perturbation will establish a transient collective cycle that decays as the individuals gradually drift apart. The generation of a collective cycle and relaxation to an incoherent state by de-phasing has been experimentally observed [6, 90] and theoretically described as a generalized Landau damping with exponential decay of oscillation amplitudes at intermediate times, but slower than exponential decay at long times [137].

Given the phase distribution $p(\theta, t)$, the degree of synchronization or phase coherency among individual cells can be estimated by the order parameter $R = \left| \int_0^{2\pi} d\theta e^{i\theta} p(\theta, t) \right|$, both for the simulated and the experimental populations (SI section 3). As expected by theory, we observed moderate degrees of synchronization ($R \approx 0.7$) prior to dilution switch-off, increasing synchronization ($R \approx 0.9$) during the off-phase and oscillatory fading-out of synchronization after dilution resumed (Fig. 2.3b). In some regards, these observations of our experimental and simulated cell cycles differ from what would be expected from the Kuramoto model. First, in contrast to the Kuramoto theory, here the order parameter does not vanish in the asynchronous state as the phase density is not uniform (see Fig. S4, SI). The reason for

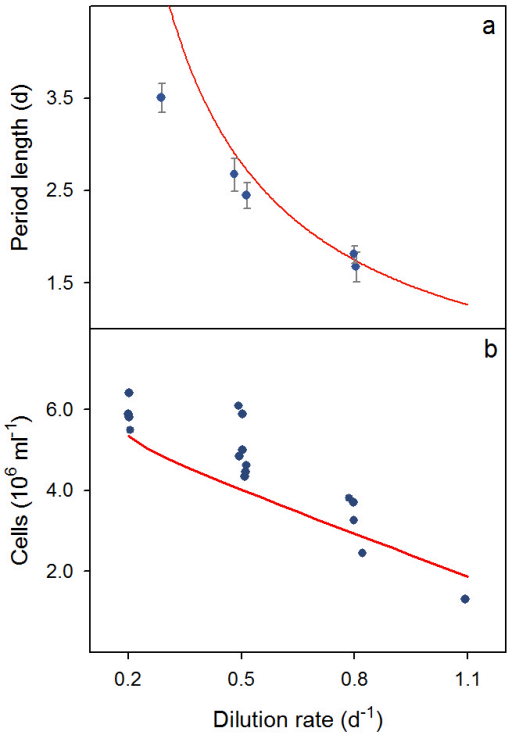

Figure 2.4: Period lengths and equilibrium densities in chemostat trials with *C. vulgaris* at different dilution rates. (**a**) Period length of oscillations arising after "off-on" manipulation of the chemostat. Blue symbols: Mean period length (± 1 SD) of oscillations in 5 separate chemostat trials. Red line: Values predicted by simulations of the structured model. Nitrogen concentration of inflowing medium $N_i = 160$ µmol·L^{-1} for all trials. (**b**) Equilibrium cell density reached in 17 separate trials (blue symbols); either before "off-on" manipulation or without such manipulation performed. Red line: model prediction. $N_i = 80$ µmol·L^{-1} for all trials.

this is that most oscillators will be located in the nutrient sensitive phase interval (due to the slow aging progression) and also have a higher probability to be washed out with increasing progress in phase (leading to a decay of phase density with θ). Second, in our system (both theory and experiment) onset of synchronization is characterized by oscillations of the order parameter (Fig. 2.3b). Oscillating order parameters can arise in modified versions of the Kuramoto model, for example in the presence of structure in the coupling topology among the oscillators [99]. But here, the oscillations of the order parameter after perturbation reflect the periodic changes in the shape of the phase density, periodically shifting between unimodal and bimodal distributions.

2.5 DISCUSSION

Our experiments show that unicellular phytoplankton can possess an internal population structure that is sufficient to affect population dynamics. In the absence of periodic external forces (in particular, under constant illumination) we observed single-species cycles that can be understood by the interaction between the nutrient pool and nutrient-dependent and -independent phases of the cell cycle. Such cycles cannot occur in standard ecological models that describe unstructured, single populations, i.e. the population behavior cannot be reduced to that of an average cell. When we removed structure from our mathematical model by making all phases of the cell cycle equally nutrient-dependent, cells were unable to synchronize and unable to oscillate in abundance.

Previous studies have established that progression through the algal cell cycle can depend on light [50] or nutrient availability [145], that algal populations can be entrained into periodic changes of illumination and that they, in theory, can maintain the entrained state for some time even in the absence of the forcing stimulus [112]. Here we show that nutrient shortage, an ecologically important condition, can lead to the entrainment of cell cycle oscillations, and that cell cycle and population oscillations remain frequency-locked for long periods of time, sometimes without any apparent signs of damping. The most likely explanation for this behavior is that the algal cells act as globally coupled, individual oscillators that interact and become synchronized with one another through a common extracellular field, the nitrogen pool. Even when synchronization is transient and oscillations are damped (Fig. 2.1b) the characteristic shape and dynamics of the phase distribution (with periodic change between unimodal and bimodal distributions, Fig. 2.2) provide strong evidence for an internal coupling by the nutrient pool. In this case, coupling is not sufficiently strong to effect sustained synchronization but it is unlikely that such phase distributions can be generated if cells simply drift apart by virtue of their different natural frequencies. Instead, the phase distribution can only sensibly be explained if internal coupling via the common nutrient pool is present. Our mathematical model corroborates this conclusion. We observed the characteristic dynamics of the phase distribution only if we included coupling to the nutrient pool via a nutrient-sensitive and non-sensitive phase interval. Similar types of synchronization (yet, at much shorter period lengths of several minutes and hours) have been observed in yeast cell cultures where glycolytic [36] or cell-cycle dependent [92, 103] oscillations became synchronized through the concentration of extracellular substrates, and in nanochemostats where bacterial cells regulated cell density through a feedback mechanism based on quorum sensing of a signaling molecule [5].

The distinction between steady state and cycles is a fundamental one [105, 141]. Our study reveals a mechanism by which small amplitude oscillations can arise in phytoplankton populations that lack obvious internal structure and that are traditionally modeled as groups of homogeneous cells. Our concrete experimental examples and mathematical model showed how complex processes occurring within individual cells may have dynamical consequences at the population level. Thereby, the interaction between within-cell processes and population dynamics goes both ways. On the one hand, population dynamics is able to induce synchrony in the cell-cycle of many individuals (through nutrient limitation). On the other hand, collective cell-cycles among individual cells generate oscillations at the population level. Because the interaction between phytoplankton and the nutrient pool is the most basic trophic module in aquatic ecosystems we suggest that cell-cycle-to-population synchronization is also likely to be an important mechanism in natural communities.

2.6 METHODS

We used experimental populations of the three green algae *Monoraphidium minutum*, *Chlorella vulgaris* and *Chlamydomonas reinhardtii*. We ran experiments in 0.8-liter chemostats at $23.3° \pm 0.4°$C and constant fluorescent illumination at 110 $\mu E \cdot m^{-2} \cdot s^{-1}$. Algae were cultured in modified Woods Hole WC medium [55] at pH = 6.8. Nitrogen concentrations in the inflow (N_i) were adjusted to limit algal growth and varied between 40 and 320 $\mu mol \cdot L^{-1}$. Peristaltic pumps transported the sterilized medium through the chemostats with a continuous flow δ (varying between 0.29 and 0.81 day^{-1} among chemostat trials) and cultures were bubbled with sterile air. We determined algal biovolume by quasi-continuous, non-invasive light extinction measurements [150]. Additionally, we took small (< 1 mL) samples of live phytoplankton from the effluent of chemostats and used a CASY particle counter (©Schärfe, Reutlingen) to measure cell size distributions as well as cell numbers and algal biovolume.

2.7 AKNOWLEDGMENTS

We thank E. Denzin for help with the chemostat experiments and A. Ryabov for help with the numerical simulations. We thank T. Hintze and N. Walz for supporting us with the extinction measuring system. We acknowledge support by the Volkswagen Foundation, the German Research Foundation (DFG), NSERC and the James S. McDonnell Foundation.

3

COMPLEX TRANSIENT DYNAMICS

by Thomas M. Massie, Ursula Gaedke, Alexei Ryabov, Guntram Weithoff, and Bernd Blasius

The manuscript is submitted to *Ecology* as

Massie, T.M.[1], U. Gaedke[1], Alexei Ryabov[2], G. Weithoff[1], and B. Blasius[2] (submitted) *Complex transient dynamics of structured populations in response to environmental changes.*

[1] Institute of Biochemistry & Biology, University of Potsdam, Maulbeeralle 2, 14467 Potsdam, Germany
[2] Institute for Chemistry and Biology of the Marine Environment, Carl von Ossietzky University, 26111 Oldenburg, Germany

3.1 ABSTRACT

Changing environmental conditions alter the demographic structure of a population and therefore its dynamics. However, the shape of the arising transients is highly complex and its prediction challenging. In experimental chemostats, we studied the response of phytoplankton populations to well-defined changes in culture conditions focusing on the interplay between stage structure and population dynamics. Starting from a stable steady state, we doubled the concentration of the growth-limiting resource and altered the dilution rate, respectively. We demonstrate that, corresponding to a memory effect, the transient behavior between two steady states crucially depended on, first, the value and direction of the parameter changed and, second, the demographic state before it changed. Together, both parameters determined whether the transition was rather smooth or whether the cell number, the biomass, and the size distribution exhibited oscillatory behavior. Further, we implemented resource-dependent cell size variability into a stage-structured model that accounts for cell cycle and population-level processes. Thereby, we were able to identify the key mechanisms determining the complex response dynamics including non-intuitive behavior, in such a way that the cell number temporarily decreased when the resource supply was increased. Our study emphasizes the paramount importance to identify the mechanisms mediating between

cell cycle and population-level processes to understand the transient dynamics originating from changes of the environment. It is of relevance to all populations possessing demographic structure including organisms of higher order which can hardly be studied with similar precision as populations of unicellular species.

3.2 INTRODUCTION

A major challenge in ecology is the identification of the critical mechanisms underlying population dynamics to predict the responses of populations to environmental changes. Being scale dependent [93], environmental changes impact the biology and the life cycle of individual organisms and cause changes in the dynamic behavior of entire populations [149, 111]. Differences between the individual life stages within a population result in a developmental heterogeneity that is denoted as population structure or, more generally, demography. This structure fundamentally determines population dynamics since the developmental stages differently interact with the environment. Demography is ubiquitous among all species on earth. Being instantly apparent in macroorganismal populations, also simple unicellular microorganisms posses a population structure [5, 63, 26, 93] that arises from physiologically distinct phases within a cell cycle [145, 4, 112]. In response to changing environmental conditions, populations perform transitions in their dynamics [23, 74, 31, 91, 56]. This transient behavior can be defined as the 'behavior that is different from the long-term behavior' [61] and reflects the behavior between two population-dynamical steady states. As environmental changes, transient population dynamics are scale dependent, too. They are directly related to the generation time of an organism (i.e., a sequoia is likely to respond on a broader timescale than a mayfly does) that is defined by the life cycle encompassing all stages of ontogenetic development.

Predicting the responses to environmental changes premises the understanding of the mechanisms by which different the developmental stages within a population are influenced. Their number strongly increases when stage-dependent interactions are relevant [140, 22] and they can stabilize or destabilize population dynamics, depending on the types of mechanisms and the given environmental conditions. One intriguing phenomenon of structured populations is the occurrence of regular fluctuations, denoted as oscillations [22, 79, 102]. Many natural populations fluctuate with frequencies that cannot be explained by diurnal, annual, or other externally forced variation. Such oscillations are often caused by multispecies interactions like predator-prey or host-parasite relations. But even single-species systems can exhibit oscillatory behavior due to inherent demographic properties: At steady state, a population possesses a characteristic demographic distribution

adapted to the prevailing environmental conditions. If this distribution is perturbated, a cohort forms (i.e. individuals that have shared a particular experience during a particular life stage) which is generally tantamount to the synchronization of a population: the higher the degree of synchronization, the higher the contribution of the cohort to the whole population. If the vast majority of individuals grows, reproduces, and dies at the same time, a population starts to oscillate. Complex dynamic behavior that results from demographic structure has most impressively been demonstrated in populations of flour beetles (*Tribolium sp.*) [66, 28, 38]. Such holometabolic insects have well-defined and morphologically distinguishable life stages (egg, larva, pupa, and imago) with distinct characteristics that certainly structure a population. Contrary, the developmental stages of a vast number of species cannot be clearly related to a morphological shape.

To investigate both, the demographic and the dynamical response of structured populations to environmental changes, we conducted chemostat experiments with physiologically structured populations of the unicellular phytoplankton species *Chlorella vulgaris*. Since a chemostat represents a highly controllable experimental system, it allows testing for changes of a specific parameter and simultaneously excludes any unwanted influences. We imposed changes of the environment by altering the supply concentration of the growth-limiting resource nitrogen, N_i, and the dilution rate, δ, the two basic parameters determining a chemostat system. By doing so, we change the environmental conditions to observe the impacts on the populations. This distinguishes our study from many others where the population structure was directly manipulated by reducing the number of individuals belonging to a specific developmental stage (selective harvesting) [28, 10, 19], because our approach is closer to natural processes. In a previous study, Massie et al. (2010) [93] synchronized *C. vulgaris* populations in a chemostat by turning off the dilution for several days. Once synchronized, the populations exhibited cyclic behavior with periods defined by the generation time. However, such a harsh "off-on" manipulation is rather uncommon in natural systems. Here, we applied gradual shifts of δ as we expected the population dynamical response to dependent on the direction of the change, the amount, and the absolute values of δ before and after they were changed.

C. vulgaris possesses a typical eukaryotic cell cycle with four physiologically distinct stages (G_1-, S-, G_2-, and M-phase) - from newly released daughter cells to proliferating mother cells that typically divide into four daughter cells. Especially the G_1-phase causes a population to exhibit demographic structure. There, all preconditions have to be fulfilled to perform DNA synthesis and replication during the next stage (S-phase) [101, 71]. Lacking nitrogen, for example, stops the transition into the S-phase [145, 110, 109, 51] and prevents the cell from entering DNA synthesis, which would not be successful without

sufficient nitrogen accumulated to perform at least one replication. The progression velocity for all other stages is nitrogen-independent. Thus, nitrogen-sensitive progression velocity in one segment of the cell cycle is a simple but effective mechanism generating a dynamic population structure whose shape depends on the availability of an external resource such as nitrogen.

A chemostat allows the maintenance of populations at steady state for many generations [108, 67]. Constant population renewal is given by the dilution which provides continuous supply with resources and removes all chemostat content defining the mortality rate of the algae. We applied environmental perturbations by (*i*) doubling the concentration of the limiting resource in the supply medium N_i, and (*ii*) by increasing or decreasing δ. A doubling of N_i allowed to investigate the dynamic behavior in response to an ameliorate resource availability, e.g. nutrient enrichment in aquatic systems due to global change [120, 75]. Varying δ mimicked changes of the system's turnover rate. This addresses the question how the population dynamics respond when higher amounts of resources enter the system per unit of time and mortality is simultaneously increased - and vice versa.

We tracked population dynamical responses by automatically measuring light extinction with a high temporal resolution. This unusually accurate time-series experiments helped identifying dynamics unlikely to be detected by 12- or 24-h sampling intervals. Size distributions as well as data on cell number, P, biovolume, V_B, and mean cell volume, V_C, were obtained by particle counter measurements every 4-8 hours. Size distribution measurements allowed to track cell size variability according to the developmental stages, from small daughter to large mother cells.

The interpretation of our experimental results is supported by a mathematical model dividing the life cycle of the phytoplankton cells into two stages: a first stage where progression is nitrogen-dependent and a second one where it is not [93]. We extended the model from Massie et al. (2010) [93] by an additional mechanism allowing the algal cells to grow larger at high nitrogen concentrations [123, 21]. That is, the size of a cell varies within the developmental stages, and also with the availability of nitrogen. Under non-limiting conditions, cells in the G_1-phase can take up surplus nitrogen (exceeding the minimum requirements to reproduce) to synthesize higher amounts of cell compounds like amino acids or proteins [123, 39]. Hence, the cells grow larger compared to growth under strongly limiting concentrations. Further, we assume Chlorella mother cells to divide by splitting into four small daughter cells. This value coincides with the ratio of the volumes between large mother and small daughter cells, which was previously found to be in a range from 3.81 to 4.29 [93]. Thus, the size of the daughter cells is defined by the size of the mother cells; e.g., a mother cell that is twice in size (volume) releases four daughter cells

that are twice in size, too. Both mechanisms, synchronization due to nitrogen limitation and nitrogen-related cell size variability are expected to provoke highly complex responses to changes of environmental parameters.

Our study shows that microbial populations may exhibit complex transient population dynamics in response to environmental changes that are directly assigned to the demographic structure. Our chemostat populations showed oscillatory dynamics and responded counterintuitively. This depended on both, the way environmental parameters changed and the population's demographic state before they changed. The experimental data agree with the predictions obtained from the mathematical model suggesting that we have identified the critical mechanisms leading to the observed dynamics.

3.3 METHODS

CHEMOSTAT SETUP We established monoclonal batch cultures of the green algae *C. vulgaris* (Chlorococcales) and kept them in a climate chamber at $23.3° \pm 0.4°$C and constant fluorescent illumination at 110 $\mu E \cdot m^{-2} \cdot s^{-1}$ (preventing synchronization by light-dark cycles). The batch cultures served as stock cultures for the chemostat experiments. Nitrogen concentrations were adjusted to be non-limiting or only weakly limiting. We used a sterile, modified Woodshole WC medium after Guillard & Lorenzen (1972, pH = 6.8) [55]. Setting $N_i = 80$ $\mu mol \cdot L^{-1}$, nitrogen concentrations were low enough to limit algal growth. The medium contained trace metals, vitamins and other nutrients in non-limiting concentrations. For stock cultures we used medium containing 320 µmol nitrogen per liter. We used glass chemostat vessels of 1.5 L volume and adjusted the culture volume to approximately 800 mL. To provide homogenous mixing and to prevent CO_2-limitation algal cultures were bubbled with pressurized, sterile air.

We measured cell number, biovolume, and cell volume by using a CASY (©Innovatis) particle counter. We used light extinction measurement devices according to Walz et al. (1997) [150]. Light extinction was measured as light transmittance (wavelength $\lambda = 880$ nm) through a sterile syringe that pulled out and pushed back 10 mL of chemostat content every 5 minutes being therefore a quasi-continuous, non-invasive method. It provided the high temporal resolution necessary to analyze population dynamics in detail. Previous investigations of the chemostat system showed that light extinction serves as an accurate proxy for algal biovolume [93]. Algal growth on the wall of the syringe was prevented due to the bidirectional movement of the syringe plunger. To automatically store the data, the extinction measurement devices were connected to a computer. Experimental design

To test for the responses of a population to a changing environment we altered the two fundamental parameters defining a chemostat system: (*a*) resource influx into the system represented by the nitrogen concentration of the supply medium N_i and (*b*) the system's turn-over rate represented by its dilution rate δ.

(*a*) The system's resource influx was increased by doubling N_i from 80 to 160 $\mu mol \cdot L^{-1}$. This is qualitatively different from applying a nutrient pulse. Here, the medium drips into the chemostat vessel according to the value of δ. The surplus of nitrogen enters the system not at once but rather gradually in time. That is, at a value of $\delta = 0.5\ day^{-1}$ 40 $\mu mol \cdot L^{-1}$ more enter the chemostat within the period of one day. In contrast, a pulse would mean that the same amount is added instantaneously. With our setup we address the response of natural populations that are affected by increasing resource amounts. We focus on the transient and lasting changes that populations experience in their demographic structure and the resulting population dynamics.

(*b*) The system's turn-over was altered by manipulating δ. By doing so, the populations experienced a higher mortality when δ was increased, and vice versa. Additionally, increasing δ leads to an ameliorated nutrient availability per cell: directly, as the inflow of nutrient-containing medium per unit time is higher and, indirectly, as more cells are washed out and, hence, do not compete for nutrients anymore. As a result, the cells remaining inside the chemostat vessel experience better conditions for individual growth than at lower δ. The opposite holds for a reduction of δ.

Each time we started a chemostat experiment, we first inoculated *C. vulgaris* at very low densities (about 25.000 to 50.000 $cells \cdot mL^{-1}$) and let the cultures grow till they reached steady state. Then, prior to each perturbation, the chemostat populations were kept at steady state for at least five days. This was done to ensure that all population-characterizing variables (P, V_B, V_C, and size distributions) remained at steady-state. Only now, changes of N_i and δ were applied.

MODEL DESCRIPTION AND PARAMETER FITTING We used numerical modeling to support our experimental findings and to explain the interplay between cell growth, demographic structure and population dynamics based on the chemostat model recently presented by Massie et al. (2010) [93]. In this model, induced population synchrony leads to sustained oscillations of cell density and demographic structure which were related to a feedback between the nitrogen-dependent maturation velocity within the G1-phase and the nitrogen concentration of the surrounding medium. Here, we extend this model by an additional mechanism allowing the nitrogen concentration to influence the duration of the G_1-phase. That is, cells can take up surplus

nitrogen that prolongs the G_1-phase and enables them to grow larger than the minimum size allowing reproduction.

The age of a cell is described by the phase variable θ_i which can be interpreted as its development index or the position along the cell cycle. For each cell, θ_i advances according to its aging velocity $g(N, \theta_i)$ and is disturbed by independent, identically distributed white noises $\xi_i(t)$:

$$\dot{\theta}_i = g(N, \theta_i) + \xi_i(t) \tag{3.1}$$

The cell cycle is subdivided into two basic segments: the G1-phase where g is nitrogen-dependent, and the rest of the cycle (comprising the S-, G2-, and M-phase) where g is constant. This results in

$$g = g(\theta, N) = \begin{cases} \omega \frac{N}{K_N + N} & \text{if } \theta \in [\theta_0, \theta_c] \\ \omega & \text{otherwise.} \end{cases} \tag{3.2}$$

with $[\theta_0, \theta_c]$ being the G_1-phase interval, N the nutrient concentration of the surrounding medium, K_N the half-saturation constant, and ω the constant maturation velocity. Within the G_1 interval, aging depends on the nutrient concentration in a Monod-wise function; it becomes zero when the nutrient concentration is exploited ($N = 0$) which ultimately causes the cells to cease developmental progression ($\dot{theta} = 0$). Moreover, the length of the G_1-phase can vary. At high nutrient concentrations the length of this phase increases, causing the cells to take up surplus nitrogen and to grow larger in size. For the length of the G_1-phase we assume an exponentially saturating dependence on the nitrogen concentration:

$$\theta_c = \widetilde{\theta}_c + \Delta\theta_c(1 - e^{\alpha N}). \tag{3.3}$$

Thus, when nitrogen is depleted, the G_1-phase has a minimal length of $\theta_0 + \widetilde{\theta}_c$ and the nutrient independent part of the cell cycle begins at $\widetilde{\theta}_c$. At infinite nitrogen concentrations, however, the G_1-phase is elongated until the phase value $\widetilde{\theta}_c + \Delta\theta_c$. The parameter α characterizes the rate of this transition with increasing nitrogen. The rest of the cell cycle is nitrogen-independent. Therefore the length of subsequent segments can be presented by a single parameter $\Delta\theta_s$ and the phase of cell division is $\theta_{div} = \theta_c + \Delta\theta s$. If the cell density at phase θ and time t is denoted as $P(\theta, t)$, their dynamics can be represented in terms of a reaction-diffusion-advection equation

$$\frac{\partial P}{\partial t} + \frac{\partial}{\partial \theta}[gP] = \frac{\partial}{\partial \theta} D(g) \frac{\partial P}{\partial \theta} - \delta P, \tag{3.4}$$

where the last term takes into account the losses by the chemostat system with dilution rate δ and the term $D > 0$ derives from the noise terms [135, 2]. The diffusion constant is assumed to scale proportional to the square of the maturation velocity $D(g) = \chi g^2$. In this way we

ensure that sharp peaks in the density distribution do not decay when maturation velocity is zero. In the usual parameterization, however, our model results are not affected by this choice of the diffusion term. To specify the boundary condition we require that all cells at the phase value θ_{div} and larger divide into n daughter cells with zero phase

$$p(0) = n \int_{\theta_{div}}^{\infty} p(\theta) d\theta. \tag{3.5}$$

Finally, the model is complemented by a dynamic equation for the nutrient concentration

$$\dot{N} = \delta(N_i - N) - \nu_m \frac{N}{K_N + N} P, \quad \text{with } P(t) = \int_0^{2\pi} p(\theta, t) d\theta, \tag{3.6}$$

where N_i is the input nutrient concentration, ν_m is maximal nutrient uptake rate, and $P(t)$ the total population density.

To fit parameters, we used the differential evolution algorithm [134]. We optimized parameters to estimate a combination of K_N, ω, χ, ν_m, α, and $\Delta\theta_c$, that minimizes the mean square deviation of the model outcome to the chemostat cell number in experimental trials 1 and 2, simultaneously. Being fitted just for two experimental trials, that parameter set yielded also remarkable agreement of the model outcome to the other experimental trials 3, 4, and 5. This verified that the qualitative model results are robust and describe the experimental data obtained under different conditions.

3.4 RESULTS

STEADY STATE CONDITIONS The populations showed characteristic size distributions depending on the chemostat dilution rate at steady state with broad size distributions at high dilution rates (Fig. 3.1). Compared to a moderate dilution rate ($\delta = 0.5$ day^1), a higher dilution rate results in higher amounts of nitrogen available for the phytoplankton cells since more nitrogen enters the vessel per unit of time and more cells are washed out of it. As a result, the cells are able to progress faster through the G_1-phase and accumulate less in it. This is shown by the size spectra (right panels of Fig. 3.1): the frequencies of smaller cells, i.e. cells in an early developmental stage, decrease with increasing dilution rates.

Moreover, the algal cells grew larger at higher dilution rates (Fig. 3.2a). While the average value of the mean cell volumes V_C at an average dilution rate of $\delta = 0.2$ day^1 ($V_C = 11.14 \pm 0.76$ μm^3, mean ± SD) and $\delta = 0.50$ day^1 ($V_C = 10.14 \pm 0.63$ μm^3) was approximately the same, it clearly increased at $\delta = 0.81$ day^1 ($V_C = 13.31 \pm 2.19$ μm^3) and $\delta = 1.09$ day^1 ($V_C = 21.53 \pm 2.14$ μm^3). Especially at the highest δ, V_C differed notably from cells at lower δ (being nearly twice as high).

The steady-state cell number, P^*, (Fig. 3.2b) as well as the steady-state biovolume, V_B^*, (Fig. 3.2c) showed a negative relationship with δ.

When doubling the nitrogen concentration of the supply medium N_i, both measures doubled, too (trial 1 and 2, dark-green dots).

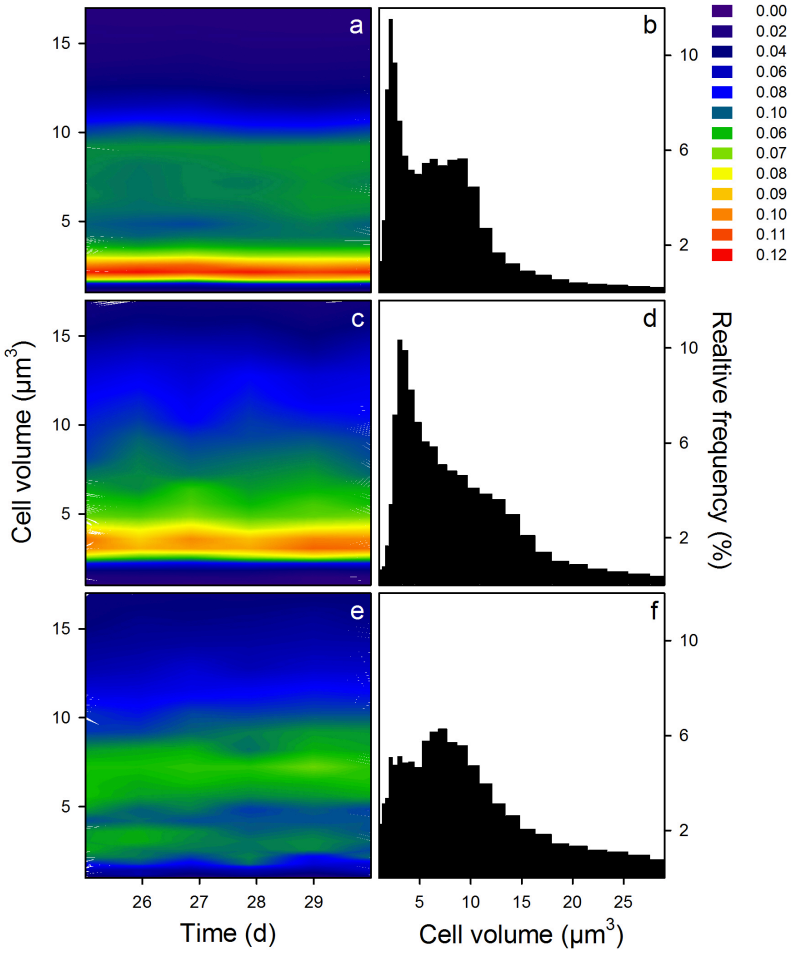

Figure 3.1: Steady-state distributions of cell size in trials 1 to 3 before perturbations were applied. The corresponding dilution rate in trial 1 was $\delta = 0.48$ day^1 (**a**,**b**), in trial 2 it was $\delta = 0.82$ day^1 (**c**,**d**), and in trial 3 it was $\delta = 1.09$ day^1 (**e**,**f**). Panels on the left (**a**,**c**,**e**) show the average size distributions over a five day sampling interval. Panels on the right (**b**,**d**,**f**) show the temporal dynamics of the size distributions within this interval. The colors code the relative frequencies from low (blue) to high values (red). In each trial, the nitrogen concentration of the supply medium was $N_i = 80$ µmol·L^{-1}

CHANGING THE NITROGEN SUPPLY CONCENTRATION In the experimental trials 1 and 2 , N_i was doubled from 80 to 160 µmol·L^{-1} at $t = 30.80$ days whereas δ remained constant in each trial. This induced transient dynamics displayed by the average population measures (Fig. 3.3 a,b) and the demographic structure (Fig. 3.3 c,d). In both trials, the populations responded with more or less pronounced

oscillations of P, V_B, V_C, and the size spectra. Damped, small amplitude oscillations occurred in trial 1 ($\delta = 0.48$ day^{-1}, period length $T = 2.67 \pm 0.18$ days, mean $\pm$ SD) and trial 2 ($\delta = 0.82$ day^{-1},$T = 1.81 \pm 0.09$ days). Directly after the perturbation, V_C increased by 33% within 0.87 days and by 94% within 1.20 days, respectively, in both trials. In trial 1, P remained at steady-state level for 1.20 days before it started to increase. In trial 2, P first decreased by 47% before it also increased after 1.20 days. V_B evolved in time according to the product of P and V_C. For instance, after the perturbation V_B in trial 2 remained around the steady-state level for 1.20 days since the increase in V_C compensated the decrease in P.

At the lower dilution rate, the oscillations were slower and the amplitude was higher (Fig. 3.3 a,c vs. Fig. 3.3 b,d). The bands in the size spectra showed how the periods of the oscillation are linked to the generation time: a cohort repetitively consists of small daughter cells becoming large mother cells that divide again into small daughter cells and so on. The increase in cell number was again higher because more cells entered mitosis at the same time compared to less synchronized conditions. This led to more pronounced ups and downs in the transient population dynamics and longer cycles. After the transient phase, P and V_B doubled approximately due to the doubling of N_i while V_C converged to the value before the change, or at least close to it (Fig. 3.3 a,b, Fig. 3.2, Tab. 1). The size spectrum resumed the dilution rate related characteristic shape prior to the change (Fig. 3.3 c,d, cf. Fig. 3.1). Simulation results of the mathematical model qualitatively corresponded to the observed behavior in trial 2 (Fig. 3.4a). After doubling N_i, P declined remarkably to approximately 60% of the steady-state value before. At the same time, the mean cell volume doubled and the daughter cells were significantly larger before their size converged to the characteristic steady-state value they showed before.

CHANGING THE DILUTION RATE In trials 3 to 5, δ was changed whereas N_i was kept constant. At $t = 34.00$ days, δ was increased from 0.21 to 0.51 day^{-1} in trial 3 and from 0.50 to 0.79 day^{-1} in trial 4, or reduced from 0.82 to 0.51 day^{-1} in trial 5 (Tab. 1). In analogy to the first series of experiments, changing δ resulted in transient dynamics of average population measures (Fig. 3.5) and demography (Fig. 3.6). After a more than twofold increase of δ in trial 3, distinct transient oscillations occurred, whereas the moderate increase of δ in trial 4 resulted in minor oscillations. No oscillations were detected in trial 5. In trial 3, δ was changed from a comparably low ($\delta = 0.21$ day^{-1}) to a moderate value ($\delta = 0.51$ day^{-1}). This resulted in damped oscillations of P, V_B and V_C (Fig. 3.5a, $T = 2.37 \pm 0.18$ days). While P (from $5.49 \cdot 10^6$ to $4.37 \cdot 10^6$ cells$\cdot$mL^{-1}) and V_B (from $5.50 \cdot 10^7$ to $4.63 \cdot 10^7$ μm$^3 \cdot$mL^{-1}) converged downwards to the new steady state

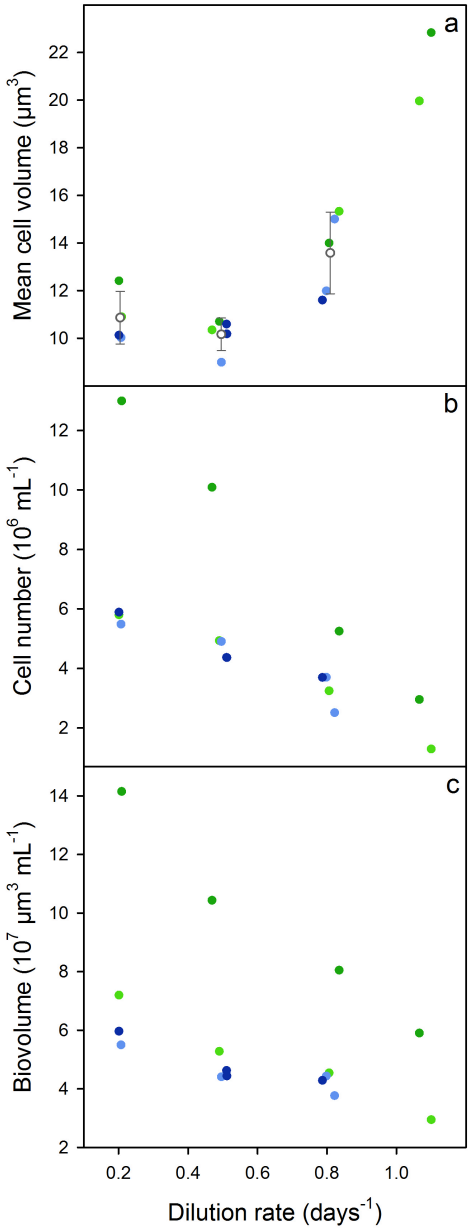

Figure 3.2: Steady-state values of the mean cell volume V_C (**a**), the cell number P (**b**), and the biovolume V_B (**c**) in relation to average value of the dilution rate δ in each cluster. Green dots refer to the first series of experiments (trial 1 and 2, doubling N_i), blue dots refer to second series of experiments (trial 3 to 5, changing δ). The values before the perturbation are light-colored, the ones after the perturbation are dark-colored. The gray circles in panel **a** give the average value of the mean cell volumes, error bars display the simple standard deviation. The average values of the mean cell volumes were calculated over 15 sampling points at steady state. Values of the dilution rates corresponded to these time intervals.

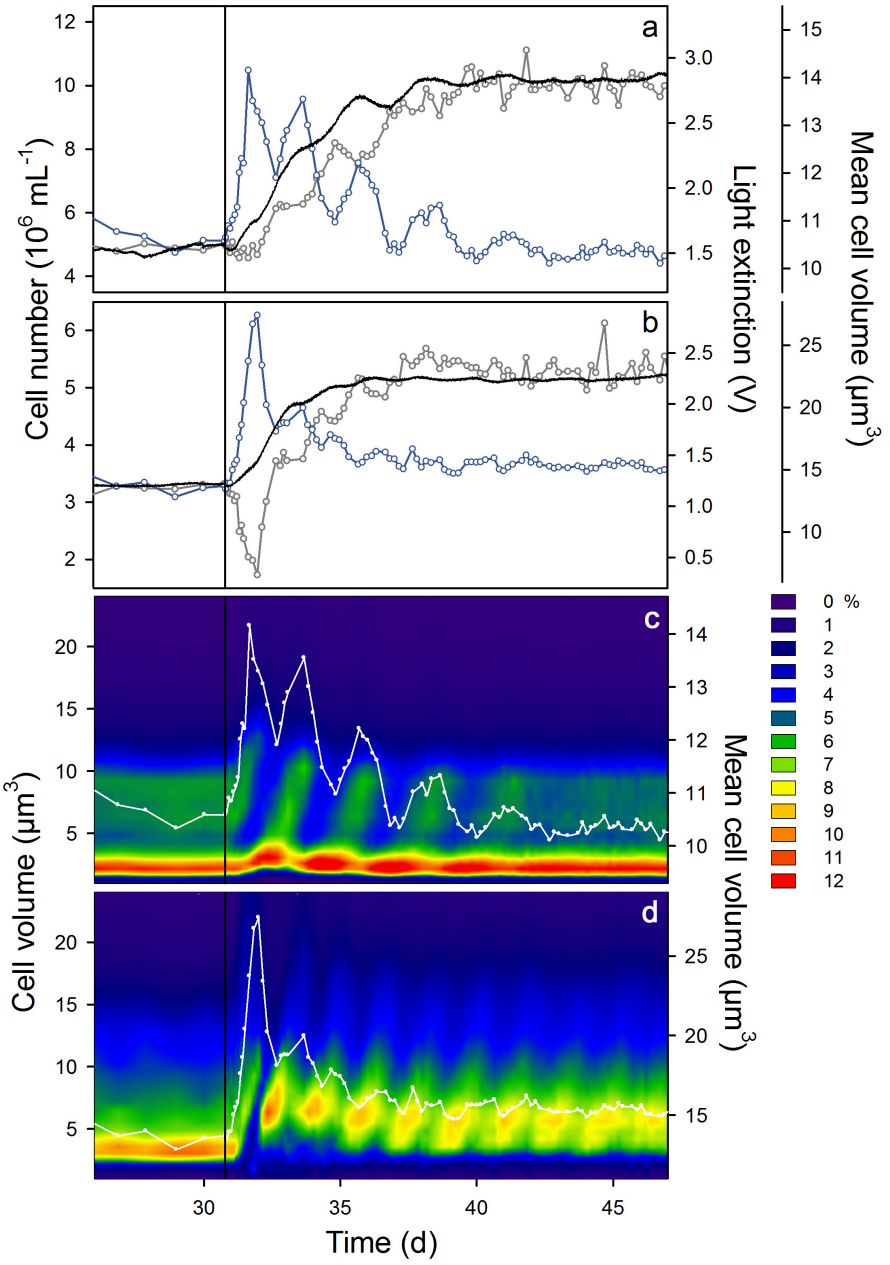

Figure 3.3: Panels **a** and **b** give the cell number (gray), the light extinction (black) and the mean cell volume (blue) in chemostat trials 1 and 2 that experienced a doubling of the nitrogen concentration from $N_i = 80$ µmol·L^{-1} to $N_i = 160$ µmol·L^{-1}; panels **c** and **d** show the corresponding size spectra and the mean cell volume (white line). Dilution rates were $\delta = 0.48$ day^{-1} (**a**,**c**) and $\delta = 0.82$ day^{-1} (**b**,**d**).

level, V_C oscillated approximately around the same value as before δ was changed ($\approx$ 10.5 µm^3). The size spectrum oscillated clearly showing repeating distinct bands from smaller to larger sized cells

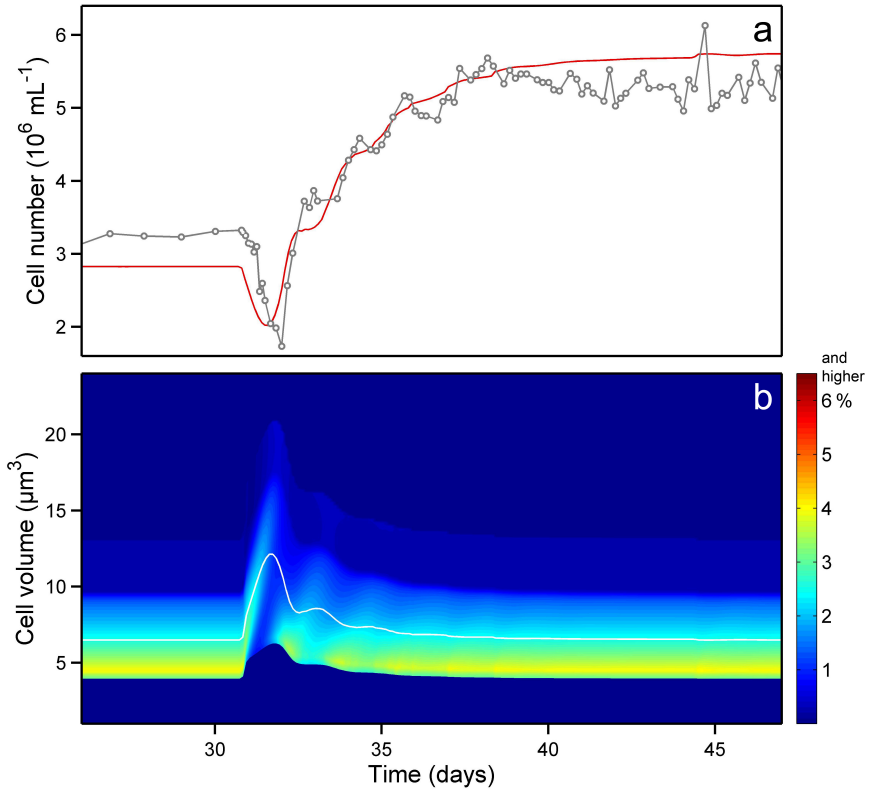

Figure 3.4: Qualitative agreement between experimental results of trial 2 and model simulations. The cell number of trail 2 (gray, c.f. Fig. 3.3b) was well-reproduced by simulation of the structured population model allowing for nitrogen-dependent cell size variability (red, **a**). Simulation results also confirmed the dynamic behavior of the size spectrum and the mean cell volume (white line) in trial 2 (**b**, c.f. Fig. 3.3d.

(Fig. 3.6a). Finally, it slowly converged to the shape characteristic for a dilution rate of about $\delta = 0.5$ day^{-1} (cf. Fig. 3.1a).

In trial 4, δ was changed from a moderate ($\delta = 0.50$ day^{-1}) to a comparably high value ($\delta = 0.79$ day^{-1}). Although δ was increased again, the average population measures showed nearly no (P, V_C) or only minor oscillations (V_B, Fig. 3.5b, $T = 1.52 \pm 0.25$ days). P (from $4.90{\cdot}10^6$ to $3.70{\cdot}10^6$ cells·mL^{-1}) and V_B (from $4.41{\cdot}10^7$ to $4.29{\cdot}10^7$ µm^3·mL^{-1}) converged downwards to the new steady state level. V_C increased from 9.0 ± 0.3 to 11.6 ± 0.3 µm^3. The size spectrum showed only minor oscillations and finally converged to the shape characteristic for a dilution rate of about $\delta = 0.8$ day^{-1} (Fig. 3.6b).

Trial 5 represents the opposite of trial 4: δ was changed from a comparably high ($\delta = 0.82$ day^{-1}) to a moderate value ($\delta = 0.51$ day^{-1}). The average population measures (Fig. 5c) as well as the size spectrum (Fig. 3.6c) did not show any oscillations related to the perturbation. The oscillations occurring after $t = 40.6$ days are due to a malfunction

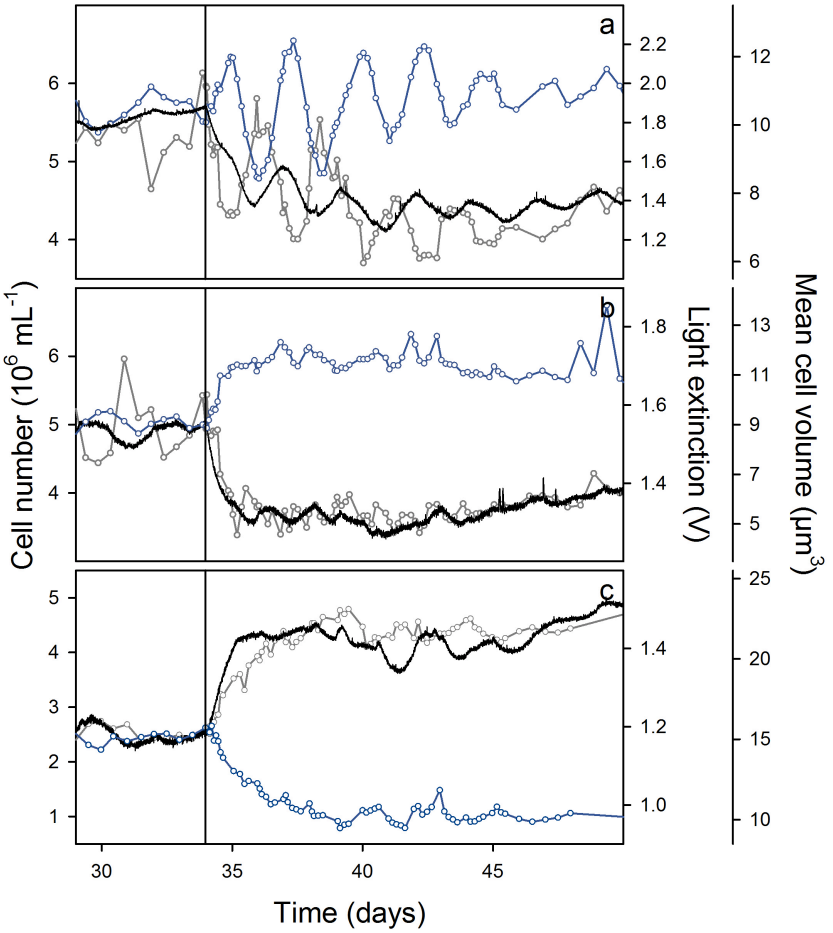

Figure 3.5: Cell number (gray), light extinction (black) and mean cell volume (blue) in chemostat trials 3 to 5 that experienced a change in dilution rate δ. Dilution rates were changed from $\delta = 0.21$ day^{-1} to $\delta = 0.51$ day^{-1} (**a**), $\delta = 0.50$ day^{-1} to $\delta = 0.79$ day^{-1} (**b**) and from $\delta = 0.82$ day^{-1} to $\delta = 0.51$ day^{-1} (**c**). The nitrogen concentration of the supply medium was constant at $N_i = 80$ µmol·L^{-1}.

of the pump that perturbed the population structure. Until that point in time, P (from $2.51{\cdot}10^6$ to $4.36{\cdot}10^6$ cells·mL^{-1}), V_B (from $3.77{\cdot}10^7$ to $4.44{\cdot}10^7$ µm^3·mL^{-1}), and V_C (from 15.0 ± 0.3 to 10.2 ± 0.4 µm^3) smoothly transitioned to values characteristic for a dilution rate of about $\delta = 0.5$ day^{-1} (Fig. 3.6b).

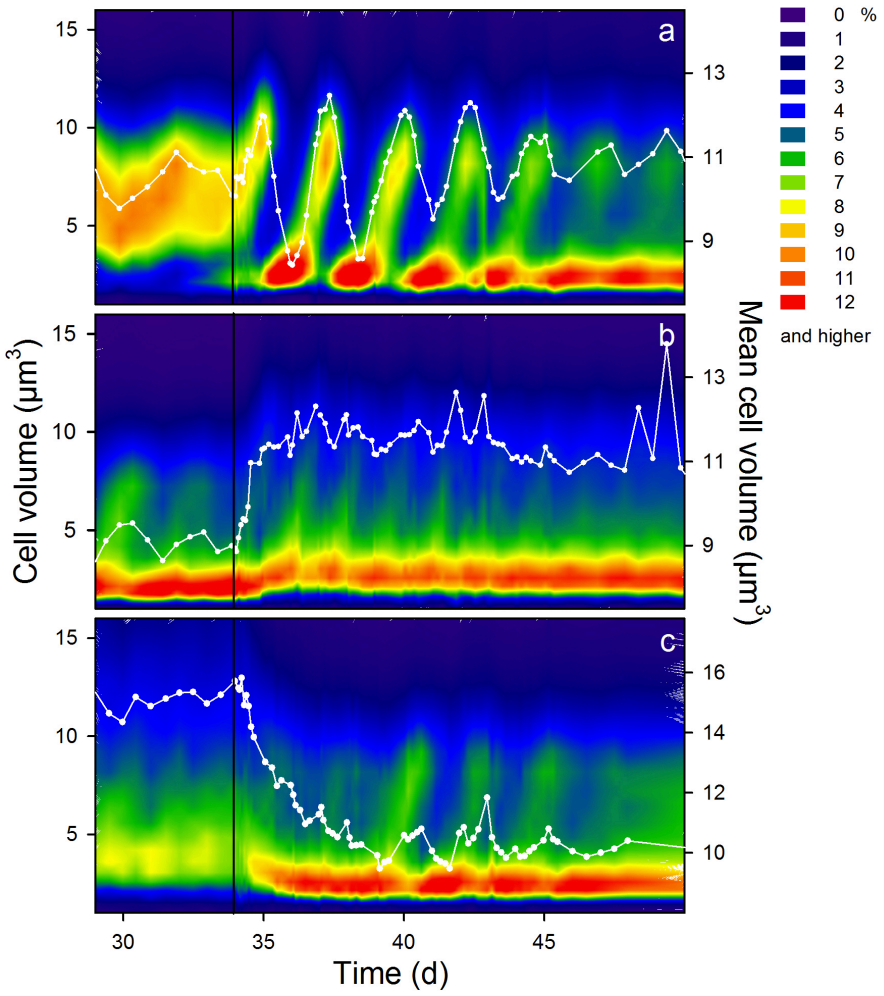

Figure 3.6: Size distribution and mean cell volume (white) of chemostat trials 3 to 5 that experienced a change in dilution rate δ. Dilution rates were changed from $\delta = 0.21$ day^{-1} to $\delta = 0.51$ day^{-1} (**a**), $\delta = 0.50$ day^{-1} to $\delta = 0.79$ day^{-1} (**b**) and from $\delta = 0.82$ day^{-1} to $\delta = 0.51$ day^{-1} (**c**). The nitrogen concentration of the supply medium was constant at $N_i = 80$ µmol·L^{-1}.

3.5 DISCUSSION

Population dynamics are determined by numerous biotic and abiotic factors differently impacting the developmental stages of individuals within a population. Growth and death rates originating from the interaction between organisms and their environment are unequally distributed over an organism's life cycle. Hence, the environment defines the shape of the population's stage distribution – its demographic structure that all potential dynamics go back to. In a constant environment, populations will adapt to the prevailing conditions to

Table 3.1: Nitrogen concentration of the supply medium, N_i, the dilution rate, δ, and the steady-state values of the cell number, P, the biovolume, V_B, and the mean cell volume, V_C, values in the two series of chemostat experiments. The period length T refers to the oscillations occurring after the chemostat system was perturbated. The overall dilution rate gives the average dilution rate over the total time of an experiment. In the first series of experiments (trial 1 and 2), N_i was doubled from 80 to 160 $\mu mol \cdot L^{-1}$ while δ remained constant. In the second series (trial 3 to 5), δ was altered while N_i remained constant. The terms "before" and "after" refer to the phases before and after perturbation at $t = 30.8$ days.

Trial	N_i			δ		P		V_B		$V_C \pm SD$		$T \pm SD$
#	($\mu mol \cdot L^{-1}$)			(day^{-1})		(10^6 cells$\cdot mL^{-1}$)		(10^7 $\mu m^3 \cdot mL^{-1}$)		(μm^3)		(days)
	before	after	overall	before	after	before	after	before	after	before	after	before
1	80	160	0.48	0.49	0.47	4.93	10.09	5.28	10.44	10.7 ± 0.3	10.4 ± 0.2	2.67 ± 0.18
2	80	160	0.82	0.81	0.84	3.24	5.25	4.54	8.05	14.1 ± 0.6	15.3 ± 0.3	1.81 ± 0.09
3	80	80	—	0.21	0.51	5.49	4.37	5.50	4.63	10.4 ± 0.5	10.6 ± 0.4	2.37 ± 0.18
4	80	80	—	0.50	0.70	4.90	3.70	4.41	4.29	9.0 ± 0.3	11.6 ± 0.3	1.52 ± 0.25
5	80	80	—	0.82	0.52	2.51	4.36	3.77	4.44	15.0 ± 0.3	10.2 ± 0.4	—

finally show a characteristic demographic distribution as it was also found in our experiments (Fig. 3.1).

Resource shortage is one of the most important factors influencing organismal processes. In our case, nitrogen was the essential resource limiting the maturation velocity by which the Chlorella cells progress through the first stage (G_1-phase) of their life cycle. This led to the hypothesis that the number of cells inside and outside of the G_1-phase can be predicted from the availability of nitrogen. Making the simplistic, but reasonable assumption that developmental progression is correlated with cell size (early developmental stages are represented by small cell sizes and vice versa, c.f. [93]) our results accurately match this prediction. The frequency distribution of cell volumes was consistently closely related to the chemostat's dilution rate δ at steady state (e.g. Fig. 3.1, Fig. 3.3, and Fig. 3.6). While moderate values of δ resulted in the dominance of small cells ($\delta = 0.49$ day^{-1} in Fig. 3.1 a,b and $\delta = 0.82$ day^{-1} in Fig. 3.1 c,d), distinctly less cells accumulated in this size interval at a high value of δ ($\delta = 1.09$ day^{-1} in Fig. 3.1 e,f). That is, cells progressed comparatively slower through their life cycle at low δ because the low ambient nitrogen concentration hampered a transition from the G_1-phase to the S-phase. The resulting formation of a cohort (principally consisting of small daughter cells) and its size are directly related to the degree of synchrony [93]. In addition to the developmental stage, the cell size also varied with the availability of nitrogen determined by δ. The mean cell volume at steady state clearly increased with increasing δ (Fig. 3.2a) supporting the model assumption that cells increase in size when taking up surplus nitrogen.

However, constant environmental conditions are rare in natural systems and always a matter of scale. Thus, most natural populations experience an environment that is characterized by fluctuations and transitions. Here, we experimentally imposed changes of environmental conditions by altering the nitrogen supply concentration, N_i, and δ, i.e. the parameters reflecting fundamental growth conditions of natural populations (resource supply and mortality). In four of the five trials, oscillations in cell number P, biovolume V_B, mean cell volume V_C, and size spectra characterized the transient behavior. Independent of which parameter was altered the oscillations showed larger amplitudes and longer periods the lower δ was before the conditions changed. This originates from the steady-state results described above. The frequency distributions of the size spectra revealed that in trial 1 ($\delta = 0.48$ day^{-1}, Fig. 3.3 a,c) more cells accumulated in the small size range than in trial 2 ($\delta = 0.82$ day^{-1}, Fig. 3.3 b,d) and strong oscillations resulted from a large cohort within the population. The high degree of synchrony arose from the strong limitation due to low δ. Thus, the oscillations in trial 1 were significantly stronger than in trial 2 since the traveling cohort in trial 1 proportionally consisted of more cells.

The dependence of the population dynamical response on the original environmental conditions becomes even clearer when comparing trial 3 and 5 in the second series of experiments. Although experiencing almost identical environmental conditions ($\delta \approx 0.5$ day^{-1}), the oscillations are stronger when coming from $\delta = 0.21$ day^{-1} (Fig. 3.5a, Fig. 3.6a) than when coming from $\delta = 0.82$ day^{-1} (Fig. 3.5c, Fig. 3.6c). This is again explicable by the stronger resource limitation, and thus synchronization at lower δ. In addition, although the dilution rate in trial 3 was increased by the same absolute value as in trial 4 ($\Delta\delta \approx 0.30$ day^{-1}), the oscillations were distinctly stronger in trial 3 since δ was lower before it changed.

Similar processes can be found in natural populations as well. Fishing, for instance, can be considered as density-independent mortality, as imposed by δ in a chemostat. It altered the demographic structure of fish stocks (mainly by truncating the size and age structure, [72, 88]) and thereby increased the population dynamical variability [68, 3]. In principle, this agrees with the dynamical behavior of our experimental Chlorella populations: altering demography led to changes in specific cohort properties and, thus generated fluctuations that increased variability.

In addition to the transient oscillations arising from demographic processes, counter-intuitive behavior of P was observed when N_i was doubled. Actually, populations are supposed to grow when resource concentrations ameliorate. This was true for V_B that immediately increased towards the new steady-state value defined by N_i (determining the carrying capacity) which is in accordance with simple, non-structured models. Surprisingly, however, after doubling N_i in trial 2, P decreased considerably to about 50% of the previous steady-state value (Fig. 3.3b) and increased again after 1.2 days. In contrast, the mean cell volume escalated to twice the value prior to the change of N_i. This supports our hypothesis that V_C increases when surplus nitrogen is available. As N_i was doubled, more nitrogen entered the system and the cells were able to take up the surplus nitrogen. Thus, the majority of the cells grew in size but did not proliferate immediately. That is, the time necessary to complete one cell cycle was prolonged compared to the previous steady-state conditions causing a decline in P due to the washout by δ. This effect was less pronounced in trial 1 since δ was lower and comparably less nutrients per unit time entered the chemostat. As a result, P increased in size merely by about 30% and the cell cycle was not substantially prolonged.

An alternative explanation for the cells growing larger might be the formation of more rather than larger daughter cells. However, we reject it for the following reason: If more daughter cells would have been formed, the cell size of the daughter cells should have been at a fixed starting value. That is, the bands of the size spectra should have always started at a cell volume of approximately 3 μm^3.

However, this is not consistent with our observations. In fact, the first generation of daughter cells occurring directly after N_i was doubled showed a distinctly higher cell volume ($\approx 6\ \mu m^3$, Fig. 3.3d). The band was clearly shifted towards higher cell volumes. This shift lasted for another generation before the minimum cell size converged to the original value of $3\ \mu m^3$ indicating that the released daughter cells had again started at a volume of $3\ \mu m^3$.

In addition to the different experimental findings complementing each other, the reliability of the hypothesized mechanism is strongly supported by the simulation results of our model. By implementing nitrogen-dependent cell size variability into the model by Massie et al. (2010) [93], we were able to imitate the two distinct dynamical features in the time series of trial 2: the temporary decrease of P (Fig. 3.5a) and the increasing size of the daughter cells (Fig. 3.5b) directly after the doubling of N_i. We also ran simulations with a model that accounted for division into more rather than larger daughter cells. The population dynamics were qualitatively the same, but we rejected this mechanism since it failed to explain the occurrence of larger daughter cells as observed in our experiments. Here, it is worth mentioning that we explicitly account for two reasonable mechanisms leading to a lagged growth response instead of just implementing a time lag into the functional response equation. Models that are solely describing overall measures of population dynamics would not lead to an adequate description of the processes leading to the dynamics we observed and would also fail to explain the discrepancy in the behavior of P, V_B, and V_C after N_i was doubled.

In chemostat systems, N_i represents the carrying capacity defining the maximum biomass or number of individuals, respectively, the system is able support. Thus, permanent changes of N_i are not equivalent to resource pulses producing temporary perturbations as it was investigated in other studies (e.g. [20]). Rather, lasting changes of N_i alter the long-term growth conditions populations have to cope with. In line with our findings there is evidence that resource shortage altered the demographic structure and synchronized plant populations also in terrestrial systems causing oscillations in numbers after the conditions ameliorated [56].

Transient dynamics become even more complex when other mechanisms come into play than those related to the shape of the demographic distribution. In our study, the Chlorella population stopped growing when the environmental conditions ameliorated (doubling of N_i). That is, not resource shortage but surplus amounts of it had temporarily a negative effect on the density of the population. This counter-intuitive effect is relevant for organisms showing plasticity in their life cycle: the generation time is prolonged by using the resource surplus to improve individual constitution. Synchronization leads to a temporary delay of population growth until the individuals start

reproducing again. Delaying reproduction implies the risk of mortality prior to reproduction. But at the same time, it can significantly increase individual fitness since they are able avoid predation when growing distinctly larger. Additionally, larger individuals will have larger and/or more offspring and may face a lower risk of extinction and starvation. Thus, this mechanism is a common life history feature and therefore expected to play a critical role in the response behavior of organisms when environmental conditions change.

Our study demonstrates the eminent influence of the environment on a population's demography and the consequences for the population dynamics arising from it. We achieved a remarkable reliability in identifying the mechanistic interplay between population dynamics and demography using large populations ($> 10^9$ cells·L^{-1}) of small organisms with short generation times. Highly controllable chemostats and advanced measurement techniques enabled an exceptional high temporal resolution combined with mathematical modeling. Corresponding to a memory effect, the future dynamics crucially depend on the past demographic state that was determined by the environment. That is, the same future state may be approached via different transients dependent on the demographic state in the past (cf. trial 3 and 5). The change-induced variability in the transient dynamics was high when arising from population synchrony caused by resource shortage at low turn-over rates. But even high-turnover rates increased variability by significantly impacting life cycle plasticity. Thus, to make any predictions about transient dynamics which are the rule rather than the exception in natural populations, identifying the acting mechanisms is a paramount requirement.

4

ENHANCED MORAN-EFFECT

by Thomas M. Massie, Nina Kuckänder, Ursula Gaedke, Guntram Weithoff, and Bernd Blasius

The manuscript is submitted to *Nature* as

Massie, T.M.[1], N. Kuckänder[2], U. Gaedke[1], G. Weithoff[1], and B. Blasius[3] (submitted) *Enhanced Moran effect in autocorrelated environments.*

[1] Institute of Biochemistry & Biology, University of Potsdam, Maulbeeralle 2, 14467 Potsdam, Germany
[2] Ecologic Institute, Pfalzburger Strasse 43/44, D-10717 Berlin, Germany
[3] Institute for Chemistry and Biology of the Marine Environment, Carl von Ossietzky University, 26111 Oldenburg, Germany

4.1 ABSTRACT

The response of biological populations to stochastic variations in their environment is a central issue in population ecology. Spatial correlations in environmental stochasticity can synchronise populations over wide areas, a fact that is known as Moran effect. Field observations and theoretical investigations suggest that the correlations of the populations must remain smaller than that of the stochastic fluctuations. However, not much is known about the Moran effect when the environmental variations are temporally correlated. Here, we perform chemostat experiments to investigate the response of phytoplankton populations to autocorrelated stochastic influcence. We show that, in contrast to naïve expectation, two uncoupled populations can be more strongly correlated than their common stochastic forcing, if the two noises differ in noise colour. Using linear theory we are able to provide analytical estimates for this correlation enhancement. Our numerical simulations show that this pattern is robust to variations in population dynamics and noise spectra. Our findings suggest that noise induced synchrony (i.e., the Moran effect) may play a larger role for population dynamics than previously thought.

4.2 INTRODUCTION

For long times ecologists have been interested in studying population fluctuations and their remarkable synchronization over wide geographical areas [69, 12, 18, 86]. Understanding the causes and mechanisms underlying spatial synchrony has become a key issue in population ecology, not least because of its intimate relation to the extinction risk in meta-populations [59, 65, 115, 40, 43]. Several mechanisms for explaining population synchrony have been put forward [12, 86], such as dispersal between populations [121, 15] or spatially extended trophic interaction (e.g., mobile predators of widespread range) [106]. However these explanations are not applicable in situations where dispersal is excluded, such as for Soay sheep populations on separate islands [54, 14]. Another explanation, which does not require direct interactions by dispersal, is synchronization through spatially correlated environmental influences (Moran effect) [100, 130]. Moran (1953) [100] suggested that spatially separated populations, which are regulated by the same density-dependent structure, will tend to fluctuate in synchrony if they are exposed to similar environmental variation. In particular, Moran pointed out that in the special case of linear density-dependence the cross-correlation r between the regional populations will be identical to that of the environment, $r = r_p$. This statement came to be known as Moran theorem [130]. Given that climatic fluctuations can be spatially correlated over large distances, the Moran effect has found a growing recognition as a major driver for generating population synchrony.

The Moran effect has been confirmed in field observations [54, 119, 47, 77, 147, 23, 81, 45] and in laboratory experiments [8, 9, 46, 143]. The Moran theorem also received considerable theoretical attention and was generalised to include nonlinear density dependence [122, 54, 14, 52, 44, 131, 1], non-identical populations [113, 125, 44, 131, 70], the influence of dispersal [124, 80, 113, 1], cyclic populations [11, 24, 13, 143, 84], species interactions [128, 143]?, and various combinations of these factors. In all these theoretical, experimental, and field studies it was found that the correlation of independent populations that are not coupled by dispersal remains bound by the environmental correlation, $r \leqslant r_p$, which potentially set limits to the role of the Moran effect as a driver of population synchrony.

In this Letter we show that the correlation between two non-interacting populations can exceed that of their environmental forcing, if the fluctuations of the environment are differently auto-correlated in time. Temporal autocorrelation refers to the relationship between successive observations in a time series and it is often referred to by its effect on the noise colour (i.e., the frequency composition in the power spectrum of a time-series) [57]. A noisy signal is said to be 'white' if it has a flat spectrum so that no frequency dominates. In this case, successive

noise values are unrelated. In contrast, red noise indicates positive temporal autocorrelation, that is successive noise values are more similar than expected by chance. Time series with positive autocorrelation are dominated by low-frequency fluctuations, and are referred to as 'red' noise by analogy to the frequency composition of red light.

Temporally autocorrelated ('coloured') noise is increasingly recognised as an important characteristics of environmental variability [133, 126, 73, 144]. Many signals in nature, such as climate variables or population densities [118], are known to exhibit positive autocorrelations. The exact nature of the environmental noise is important for population dynamics [114] and can be crucial for population persistence [127, 115, 64, 32, 151]. However, the effect of coloured noise on population synchrony has only been rarely addressed. The Moran effect and population synchrony of under the influence of autocorrelated noise was investigated [64, 142, 87]. It was found that the noise colour has a major influence on population synchrony. In particular, reddened environmental noise is able to intensify spatial synchrony in spatially heterogeneous populations.

These few studies on the Moran effect with autocorrelated noise considered identical noise colours in the two populations. The autocorrelation parameters can vary between different measured data sources and geographic location [34, 48]. Steele suggested in 1985 that terrestrial noise should be white, while marine noise should be reddened [133]. Here we show that the Moran effect is enhanced if the noise colour between the two population differs. In this case it is possible that the cross-correlation between the two noises can be enhanced by the population dynamics. Thus our major finding is the counter-intuitive result that in auto-correlated environments, the correlation between the populations can be larger than that of the environment.

To test these ideas in experiments with living organisms under well defined conditions we performed experiments with chemostat systems containing isolated populations of the green algae *Chlorella vulgaris* (Chlorococcales). We investigated the population dynamics of two uncoupled isolated populations, A and B, that experience correlated environmental stochasticity (Fig. 4.1). We imposed environmental variation on chemostat populations by altering the dilution rates, $\delta_A(t)$, $\delta_B(t)$. Dilution rates changed in defined intervals (Δt) of one or two hours and were cross-correlated by $r = C(\delta_A, \delta_B)$. This stochastically correlated forcing was the only way in which the two systems were coupled. Using light extinction as a proxy of algal biomass [93] allowed us to measure population densities with an unusually high temporal resolution of five minute intervals. As shown in Fig. 4.1, the two populations responded to the stochastic forcing with fluctations that were cross-correlated by $r = C(\delta_A, \delta_B)$. This population correlation, in general, was different to the correlation of the input signals. Thus,

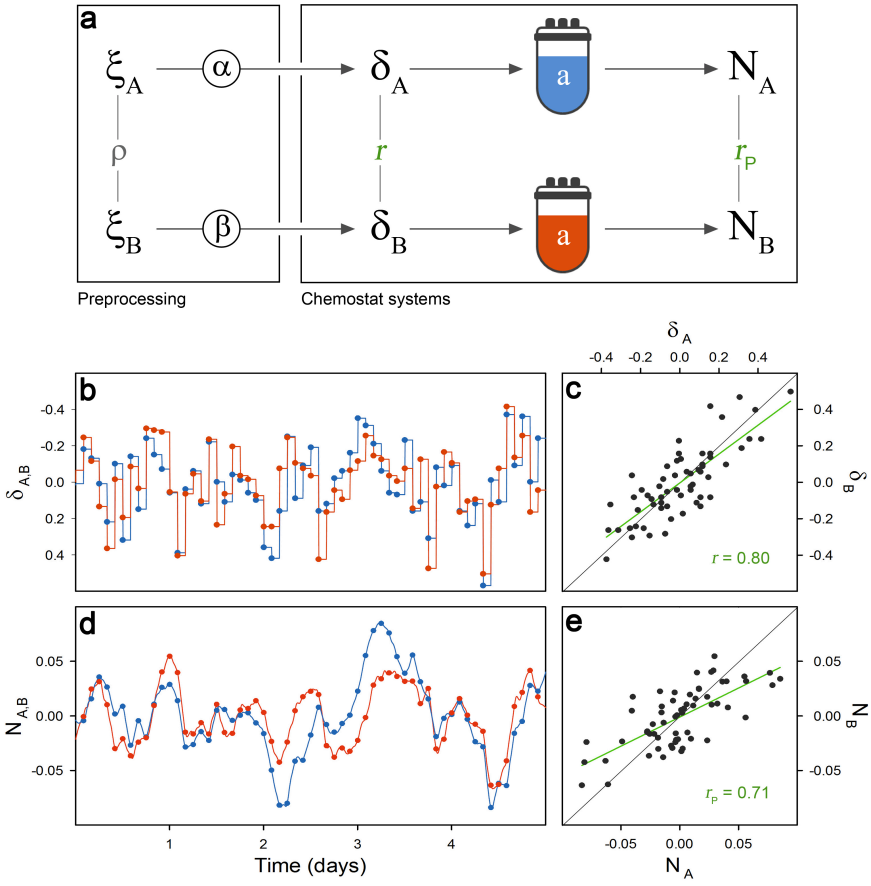

Figure 4.1: Noise induced synchronization in two independent populations. **a**, Experimental set-up to explore the response of two populations A and B to correlated stochastic forcing, realized as chemostat systems of *Chlorella vulgaris*. The two systems are coupled only by their correlated noise input, which is generated by data-preprocessing. For each system, Gaussian distributed white noises, $\xi_A(t)$ and $\xi_B(t)$, are generated that are cross-correlated by $\rho = C(\xi_A, \xi_B)$. To implement temporal structure, the generating noises are filtered through an autoregressive AR(1) process with autocorrelation parameters α and β, respectively. The resulting time series determine the experimental dilution rates ($\delta_A(t)$, $\delta_B(t)$) in defined time intervals Δt and are cross-correlated by $r = C(\delta_A, \delta_B)$. The correlation between chemostat population densities $N_A(t)$ and $N_B(t)$ is then measured by $r_p = C(N_A, N_B)$. **b-e**Typical population response (here shown for the case of two identical populations and white noise, $\alpha = \beta = 0$). **b**, Normalized dilution rates $\delta_A(t)$ and $\delta_B(t)$ and **d**, normalized population densities $N_A(t)$ and $N_B(t)$ of system A (blue) and system B (red). Circles indicate the respective values at the time instances when dilution rates were set to a new value. Further shown is the pairwise correlation (black circles) and the regression line (green) of normalized dilution rates $r = 0.80$ **c**) and population densities $r_p = 0.71$ **e**). For illustration the diagonal is indicated as black line.

the experimental set-up allowed us to test the Moran effect in a well-controlled laboratory system.

4.3 RESULTS

We present results from three different experimental scenarios, where we investigated the response of uncoupled populations to correlated stochastic forcing. In the first scenario we tested whether identical populations would follow the behaviour as expected from the Moran theorem. For this we parameterised both chemostat systems to be identical, i.e., the average dilution rates $\langle \delta_A \rangle = \langle \delta_B \rangle = 0.75$ day^{-1} and the nitrogen supply concentrations $N_A = N_B = 80$ µmol·L^{-1} were chosen to have the same value for both systems (parameter values are shown in Table 1). In six consecutive runs, the population experienced white noise with standard deviation $\sigma = 0.2$ that was cross-correlated between the two populations with coefficients r of approximately 0.8, 0.2, 0.6, 0.0, 0.4 and 1.0 (for exact values see Table 1). The populations responded to the stochastic forcing with correlated population dynamics, with cross-correlations that correspond to that of the environmental forcing, $r_p \approx r$ (see Fig. 4.2a, and Fig. 2.1, Appendix). These results agree with the prediction from the Moran theorem and confirm the hypothesis that correlated stochastic forcing can synchronise the dynamics of non-interacting populations.

In the second scenario we tested whether stochastic forcing is able to synchronise populations that differ in key ecological properties, such as turn-over rate (dilution) and carrying capacity (nitrogen supply). For this we adjusted the two systems to differ in average dilution rate $\langle \delta_A \rangle = 0.75$ day^{-1}, $\langle \delta_B \rangle = 0.40$ day^{-1} and nitrogen supply concentration $N_i = 80$ µmol·L^{-1}, $N_i = 40$ µmol·L^{-1}. Additionally, we reduced the standard deviation of the input noises in both systems to $\sigma = 0.15$, to avoid negative values of dilution rates. Again, the cross-correlation coefficients were approximately 0.8, 0.2, 0.6, 0.0, 0.4 and 1.0 (for exact values see Table. 3). In our experiments we observed that stochastic forcing is able to synchronise even populations with non-identical population parameters (Fig. 4.2b, Fig. 2.1, Appendix). However, the cross-correlation of population density, was systematically smaller than that of the environmental driving, $r_p < r$. This finding confirms results from field-studies [113], and theoretical studies [125, 44, 131, 70].

In the third scenario we tested the response of two identical populations under the influence of differently autocorrelated noise. In theory (see methods) this would allow for an enhancement of the input noise correlations. We performed experiments, where the two populations were adjusted to have identical conditions, with average dilution rates $\langle \delta_A \rangle = \langle \delta_B \rangle = 0.75$ day^{-1} and nitrogen supply concentrations $N_A = 80$ µmol·L^{-1}. However, in contrast to the previous

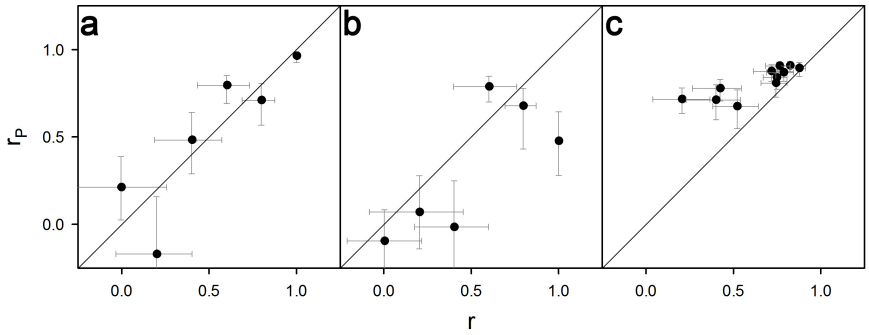

Figure 4.2: Moran effect in different experimental treatments. Population correlation r_p in dependence of the environmental correlation r (black circles). **a**, Identical systems, white noise: the correlation of the population equals that of the environment $r_p = r$ (Moran theorem). **b**, Non-identical systems, white noise: the population correlation is smaller than the environmental correlation $r_p \leqslant r$. **c**, Identical populations, differently autocorrelated noise: Even though the two populations are non-interacting, the correlation of the populations exceeds that of the environment $r_p > r$ (correlation enhancement). Error bars show 95% confidence intervals from a sample of $10,000$ noise replicates (r), and from resampling measured correlations by bootstrapping (r_p). The black lines indicate the expected outcome of the Moran theorem $r_p = r$.

scenarios, we implemented temporal autocorrelations (noise color) in the time series of dilution rates (see methods). We performed a series of 15 experimental runs, each representing a combination of differing autocorrelation parameters α and β roughly adjusted within the range $[0, 0.9]$ (see Table 2.3).

In our experiments we observed that in autocorrelated environments the correlation of the populations can significantly exceed that of the environmental shocks (Fig. 4.2c). To compare this experimental finding with theoretical expectations in Fig. 4.3 we plot the correlation enhancement factor r_p/r as a function of the realised noise correlation r and the difference in autocorrelation parameters $\alpha - \beta$. A value of $r_p/r = 1$ (solid line in Fig. 4.3) would correspond to the expectation from the Moran theorem. However the experimental findings demonstrate that, in contrast to the naïve expectation, the input correlation of the environmental fluctuations is amplified by the population dynamics, with a factor of more than 300% for large difference in autocorrelation parameters.

This finding is confirmed by theoretical analysis. Linear theory (see methods) allows to calculate the correlation enhancement for linear population demography (Eq. 4.1). Expansion of this result for small values of a and differences in autocorrelation $|\beta - \alpha|$ yields

$$\frac{r_p}{r} \approx 1 + \frac{1}{2} a^2 (\beta - \alpha)^2 \,. \tag{4.1}$$

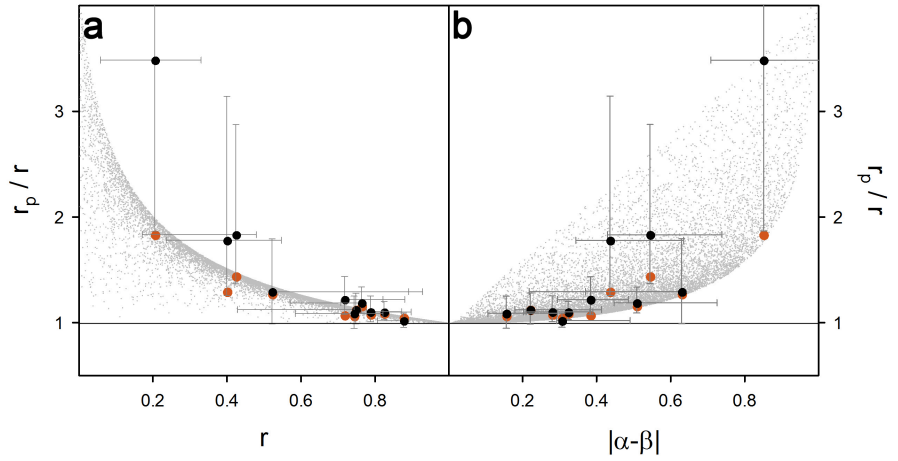

Figure 4.3: Correlation enhancement in differently autocorrelated environments. Correlation enhancement factor r_p/r (black circles) as a function of (**a**) the environmental correlation $r(\alpha, \beta)$ and (**b**) the difference in autocorrelation parameters $|\alpha - \beta|$. Red circles show the theoretically expected enhancement factor (Eq. 4.1) for the respective, experimentally realized parameter combination (r, α, β). Grey dots show simulated enhancement factors for 20,000 randomly chosen autocorrelation parameters α and β, taken from a uniform distribution in the range $[0, 1]$. Error bars show 95% confidence intervals from a sample of 10,000 noise replicates (r, and $|\alpha - \beta|$), and from resampling measured correlations by bootstrapping (r_p/r). The horizontal lines $r_p/r = 1$ indicate the expected outcome according to the Moran theorem.

The amplification factor r_p/r scales quadratically with both the difference $\alpha - \beta$ of the autocorrelation parameters and the population dynamics parameter a. Thus, in identical linear systems the correlation of the population can be larger than that of the oscillations, $r_p \geqslant r$. Correlation enhancement arises if the noise colour differs between the two populations. If both autocorrelation parameters are equal, $\alpha = \beta$, the Moran effect $r_p = r$ is reproduced. Further, the correlation enhancement is most pronounced for more unstable systems $a \approx 1$. These results are confirmed by the experimental findings (Fig. 4.3). Interestingly, in general the experiments showed even larger correlation enhancement than predicted from linear theory. Numerical simulations showed that these results are robust.

4.4 DISCUSSION

How can this counter-intuitive behaviour be explained? Based on fundamental information theoretic concepts the mutual information between two non-interacting systems cannot increase. Thus, the mutual information between the population densities $\{N_A(t), N_B(t)\}$

cannot exceed the mutual information between the driving signals $\{\delta_A(t), \delta_B(t)\}$. However this does not apply to the linear (Pearson) cross-correlations coefficient, which does not capture the full statistical interdependence of two signals. The common praxis in ecological field studies is to investigate the cross-correlation coefficients, which thus yields a restricted insight into time series. The cross-correlation coefficient evaluates the signal values in both systems at the same times, while the full linear relationship between two signals is coded in the cross-correlation function, or equivalently the cross-spectrum [25]. In autocorrelated signals with $\alpha \neq \beta$ the cross-correlation is distributed differently in the frequency components of the noises. In other words, some mutual interdependence that is implemented in the signals can not be detected by means of the cross-correlation coefficient. This is evident, for example, in the reduced correlation r of autocorrelated dilution rates compared to the larger correlation of the white generating noises, ρ (Fig. 4.1a). This hidden correlation can however be unmasked, when it is imposed on a population that effectively responds as a low-pass filter (see appendix) which finally leads to the correlation enhancement.

Our findings may have widespread importance for the investigation of field data, where autocorrelated time series are abundant. Finally, the reported mechanism is not restricted to ecology. Similar correlation enhancement should play an important role also in other systems, such as correlated firing in populations of neurons [35].

4.5 METHODS

DATA ANALYSIS Population synchrony is measured as Pearson's correlation coefficient

$$r = C(x(t), y(t)) = \frac{\langle x(t)y(t)\rangle - \langle x(t)\rangle\langle y(t)\rangle}{\sqrt{\langle x(t)^2\rangle - \langle x(t)\rangle^2}\sqrt{\langle y(t)^2\rangle - \langle y(t)\rangle^2}}.$$

NOISE GENERATION We generate spatially and temporally correlated noise using a two-step data preprocessing (see Fig. 4.1). First, we implement generating noises $\xi_A(t)$ and $\xi_B(t)$ at discrete times $t = 0, \ldots n$. They are drawn from a bivariate Gaussian distribution with correlation coefficient $C(\xi_A(t), \xi_B(t)) = \rho$, zero mean and variance σ^2. This is realised as a linear superposition $\xi_A(t) = \sigma\zeta(t)$ and $\xi_B(t) = \rho\xi_A(t) + \sigma\sqrt{(1-\rho^2)}\zeta'(t)$ of independent Gaussian white noise sources $\zeta(t)$ and $\zeta'(t)$. Note, that the generating noises are introduced for computational convenience and bear no ecological meaning.

Next, we introduce temporal structure into the cross-correlated generating noises to generate the actual environmental noise that is acting on the two populations, $\delta_A(t)$ and $\delta_B(t)$. Several approaches have been put forward how autocorrelated time series can be modeled

[130, 126, 32, 125, 25, 151, 53]. Here, we use a first-order autoregressive AR(1) process with autocorrelation parameters $\alpha, \beta < 1$

$$\begin{aligned} \delta_A(t+1) &= \alpha\, \delta_A(t) + \xi_A(t), \\ \delta_B(t+1) &= \beta\, \delta_B(t) + \xi_B(t). \end{aligned} \tag{4.2}$$

Assuming stationarity, $\delta_A(t)$ and $\delta_B(t)$ are correlated by [18, 125, 70, 131]

$$r = C(\delta_A(t), \delta_B(t)) = \rho \frac{\sqrt{1-\beta^2}\sqrt{1-\alpha^2}}{1-\alpha\beta}. \tag{4.3}$$

Note, that the correlation of the environmental processes will always be smaller than or equal to the correlation of the generating noise, $r \leqslant \rho$. In experiments without autocorrelation we set $\alpha = \beta = 0$ so that $r = \rho$.

MORAN EFFECT We model the population dynamics of population densities by an AR(1) process

$$\begin{aligned} N_A(t+1) &= a N_A(t) + \delta_A(t) \\ N_B(t+1) &= a N_B(t) + \delta_B(t)\,, \end{aligned} \tag{4.4}$$

where $N_A(t), N_B(t)$ are the population densities at time t and the noise terms $\delta_A(t), \delta_B(t)$ are taken from Eq. (4.2) and $|a| < 1$ so that the process (4.4) is stationary. The variance and the first joint moment of the two AR(1) processes can be calculated [126, 125, 128]

$$\begin{aligned} \langle N_A(t)^2 \rangle &= \frac{(1+a\alpha)}{(1-a^2)(1-a\alpha)} \langle \delta_A(t)^2 \rangle, \\ \langle N_A(t) N_B(t) \rangle &= \frac{(1-a^2\alpha\beta)}{(1-a^2)(1-a\beta)(1-a\alpha)} \langle \delta_A(t)\delta_B(t) \rangle. \end{aligned}$$

Assuming stationarity, the correlation coefficient of two AR(1) processes computes to

$$r_p = r \frac{1-a^2\alpha\beta}{\sqrt{(1-a^2\beta^2)(1-a^2\alpha^2)}}. \tag{4.5}$$

If the autocorrelation parameters differ, $\alpha \neq \beta$, the correlation between the two uncoupled populations is always larger than the correlation of the noise inputs $r_p \geqslant r$, while for identical autocorrelation $\alpha = \beta$ the Moran theorem is reproduced, $r_p = r$.

CHEMOSTAT SETUP We established monoclonal batch cultures of the green algae C. *vulgaris* (Chlorococcales) that were kept in a climate chamber at $23.3° \pm 0.4°$C and constant fluorescent illumination at 110 $\mu E \cdot m^{-2} \cdot s^{-1}$ (preventing synchronization by light-dark cycles). The batch cultures served as stock cultures for the chemostat experiments.

Nitrogen concentrations were adjusted to be non-limiting or only weakly limiting. We used sterile, modified Woodshole WC medium after Guillard & Lorenzen (1972, pH = 6.8) [55]. Nitrogen concentrations were sufficiently low to limit algal growth and were set to 80 $\mu \cdot L\text{-}^{1}$ (phosphorus to nitrogen ratio $P/N_{80} = 1/1.6$) by adjusting the amount of $NaNO_3$. The medium contained trace metals, vitamins and other nutrients in non-limiting concentrations. For stock cultures we used medium containing 320 $\mu mol \cdot L^{-1}$. We used glass chemostat vessels of 1.5 L volume and adjusted the culture volume to approximately 800 mL. To provide homogeneous mixing and to prevent CO_2-limitation algal cultures were bubbled with pressurised, sterile air.

We used light extinction measurement devices according to [150]. Previous investigations of the chemostat system showed that light extinction is an accurate proxy for algal biovolume [93]. Light extinction was measured as light transmittance (wavelength = 880 nm) through a sterile syringe that pulled out and pushed back 10 mL of chemostat content every 5 minutes being therefore a quasi-continuous, non-invasive method. It provided the high resolution of population dynamics necessary to analyse correlations between chemostat systems. Algal growth on the wall of the syringe was prevented due to the bidirectional movement of the syringe plunger. To automatically store the data, the extinction measurement devices were connected to a computer. The computer also controlled the peristaltic pumps by which noise applied.

EXPERIMENTAL PROCEDURE The experimental set-up consisted of two uncoupled chemostats, A and B (see Fig. 4.1a). Prior to each experimental run we let the phytoplankton populations first grow towards steady-state before disturbance of the dilution rate were initiated. In the experimental runs, subsequent values of correlation coefficients were chosen not to be in ascending or descending order to avoid systematic errors. Number of data points to calculate r_p was reduced to match the number of data points when δ was changed. Every experimental run took 5 days in which correlated noise was applied to the chemostat populations. This is, with an interval length of two hours this allowed for a total number of $n = 60$ random shocks in experiments where the interval length was $\Delta t = 2h$, and $n = 120$ random shocks for $\Delta t = 1h$.

Part III

GENERAL DISCUSSION

5

POPULATION DYNAMICS & SYNCHRONIZATION

5.1 SYNCHRONIZATION IN SINGLE POPULATIONS

My doctoral thesis addresses the dynamic behavior of populations that are far from steady state. Generally, nature is complex and unstable, and environmental variability influences organisms and their populations on many scales. Thus, it is only natural that populations vary in time and space according to the prevailing environmental conditions. But not only extrinsic factors but also intrinsic mechanisms provoke nonsteady-state dynamics. These originate either from the interactions between populations, like predator-prey interactions [129, 94] or competition for resources [89, 139]. Or they are the result of the interactions between the individuals within a single population.

Extrinsic and intrinsic factors determine the dynamics of a population.

Variability in single-species populations originating from intrinsic processes is most often explained by density regulation according to discrete logistic growth. The theory of logistic growth goes way back to the middle of the nineteenth century [146]. It was intensively studied since the 1970s and has not lost its attraction in the analyses of population dynamics to date. The simple logistic equation explains cyclic as well as chaotic behavior depending on the growth rate of a population [95, 96, 60]. However, most dynamical features of the logistic difference equation disappear when dealing with populations having over-lapping generations. Then, the logistic differential equation replaces the difference equation since reproduction does not occur in discrete steps but is rather continuous. Nevertheless, cyclic dynamics in single-species populations are possible due to time delays that often originate from demographic structure [97, 33].

ENTRAINED PHYTOPLANKTON POPULATIONS The oscillations described in chapters two and three are the result of extrinsic *and* intrinsic processes. In both studies, environmental influences caused alternations in the structure of the populations that led to oscillatory behavior. To be more precise, the populations were entrained by resource shortage and accumulated in a specific stage of their life cycle since individual development was temporarily ceased (Fig. 5.1). Especially in chapter two, when applying a strict "off-on" manipulation of the dilution rate, a high degree of synchrony was achieved. In these strongly synchronized populations the vast majority of the individuals (forming a cohort) reproduces at the same point in time. Therefore, periods of somatic growth and population growth alternated and caused the populations to increase and decrease in accordance to the

generation time. This means, that the dynamics of a population in perfect synchrony can be described in analogy to the discrete logistic equation.

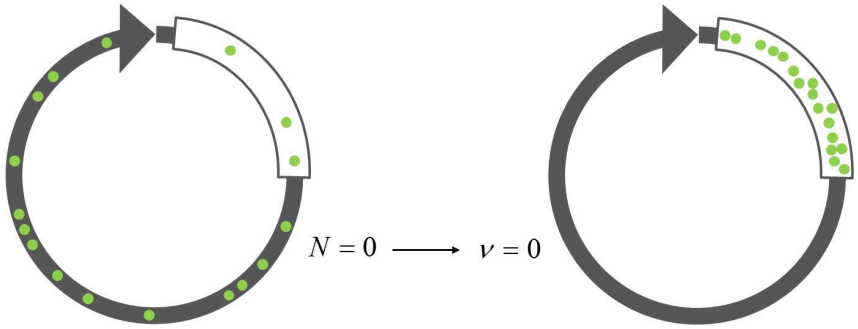

Figure 5.1: Schematic description of entrainment. *C. vulgaris* cells growing under non-limiting nitrogen concentrations are distributed all over their life cycle (left cycle). If all nitrogen in the medium is depleted ($N = 0$), the cells accumulate in the G_1-phase since progression in this phase becomes zero, $\nu = 0$ (right cycle).

Synchronized cells could be described in terms of phase-locked oscillators.

Moreover, the study is the first that clearly demonstrates in theory (model simulations) and experiments that single-species oscillations can be described in terms of phases-coupled oscillators [135, 152, 117]. From the interaction between cells and nitrogen arose a mean field that coupled the cells and synchronized their phases. Once phase-locked, the cells progressed through their life cycles in lockstep which led to sustained oscillations in population density. Since the dilution rate determined the amount of nitrogen in the medium (at constant supply concentration), it also determined the degree of synchrony and, hence, amplitude and frequency of the oscillations. The relationship the between dilution rate and the intensity of the oscillations can be described by the following cascade: low dilution rate $\rightarrow$ strong nitrogen-limitation $\rightarrow$ high degree of synchronization $\rightarrow$ large amplitude and long periods. The long periods are caused by long generation times due to slow cell cycle progression in the G_1-phase when nitrogen concentrations are low.

ENVIRONMENTAL IMPACTS ON DEMOGRAPHY A harsh off-on manipulation as performed in chapter two does not apply to most natural systems where rather gradual changes are the rule. Against this background, the focus in chapter three laid on the transient behavior in response to a series of complementary changes. Therefore, populations that were previously at steady state experienced changes of resource supply and turn-over rate differing in direction and value. By directly changing the environmental conditions, this study is fundamentally different from others investigating environmental effects by harvesting of specific developmental stages [28, 38]. Moreover, measuring the size spectra in comparably small intervals (4-8 hours) gave a temporal

record of the demographic structure with unusual high resolution. This allowed for the detailed analysis of the processes underlying the population dynamics.

Transient population dynamics depended on the kind of perturbation and the demographic state before it occurred.

The transient behavior was again characterized by oscillations resulting from an unbalanced demographic structure and the formation of a cohort. The intensity of the oscillations crucially depended on the demographic steady state before environmental changes were applied. That is, to predict the future population dynamics after changes of the environment, it is of prime importance not only to know how a population is affected, but also in which demographic state. Here, it was made clear that (*i*) although the environmental conditions after having changed in two habitats are identical and (*ii*) although the changes occurred with identical direction and value, the transient dynamics towards the new steady state can vary significantly when the steady-state demography of the populations differed before.

The study also showed that knowledge of the critical mechanisms underlying population dynamics is paramount. Here, cell size was not only related to the developmental stage, but varied with the availability of nitrogen. When available in excess, cells are able to take up surplus nitrogen that is used in various cell compounds and enables a cell to grow larger than compared to strongly limited conditions. On the one hand, by growing larger cells might be able to avoid predation [78]. On the other hand, larger mother cells might produce more or larger daughter cells, respectively. Either way, increasing body size might significantly increase the fitness of a species. Therefore, this mechanisms is not only relevant for *C. vulgaris* populations, but for all species that posses sufficient plasticity in their life cycle to show resource-dependent variability in size and reproduction.

An important mechanism underlying population dynamics was revealed only through transient behavior.

Chapters two and three emphasized the important role of synchronization for single-species population dynamics. Originating from demographic processes, synchrony is likely be an important feature in the dynamics of any population. However, both chapters also show that synchrony among individuals within a population is more than just simultaneous development. It implies coupling between the individuals and the potential for phase-locking leading to self-sustained oscillations.

5.2 SYNCHRONIZATION AMONG VARIOUS POPULATIONS

Populations can be synchronized across large distances in space. In the absence of migration or trophic interactions, environmental stochasticity is likely to cause the high coherence observed in many populations, commonly denoted as Moran effect. The best example for the Moran effect in natural populations are the feral sheep on the St. Kilda archipelago of the Outer Hebrides, Scotland (Fig. 5.2) [54, 14, 30]. The

correlation between the populations r_p reached nearly 0.7. The problem in natural systems, however, is that one cannot exactly determine the influence of the environment as there is no single environmental parameter determining alone the time series of a population. Estimating the environmental correlation r necessary to cause a specific value of r_p is problematic since natural time series often lack a critical number of data points to obtain reliable values of r [14].

Figure 5.2: The feral Soay sheep living on the islands of the St. Kilda archipelago (Outer Hebrides, Scotland) are probably the best system to study the Moran effect in field populations. (Photo copyright: Bill Lockhart, top; Emily Brown, bottom)

Chemostats allowed for perfect control of environmental variability and, hence, were ideal systems to study the Moran effect.

Laboratory experiments provide a solution to this problem. Under well-controlled conditions, one can investigate the Moran effect by altering a specific parameter that alone determines population growth. However, nonlinearities in density dependence might also cause deviations from the expected picture that $r_p = r$ [54, 131]. In the chemostat experiments of chapter four, the dilution rate was changed in intervals large enough to cause detectable changes in population density, and small enough not to cause any nonlinear behavior (population densities converging towards steady state). Thus, this accurate

system reproduced well the Moran effect when Gaussian distributed white noise was applied to identical chemostat populations. Since completely identical populations in identical habitats do not exist (meaning talking about one and the same population), we tested for the Moran effect in two chemostat populations differing in average dilution rate and nitrogen supply concentration. Results showed that $r_p < r$ confirming results from field-studies [113] and theoretical studies [44, 70]. However, when applying differently autocorrelated environmental fluctuations (colored noise) on identical populations, r_p was significantly higher than r. This result is surprising, absolutely nonintuitive and has not been reported before. Although explainable by theoretical analysis, an easy and intuitive explanation is difficult. Some interdependence that is implemented in the environmental fluctuations can not be detected by means of cross-correlation. This hidden correlation can however be unmasked, when it is imposed on a population that effectively responds as a low-pass filter which finally led to an enhanced Moran effect. Since autocorrelated time series are common, these results have widespread relevance not only in ecological research.

Experiments supported theoretical findings that $r_p \geqslant r$ when differently autocorrelated noises influenced the populations.

5.3 SYNCHRONY IN ECOLOGY

Synchronous behavior is one of the most pervasive and apparent dynamical patterns in nature. Gravitational synchrony in the solar system; fireflies flashing in unison; coordinate firing of pacemaker cells in the heart; electrons in a superconductor marching in lockstep [136]. Whatever scale one looks at, in animate as well as inanimate systems, one is likely to encounter synchrony.

In ecology, there are two types of synchrony: single populations whose individuals are synchronized in analogy to the phase synchronization of coupled oscillators; and synchronous fluctuations of spatially disjunct populations experiencing correlated environmental stochasticity (Moran effect). Either type has strong relevance in ecology since synchrony is destabilizing population dynamics and is assumed to decrease the persistence of populations [65, 41].

In March 2011, I was part of a diverse group of researchers form mathematics and statistics and the biological sciences that met at a workshop held at the National Institute of Mathematical and Biological Synthesis (NIMBioS) in Knoxville, Tennessee (USA) to discuss '*Synchrony in Biological Systems Across Multiple Scales*', as the workshop was entitled. Unfortunately, we failed to find a general definition to describe synchronous behavior in biological systems. Nevertheless, ideas about the study of synchrony in one field provided novel insights into questions of synchrony in other fields. Thus, I believe that ecologists will strongly benefit from interdisciplinary collaborations

filling the gaps in knowledge to explain the dynamics of populations and to identify the underlying mechanisms.

Part IV

APPENDIX

A

CYCLES, PHASE SYNCHRONIZATION, AND ENTRAINMENT

A.1 ALGAL CULTURES AND EXPERIMENTAL PROCEDURE

STOCK CULTURES We established monoclonal batch cultures of the three green algae *Monoraphidium minutum* (Clorococcales, former *Kirchneriella lunaris*), *Chlorella vulgaris* (Chlorococcales) and *Chlamydomonas reinhardtii* (Volvocales). Batch cultures were kept in a climate chamber at $23.3° \pm 0.4°C$ and constant fluorescent illumination at 110 $\mu E \cdot m^{-2} \cdot s^{-1}$. Light inside the climate chamber consisted of neutral-white (4000K) and warm-white (3000K) light in equal amounts. These batch cultures served as stock cultures for the chemostat experiments. We kept the batch cultures under constant illumination to prevent synchronization by light-dark cycles. One week prior to each chemostat experiment, we started a new batch culture. Nitrogen concentrations were adjusted to be non-limiting or only weakly limiting to avoid pre-synchronization by limitation (unless this was specifically desired).

MEDIUM We used sterile, modified Woodshole WC medium after Guillard & Lorenzen (1972, pH = 6.8) [55]. Nitrogen concentrations were sufficiently low to limit algal growth and were set to 40 (phosphorus to nitrogen ratio $P/N_{40} = 1/0.8$), 80 ($P/N_{80} = 1/1.6$), 160 ($P/N_{160} = 1/3.2$), 240 ($P/N_{240} = 1/4.8$) or 320 ($P/N_{320} = 1/6.4$) $\mu mol \cdot L^{-1}$ by adjusting the amount of $NaNO_3$. The medium contained trace metals, vitamins and other nutrients in non-limiting concentrations. For stock cultures we used medium containing 320 $\mu mol \cdot L^{-1}$.

CHEMOSTAT SETUP A chemostat is a continuous flow-through culturing system, designed to keep a population of microorganisms at a steady-state over a long period of time. We used glass chemostat vessels of 1.5 L volume and adjusted the culture volume to approximately 800 mL. To prevent CO_2 limitation algal cultures were bubbled with pressurized, sterile air. We measured extinction at 880 nm as a proxy for algal biovolume (biomass) (for details see section 'Light extinction measurement apparatus'). We also sampled the outflow of chemostats and determined algal cell numbers and biovolume of the samples using a CASY particle counter (©Schärfe, Reutlingen). Assuming spherical cell shapes, we used CASY measurements to generate cell size spectra with a resolution of 0.1 µm.

CHEMOSTAT EXPERIMENTS We performed two types of chemostat experiments. The dilution rate varied between $\delta = 0.29$ and $\delta = 0.81$ day^{-1}. Type 1 experiments: Chemostat cultures were inoculated from strongly nitrogen-limited batch cultures. After inoculation, we performed no further experimental manipulations and the populations could grow towards steady-state. Here, we investigated the dynamics of populations that are potentially already synchronized when they start growing in the chemostat system. Type 2 experiments: Chemostat cultures were inoculated from non-limited, non-synchronous batch cultures. First, we let the populations grow without any experimental manipulation towards steady-state. Then, we switched off the dilution (= flow through the chemostat) for 5-7 days, as described by Pascual & Caswell (1997) [112]. During this time, algal cells were expected to take up the remaining nitrogen, became strongly nitrogen-limited and thereby synchronized. With this series of experiments we directly tested for mechanisms by which synchronization could be induced in previously non-synchronized cultures. All chemostat experiments were conducted in the same climate chamber in which the stock cultures were located and experienced identical environmental conditions.

A.2 LIGHT EXTINCTION MEASUREMENT APPARATUS

We used light extinction measurement devices according to Walz et al. (1997) [150], an improved method of Boraas & Bennett (1988) [16]. Light extinction was measured as the light transmittance (wavelength $\lambda = 880$ nm) through a sterile syringe (inner diameter = 11 mm, outer diameter = 14 mm) that pulled out and pushed back 10 mL of chemostat content every 5 minutes. Thus, it is a quasi-continuous, non-invasive method. Traditional methods based on sampling would have failed to show the regularity of the population cycles. Algal growth on the wall of the syringe was prevented due to the bidirectional movement of the syringe plunger. To automatically store the data, the extinction measurement devices were connected to a computer. An analogue input/digital output unit converted the measured voltage of the light extinction sensor into digital units of Volts and amplified the signal negatively. This means that the higher the biovolume in the chemostat was the less light passed the syringe and the higher was the measured voltage.

Figure 1.1a shows that, during small-amplitude oscillations, light extinction is an accurate proxy only for algal biovolume. Light extinction measurements are in phase with biovolume but in anti-phase with the cell density measurements (Fig. 1.1b). That is, the light extinction is low when the biovolume is low and the cell density is high, and vice versa. Under all other dynamic conditions (steady-state, monotonous

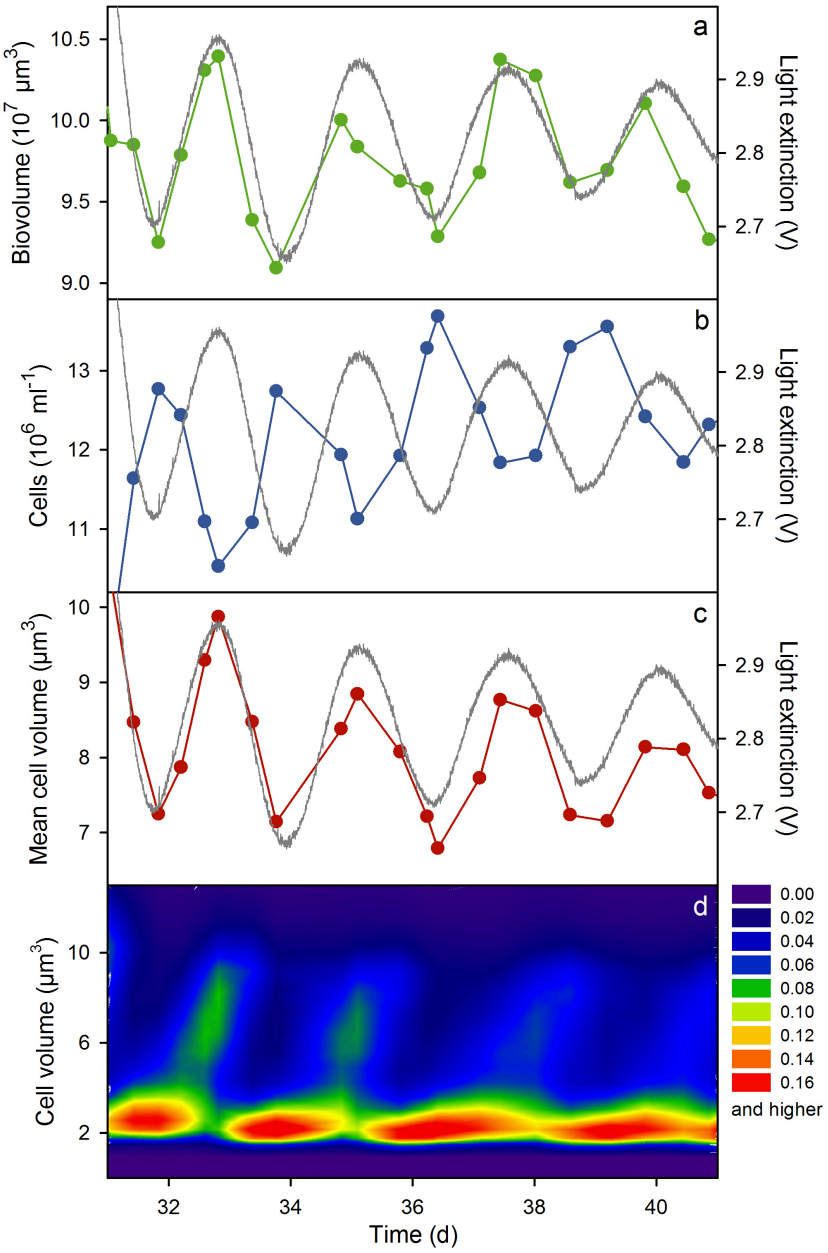

Figure 1.1: Oscillations of (**a**) algal biovolume (green), (**b**) cell density (blue) and (**c**) mean cell volume (red) in relation to light extinction (grey) in chemostat trial number 6 of Table 2.1 ($\delta = 0.52$ day^{-1}, $N_i = 160$ µmol·L^{-1}). (**d**) Oscillations of population density structure.

increase etc.) light extinction is a good proxy for both biovolume and cell density.

The mean cell volume (Fig. 1.1c) and the size spectrum (Fig. 1.1d) show that the majority of the cells are rather big (8-10 µm^3) when the biovolume is high and the cell density is relatively low. Conversely, the cells are comparatively small when the biovolume is low and the

cell density is high. Thus, when the majority of the cells are small one can assume that most cells are newly released daughter cells and the cell density is high due to a growing population. In contrast, when most cells are rather big they recently invested into cellular growth to finally become mother cells, i.e. biovolume is high but cell numbers are not.

A.3 STAGE-STRUCTURED SIMULATION MODEL

Our model (compare to Pascual & Caswell, 1997 [112]) describes the distribution $p(\theta, t)$ of cells in phase $\theta_i \in [0, 2\pi]$ along the cell cycle at time t. The total population number is obtained by integrating the distribution over θ

$$P(t) = \int_0^{2\pi} p(\theta, t) d\theta$$

The dynamics of the distribution is determined by

$$\frac{\partial P}{\partial t} + \frac{\partial}{\partial \theta}[gP] = \frac{\partial}{\partial \theta} D(g) \frac{\partial P}{\partial \theta} - \delta P.$$

Here, the term with δ corresponds to a constant loss rate for each oscillator of strength δ equal to the chemostat dilution rate, $D(g)$ is the effective diffusion constant and $g(\theta, N)$ is the maturation velocity of a cell, described as follows (for the numerical realization see below)

$$g = g(\theta, N) = \begin{cases} \omega \frac{N}{K_N + N} & \text{if } \theta \in [\theta_0, \theta_c] \\ \omega & \text{otherwise.} \end{cases}$$

In the phase subinterval $[\theta_0, \theta_c]$ the maturation velocity is nutrient dependent with half-saturation constant K_N and maximal velocity ω, while through the rest of the cycle the maturation velocity is constant. We used the same maximum maturation velocity ω in the nutrient sensitive and in the nutrient insensitive phase interval.

As phases are only defined in the interval $0 \leqslant \theta \leqslant 2\pi$, the model needs to be applied with a boundary condition at both sides of the phase range. Here we assume that the inflow $J_{in} = g(0, N)p(0)$ of daughter cells from the left boundary is ν times larger than the outflow $J_{out} = g(2\pi, N)p(2\pi)$ of dividing cells into the absorbing boundary at $\theta = 2\pi$, where ν denotes the average number of daughter cells after cell division. Since the maturing velocity attains the same value at both ends of the phase range $g(0, N) = g(2\pi, N)$ we arrive at

$$p(0, t) = \nu p(2\pi, t).$$

We do not explicitly consider the heterogeneity in the aging velocity of different cells. Instead, phase dispersion is incorporated into the model in the form of an effective diffusion term. This term can be

thought to describe the effect of stochastic forces on the maturation of each cell (eq. 2.1, main text). The diffusion constant is assumed to scale proportional to the square of the maturation velocity

$$D(g) = \chi g^2.$$

In this way we assure that sharp peaks in the density distribution do not decay when maturation velocity is zero. In the usual parameterization however, our model results are not affected by this choice of the diffusion term.

The dynamics of the nutrient is similar to standard Monod-type chemostat models, given by

$$\dot{N} = \delta(N_i - N) - \nu_m \frac{N}{K_N + N} P.$$

PARAMETER VALUES Parameter values were taken as follows:
Number of daughter cells: $\nu = 4$
Nutrient sensitive phase interval: $\theta_0 = 2\pi{\cdot}0.05$, $\theta_c = 2\pi{\cdot}0.45$
Diffusion strength: $\chi = 0.018$ days
Half saturation constant: $K_N = 350$ μmol$\cdot$L^{-1}
Maximal maturation velocity: $\omega = 2.94{\cdot}2\pi{\cdot}$day^{-1}
Maximal nutrient uptake rate: $\nu_m = 1.74{\cdot}10^{-4}$ μmol$\cdot$day$^{-1}\cdot$cell^{-1})
Dilution rate: $\delta = 0 \ldots 0.81$ day^{-1}
Nutrient concentration in external medium: $N_i = 40$-320 μmol$\cdot$L^{-1}

We used maximum likelihood parameter estimation. We estimated the set of parameter values that minimized the mean square deviation of the model outcome to the chemostat population density represented in Fig. 2.3 ($\delta = 0.8$ day^{-1}, $N_i = 160$ μmol$\cdot$L^{-1}) using a stochastic gradient descent method. The model parameters that we obtained in this way by fitting to one data set were then used to independently generate simulations for the remaining data sets. We found that this single set of parameters yielded remarkable agreement of the model outcome to all experimentally measured time series. Accordingly, all simulations were performed with these parameters. Using extensive simulation runs we verified that the qualitative model results are robust to changes in all parameter values.

Parameter justification:
• The nutrient concentration of the external supply medium N_i and the dilution rate δ are the values that were used in the chemostat experiments.
• The number of daughter cells was fixed to $\nu = 4$, since in our experiments large *Chlorella* mother cells divide by splitting into four small daughter cells. This value further coincides to the ratio of the volumes between large mother and small daughter cells, which in our experiments was found to be in a range from 3.81 to 4.29.

• The interval length of the nutrient sensitive phase $[\theta_0, \theta_c]$ (G_1-phase) makes about 30 to 40% of the cell cycle under optimal, non-limiting conditions [110]. Similar to Pascual & Caswell (1997) [112] we decided to place the interval at the beginning of the cycle as $[\theta_0, \theta_c] = [2\pi{\cdot}0.05, 2\pi{\cdot}0.45]$.
• The maximum nutrient uptake rate v_m, the half-saturation constant K_N, the maximum maturation velocity ω and the diffusion parameter χ were simultaneously obtained by maximum likelihood estimation. This resulted in a value of $v_m = 1.74{\cdot}10^{-4}$ μmolůday^{-1}·cell^{-1} which deviates marginally from values reported by Halterman (1984) [58] that are $3.34{\cdot}10^{-4}$ μmol·day^{-1} ·cell^{-1} (*C. vulgaris*) or $3.00{\cdot}10^{-4}$ μmol·day^{-1} ·cell^{-1} (*C. pyrenoidosa*).
• Parameter estimation for the half-saturation constant yielded $K_N = 350$ μmol·L^{-1}. Reported values of the half-saturation constant K_N in the literature vary over a large range: e.g., 0.89 μmol·L^{-1} (*C. vulgaris*) [58], 4.5 μmol·L^{-1} (*C. pyrenoidosa*) [116], 148 μmol·L^{-1} (*C. reinhardtii*) [148], 230 μmol·L^{-1} (*C. pyrenoidosa*) [132].
• Parameter estimation for the maximum maturation velocity ω yielded a value of $\omega = 2.94{\cdot}2\pi$ day^{-1}, meaning that under optimal conditions a cell could fulfill approximately three cycles a day.
• Parameter estimation for the diffusion parameter χ resulted in a value of $\chi = 0.018$ days.

For the numerical solution of the partial differential equation we discretized all variables on a grid which consisted of 200 points. The diffusion term was approximated by a second order central discretization scheme and the 'advection' term was represented by a third-order upwind biased formula. The resulting system of ordinary differential equations was integrated using a backward differentiation formula, by the CVODE package (). We have verified that our results do not change by various alterations of the numerical procedure. Additionally we have found practically identical simulation results using the escalator boxcar train method [37].

To avoid numerical problems when solving the model's partial differential equations we chose a continuous formula to describe nutrient dependent maturation velocity (see Fig. 1.2)

$$g(\theta, N) = \omega\,(1 - f(N)))\,[1 + _{\theta_0}(\theta) - F_{\theta_c}(\theta)] + \omega f(N),$$

with the Fermi-function

$$F_\vartheta(\theta) = \left(1 + \exp\frac{\theta - \vartheta}{\alpha}\right)^{-1},$$

of width $\alpha = 0.01{\cdot}2\pi$ and the Monod function

$$f(N) = \frac{N}{K_N + N}.$$

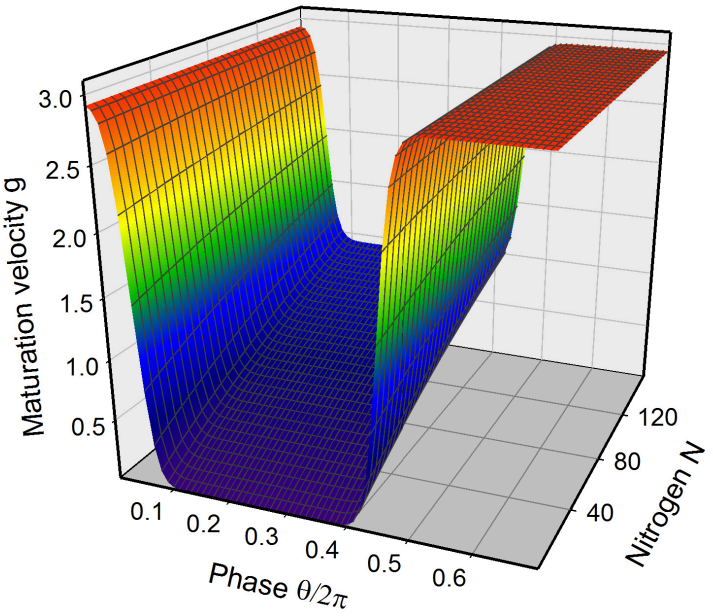

Figure 1.2: Maturation velocity $g(\theta, N)$ as a function of the normalized phase $\theta/2\pi$ and the nutrient concentration N.

To measure the order parameter R of the Kuramoto model in experimental populations cell volume V was translated to phase according to the following formula

$$\theta = 2\pi \frac{V - V_{min}}{V_{max} - V_{min}}$$

with $V_{min} = 1.15 m^3$ and $V_{min} = 18.82 m^3$. The complex order parameter [117] can then be estimated from the phase density as

$$Re^{i\psi} = \int_0^{2\pi} d\theta e^{i\theta} p(\theta, t).$$

The complex order parameter indicates the center of gravity of all oscillators, distributed according to their phase on a unit circle in the complex plane (see Fig. 1.3). The order parameter equals $R = 0$ when all cells oscillate out of phase with each other (incoherent state) and R=1 when all cells are perfectly locked in phase.

A.4 STATIONARY DISTRIBUTIONS

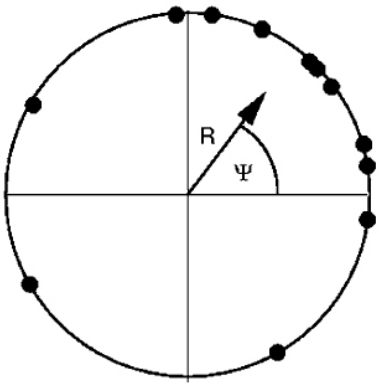

Figure 1.3: Schematic representation of the complex order parameter. Shown is the distribution of oscillators on the unit circle in the complex plane. The order parameter $Re^{i\psi} = \left(\sum_{j=1}^{n} e^{i\theta}\right)/n$ points to the center of gravity. The absolute value R measures the phase coherency or degree of synchronization and ψ describes the average phase of the oscillators.

A.5 RESULTS OF ADDITIONAL CHEMOSTAT TRIALS

We ran chemostat trials in addition to the examples shown in the main paper. In Table 2.1 we give a comparative summary of the results of the 9 trials performed as Type 2 experiment (i.e. with off-on manipulation of the chemostat leading to synchronization).

Fig. 1.5 shows the relationship between period length, supplied nitrogen N_i and dilution rate δ. Blue dots represent the 9 chemostat trials summarized in Table 2.1. The three red lines show model predictions for the period length once along a gradient of dilution rates (constant nitrogen supply, $N_i = 160$ μmol·L^{-1} and $N_i = 320$ μmol·L^{-1}) and along a gradient of supplied nitrogen (constant dilution rate, $\delta = 0.5$ day^{-1}).

Figures 1.6-1.8 show examples of time series of synchronization experiments for *C. reinhardtii* (Fig. 1.6), *M. minutum* (Fig. 1.7) and *C. vulgaris* (Fig. 1.8).

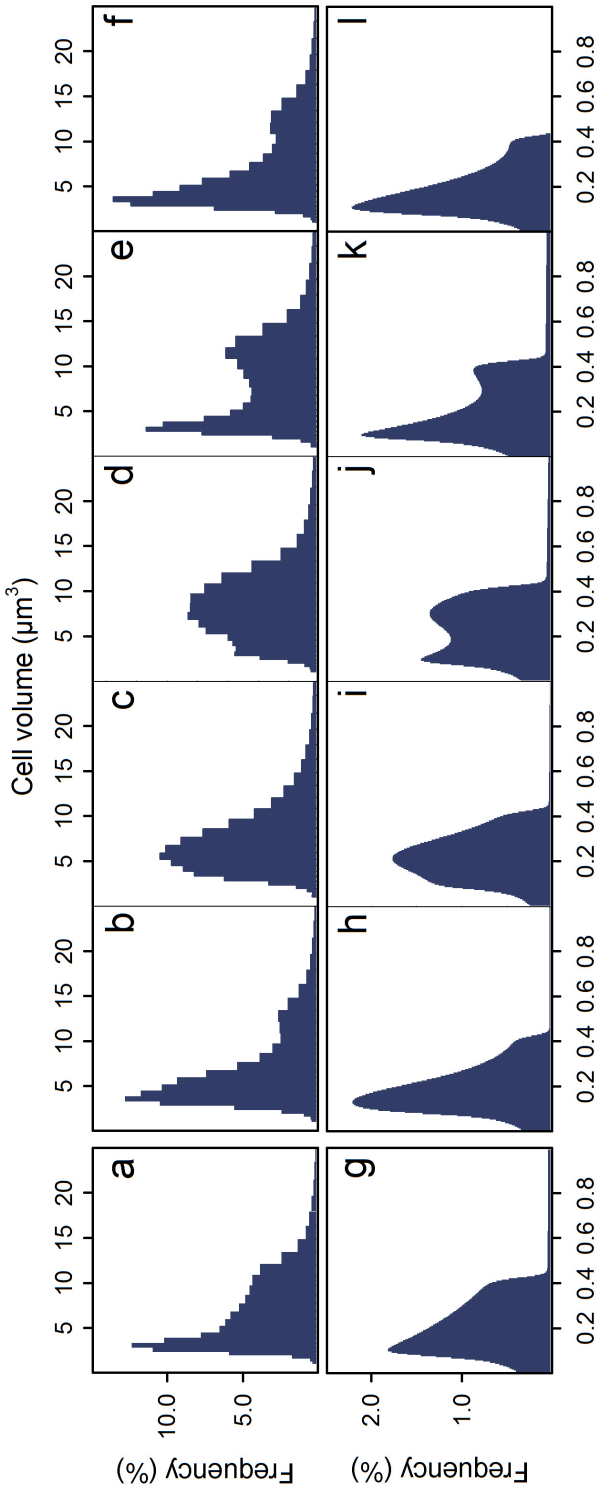

Table 1.1: Comparison of experimental and simulated phase distributions in the oscillatory regime. Shown are the distributions of position along the cell cycle at 5 consecutive sampling points within one period of oscillation. (**b-f**) Data from chemostat trial with *C. vulgaris* for $\delta = 0.81$ day^{-1} and $N_i = 160$ µmol·day^{-1} (Fig. 2.1b, main text). (**h-l**) Corresponding model simulation. Stationary distributions (**a**, **g**) are shown for comparison.

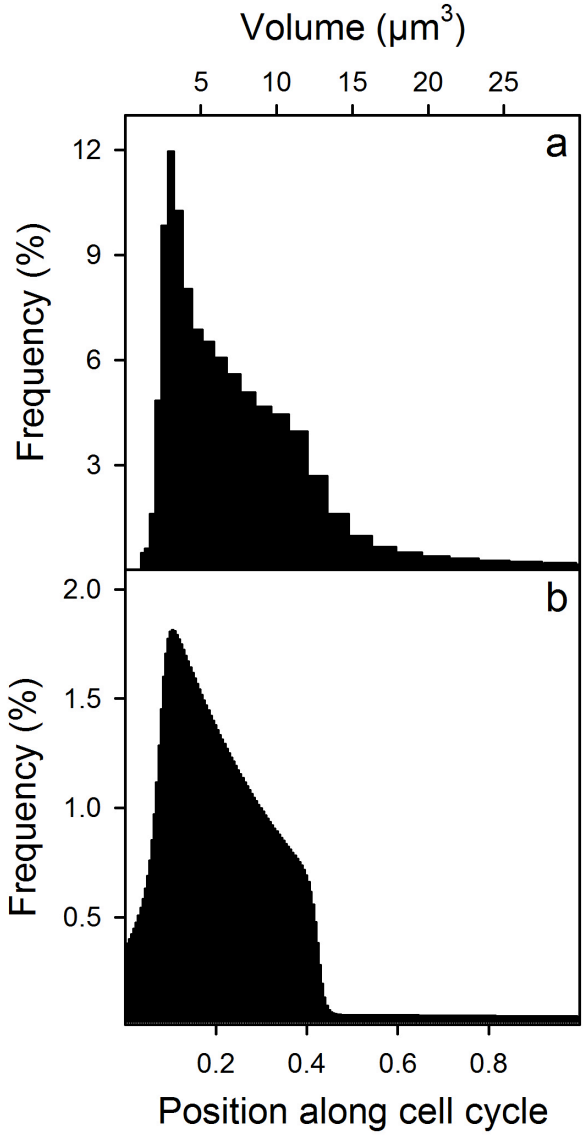

Figure 1.4: Comparison of (**a**) experimental and (**b**) model relative frequency distributions at steady-state (t = 19.89 days). Data were taken from chemostat trial 5 with $\delta = 0.81$ day^{-1} and $N_i = 160$ μmol·L^{-1} and the corresponding model simulation. The characteristic shape can be explained as the combined effect of three processes: (*i*) as the cell progression through the G_1-phase of the cell cycle is slow, this yields an elevated number of oscillators in this phase (i.e. a peak for small cell volumes). (*ii*) as cells are washed out of the chemostat system during their growth process there is tendency for an exponential decay of cell numbers with volume. (*iii*) from a certain cell volume most cells divide into smaller daughter cells, which results in a sharp drop in cell numbers around $V = 13m^3$.

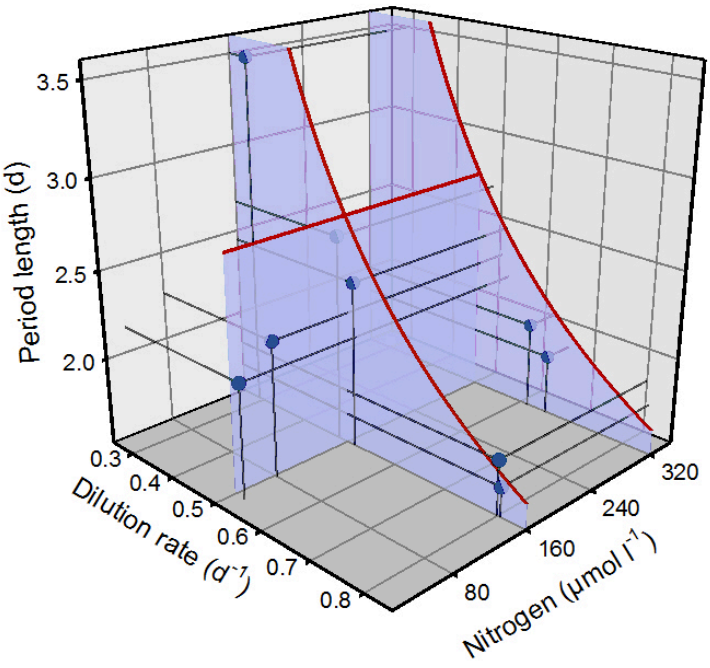

Figure 1.5: Comparison of chemostat trials with off-on manipulation (blue dots) against model predictions (red lines).

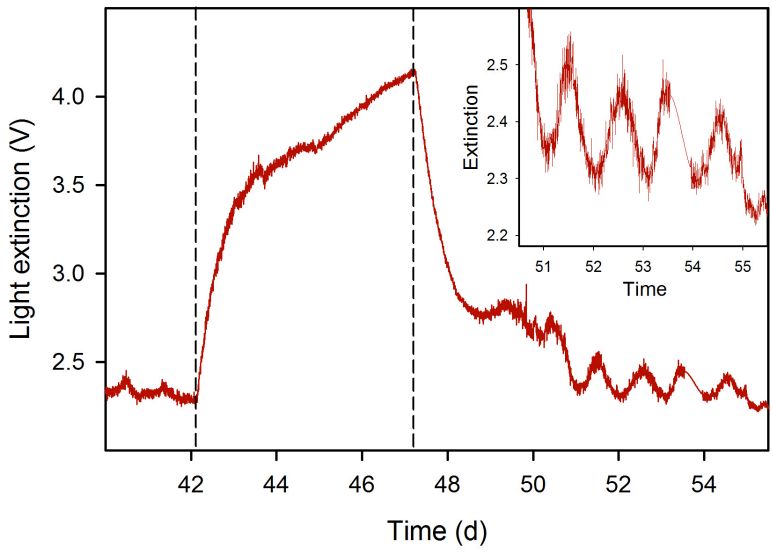

Figure 1.6: Trial 1 with *C. reinhardtii*: $\delta = 0.51$ day^{-1}, $N_i = 160$ µmol·L^{-1}, $\Delta t_{off} = 5.1$ days. (sine interpolation between day 53.5 and 53.8)

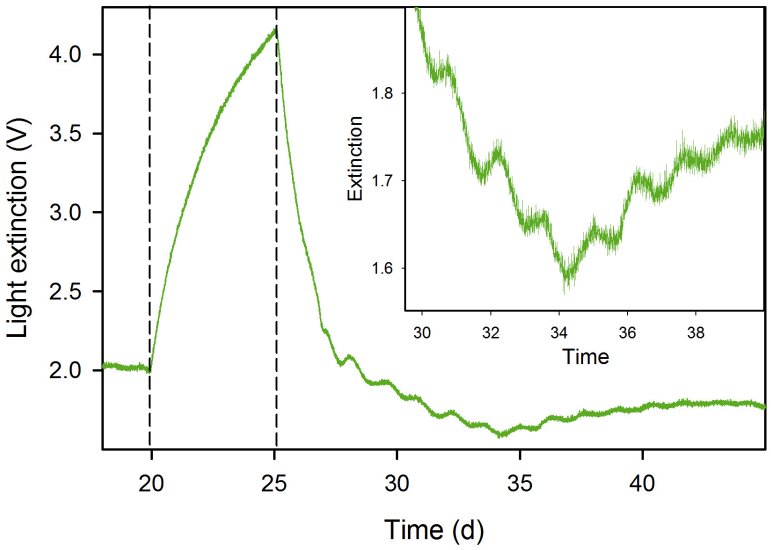

Figure 1.7: Trial 2 with *M. minutum*: $\delta = 0.51$ day^{-1}, $N_i = 160$ µmol·L^{-1}, $\Delta t_{off} = 4.9$ days.

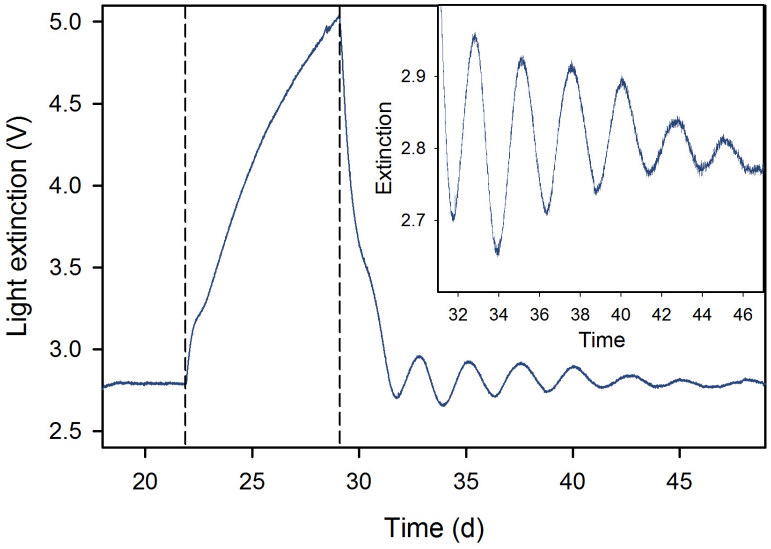

Figure 1.8: Trial 6 with *C. vulgaris*: $\delta = 0.52$ day^{-1}, $N_i = 160$ µmol·L^{-1}, $\Delta t_{off} = 7.2$ days.

Table 1.2: Summary statistics of chemostat trials with off-on manipulation. *Trial was aborted due to technical problems before steady state was reached. **No steady state reached before end of trial.

Trial #	Species	δ (day^{-1})	N_i $\mu mol \cdot L^{-1}$	No. of oscillations	Period length (days)	SD (days)
1	*C. reinhardtii*	0.51	160	5	1.03	0.07
2	*M. minutum*	0.51	160	12	1.35	0.12
3	*C.vulgaris*	0.65	320	3*	1.84	0.08
4	*C.vulgaris*	0.61	320	16**	2.00	0.17
5	*C.vulgaris*	0.81	160	7	1.67	0.16
6	*C.vulgaris*	0.52	160	5	2.45	0.14
7	*C.vulgaris*	0.29	160	2	3.50	0.16
8	*C.vulgaris*	0.50	80	3	2.27	0.10
9	*C.vulgaris*	0.52	40	2	2.15	0.01

B

ENHANCED MORAN EFFECT

B.1 EXPERIMENTAL SETUP

STOCK CULTURES We established monoclonal batch cultures of the green alga *Chlorella vulgaris*. Batch cultures were kept in a climate chamber at $23.3° \pm 0.4°C$ and constant fluorescent illumination at 110 $\mu E \cdot m^{-2} \cdot s^{-1}$. Light inside the climate chamber consisted of neutral-white (4000K) and warm-white (3000K) light in equal amounts. The batch cultures served as stock cultures for the chemostat experiments. Constant illumination prevented synchronization by light-dark cycles. One week prior to each chemostat experiment, we started a new batch culture. Nitrogen concentrations were adjusted to be non-limiting to avoid synchronization by limitation.

MEDIUM We used sterile, modified Woodshole WC medium after Guillard & Lorenzen (1972, pH = 6.8) [55]. Nitrogen concentrations were sufficiently low to limit algal growth and were set to 80 $\mu mol \cdot L^{-1}$ by adjusting the amount of $NaNO_3$. The medium contained trace metals, vitamins and other nutrients in non-limiting concentrations. For stock cultures we used medium containing 320 $\mu mol \cdot L^{-1}$.

CHEMOSTAT SETUP A chemostat is a continuous flow-through culturing system, designed to maintain a microorganismal population at steady-state over a long period of time. We used glass chemostat vessels of 1.5 L volume and adjusted the culture volume to approximately 800 mL. To prevent CO_2 limitation, algal cultures were bubbled with pressurized, sterile air. We measured light extinction at $\lambda = 880$ nm as a proxy for algal biovolume (biomass) [93]. We also sampled the outflow of chemostats and determined algal cell numbers and biovolume of the samples using a CASY particle counter (©Innovatis). Assuming spherical cell shapes, we used CASY measurements to generate cell size spectra with a resolution of 0.1 µm.

LIGHT EXTINCTION MEASUREMENTS We used light extinction measurement devices according to Walz et al. (1997) [150]. Light extinction was measured as the light transmittance (wavelength $\lambda = 880$ nm) through a sterile syringe (inner diameter = 11 mm, outer diameter = 14 mm) that pulled out and pushed back 10 mL of chemostat content every 5 minutes. It is a quasi-continuous, non-invasive method allowing to detect the regularity of the population cycles. Algal growth on the wall of the syringe was prevented due to the bidirectional

movement of the syringe plunger. To automatically store the data, the extinction measurement devices were connected to a computer.

B.2 TABLES

Table 2.1: Series 1: Characteristic parameter values and statistics for trails 1 to 6; Gaussian distributed white noise in identical populations.

Trial #	N_i ($\mu M\ L^{-1}$)	$\langle \delta_A \rangle$ (day^{-1})	$\langle \delta_B \rangle$ (day^{-1})	σ (day^{-1})	r	r_p
1	80	0.74	0.73	0.20	0.80	0.71
2	80	0.76	0.71	0.20	0.20	-0.17
3	80	0.75	0.75	0.20	0.60	0.80
4	80	0.72	0.76	0.20	0.00	0.21
5	80	0.75	0.77	0.20	0.40	0.48
6	80	0.72	0.72	0.20	1.00	0.96

Table 2.2: Series 2: Characteristic parameter values and statistics for trails 7 to 12; Gaussian distributed white noise in differing populations.

Trial #	$N_{i,A}$ ($\mu M\ L^{-1}$)	$N_{i,B}$ ($\mu M\ L^{-1}$)	$\langle \delta_A \rangle$ (day^{-1})	$\langle \delta_B \rangle$ (day^{-1})	σ (day^{-1})	r	r_p
7	80	40	0.76	0.39	0.15	0.80	0.68
8	80	40	0.74	0.43	0.15	0.20	0.07
9	80	40	0.77	0.40	0.15	0.60	0.79
10	80	40	0.76	0.44	0.15	0.00	-0.09
11	80	40	0.75	0.38	0.15	0.40	-0.02
12	80	40	0.77	0.42	0.15	1.00	0.48

Table 2.3: Series 3: Characteristic parameter values and statistics for trails 13 to 23; auto-correlated noise in identical populations.

Trial #	N_i ($\mu M\ L^{-1}$)	$\langle \delta_A \rangle$ (day^{-1})	$\langle \delta_B \rangle$ (day^{-1})	σ (day^{-1})	α	β	$\lvert\alpha - \beta\rvert$	r	r_p
13	80	0.84	0.82	0.25	0.87	0.65	0.22	0.75	0.84
14	80	0.84	0.80	0.25	0.87	0.33	0.54	0.42	0.78
15	80	0.84	0.77	0.25	0.87	0.02	0.85	0.20	0.72
16	80	0.82	0.80	0.25	0.65	0.33	0.32	0.82	0.91
17	80	0.82	0.77	0.25	0.65	0.02	0.63	0.52	0.67
18	80	0.80	0.77	0.25	0.33	0.02	0.31	0.88	0.89
19	80	0.77	0.78	0.25	-0.18	0.20	0.38	0.72	0.88
20	80	0.72	0.71	0.25	0.04	0.55	0.51	0.76	0.91
21	80	0.85	0.86	0.25	0.42	0.70	0.28	0.79	0.87
22	80	0.85	0.84	0.25	0.42	0.85	0.43	0.40	0.71
23	80	0.86	0.84	0.25	0.70	0.85	0.15	0.74	0.81

B.3 DATA PROCESSING

Before computing the correlation coefficients, all time series underwent identical data processing (Fig.1 2.2). First, the logarithmic light extinction values were normalised to zero mean, denoted as X' (Supplementary Fig. 2.2a, light blue). Then, X' was smoothed by a local regression filter that uses weighted linear least squares and a 2^{nd} degree polynomial model ('rloess' filter from Matlab's curve fitting toolbox, the span was set to 2% of the data points). This gave the smoothed time series X (Supplementary Fig. 2.2a, dark blue).

Next, we gently detrended X by subtracting a coarse fit F generated with a Savitzky-Golay filter. This filter comprises a generalized moving average with coefficients determined by an unweighted linear least-squares regression and a 2^{nd} degree polynomial model ('sgolay' filter from Matlab's curve fitting toolbox, the span was set to 100% of the data points; Supplementary Fig. 2.2b, green). Detrending was applyed to account for changes influencing the times series after the start of a new experimental trial. This gave the detrended times series N' (Supplementary Fig. 2.2b, red). Finally, N' was discretised according to the intervals when δ was changed. This gave the discrete times series N used in the correlations (Fig. 2.2c).

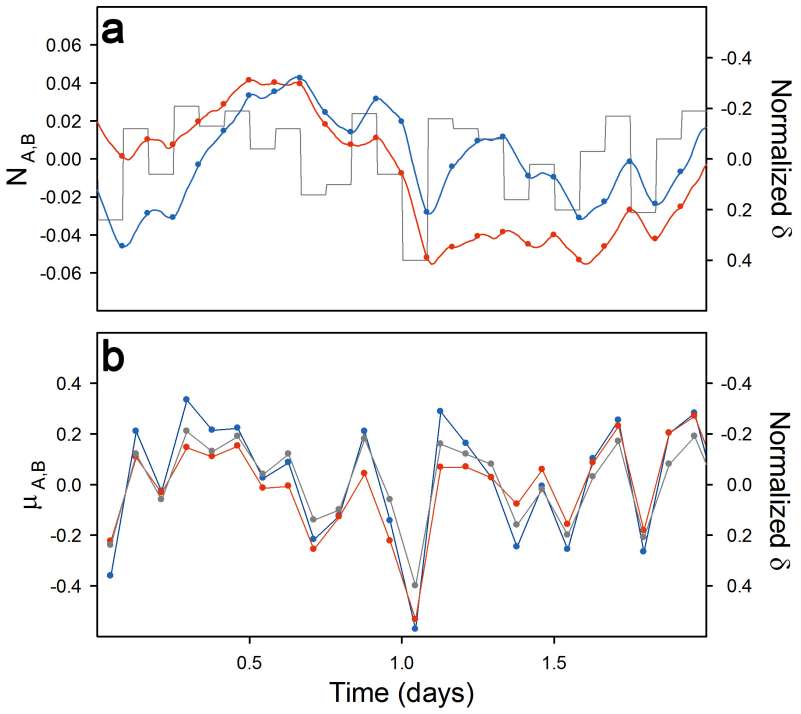

Figure 2.1: Synchronization by Gaussian distributed white noise in two differing populations (trial 12). Although differing in $\langle\delta\rangle$ and N_i, both populations deviated only minor in densities (**a**) and growth rates (**b**).

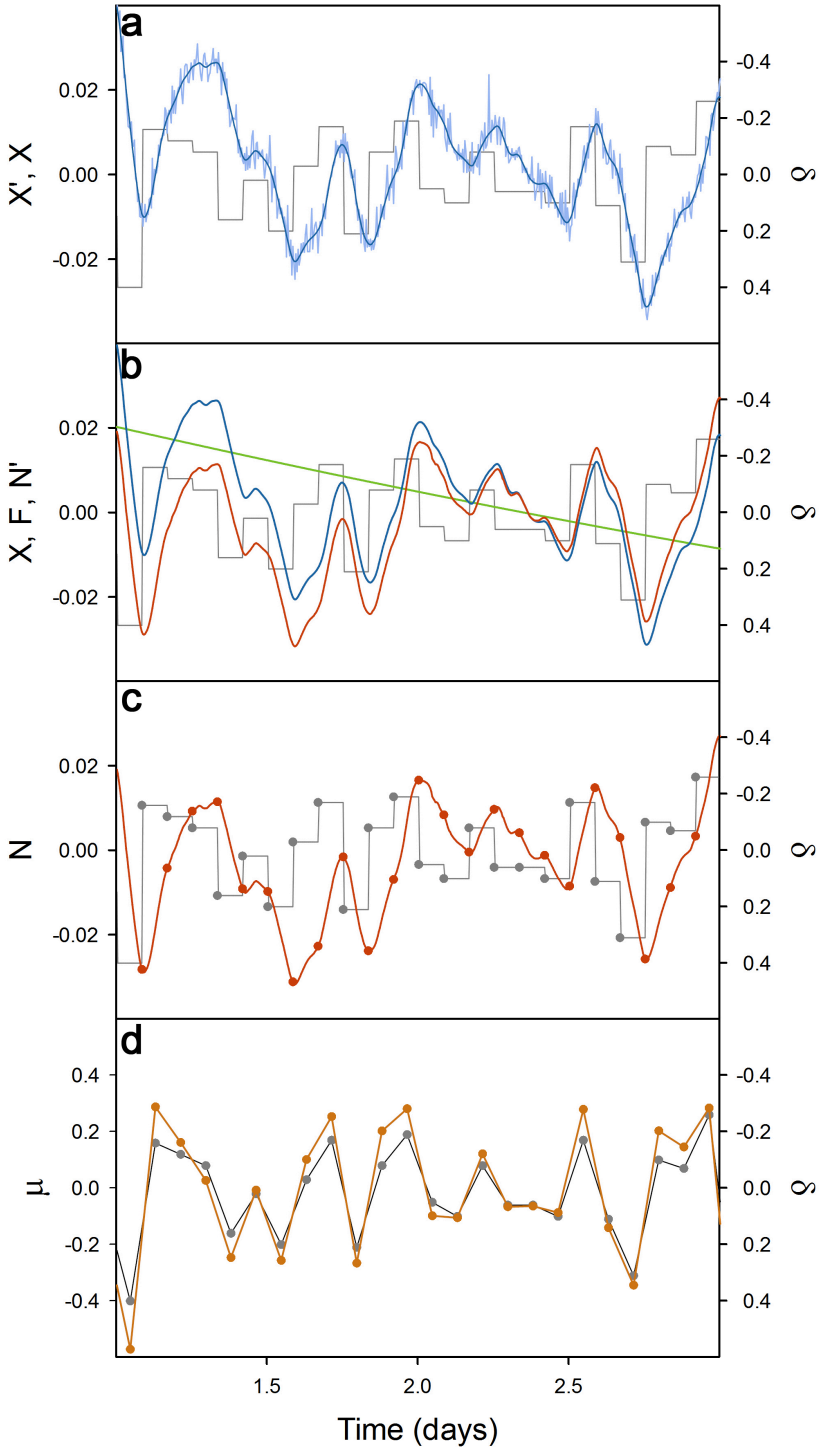

Figure 2.2: Data processing example for one chemostat of trial 1; Gaussian distributed white noise in identical populations. The normalized, logarithmic light extinction measurements were first smoothed (**a**) and then detrended (**b**). Discretizing of the continuous detrended time series according to the changing steps of the dilution rate gave the population time series used for calculating correlations (**c**). The growth rate of the population corresponded well with the normalized dilution rate (**d**)

BIBLIOGRAPHY

[1] K. C. Abbott. Does the pattern of population synchrony through space reveal if the Moran effect is acting? *Oikos*, 116(6):903–912, 2007.

[2] J. Acebrón, L. Bonilla, C. Pérez Vicente, F. Ritort, and R. Spigler. The Kuramoto model: A simple paradigm for synchronization phenomena. *Reviews of Modern Physics*, 77(1):137–185, 2005. ISSN 0034-6861.

[3] C. N. K. Anderson, C.-H. Hsieh, S. A. Sandin, R. Hewitt, A. Hollowed, J. Beddington, R. M. May, and G. Sugihara. Why fishing magnifies fluctuations in fish abundance. *Nature*, 452:835–9, 2008.

[4] O. Arino and M. Kimmel. Comparison of approaches to modeling of cell population dynamics. *Journal on Applied Mathematics*, 53(5):1480–1504, 1993.

[5] F. K. Balagaddé, L. You, C. L. Hansen, F. H. Arnold, and S. R. Quake. Long-term monitoring of bacteria undergoing programmed population control in a microchemostat. *Science*, 309 (5731):137–40, 2005.

[6] F. Beck, B. Blasius, U. Lüttge, R. Neff, and U. Rascher. Stochastic noise interferes coherently with a model biological clock and produces specific dynamic behaviour. *Proceedings of the Royal Society of London. Series B: Biological Sciences*, 268(1473):1307–13, 2001.

[7] L. Becks, F. M. Hilker, H. Malchow, K. Jürgens, and H. Arndt. Experimental demonstration of chaos in a microbial food web. *Nature*, 435:1226–1229, 2005.

[8] T. G. Benton, C. T. Lapsley, and A. P. Beckerman. Population synchrony and environmental variation: an experimental demonstration. *Ecology Letters*, 4(3):236–243, 2001.

[9] T. G. Benton, C. T. Lapsley, and A. P. Beckerman. The population response to environmental noise: population size, variance and correlation in an experimental system. *Journal of Animal Ecology*, 71(2):320–332, 2002.

[10] T. G. Benton, T. C. Cameron, and A. Grant. Population responses to perturbations: predictions and responses from laboratory mite populations. *Journal of Animal Ecology*, 73(5):983–995, 2004.

[11] O. N. Bjørnstad. Cycles and synchrony: two historical 'experiments' and one experience. *Journal of Animal Ecology*, 69(5): 869–873, 2000.

[12] O. N. Bjørnstad, R. A. Ims, and X. Lambin. Spatial population dynamics: analyzing patterns and processes of population synchrony. *Trends in Ecology & Evolution*, 14(11):427–432, 1999.

[13] O. N. Bjørnstad, A. M. Liebhold, and D. M. Johnson. Transient synchronization following invasion: revisiting Moran's model and a case study. *Population Ecology*, 50(4):379–389, 2008.

[14] B. Blasius and L. Stone. Nonlinearity and the Moran effect. *Nature*, 406:846–847, 2000.

[15] B. Blasius, A. Huppert, and L. Stone. Complex dynamics and phase synchronization in spatially extended ecological systems. *Nature*, 399:354–9, 1999.

[16] M. E. Boraas and W. N. Bennett. Steady-state rotifer growth in a two-stage, computer-controlled turbidostat. *Journal of Plankton Research*, 10(5):1023–1038, 1988.

[17] J. Buck. Synchronous rhythmic flashing of fireflies. II. *Quarterly Review of Biology*, 63(3):265–289, 1988.

[18] J. P. Buonaccorsi, J. S. Elkinton, S. R. Evans, and A. M. Liebhold. Measuring and Testing for Spatial Synchrony. *Ecology*, 82(6): 1668–1679, 2001.

[19] T. C. Cameron and T. G. Benton. Stage-structured harvesting and its effects: an empirical investigation using soil mites. *Journal of Animal Ecology*, 73(5):996–1006, 2004.

[20] J. Caperon. Time lag in population growth response of Isochrysis galbana to a variable nitrate environment. *Ecology*, 50(2):188–192, 1969.

[21] J. Caperon and J. Meyer. Nitrogen-limited growth of marine phytoplankton–I. changes in population characteristics with steady-state growth rate. *Deep Sea Research and Oceanographic Abstracts*, 19(9):601–618, 1972.

[22] H. Caswell. *Matrix Population Models: Construction, Analysis and Interpretation*. Sinauer Associates, 2000.

[23] I. M. Cattadori, D. T. Haydon, and P. J. Hudson. Parasites and climate synchronize red grouse populations. *Nature*, 433:737–41, 2005.

[24] B. Cazelles. The Moran effect and phase synchronization in complex spatial community dynamics. *The American Naturalist*, 157(6):670–676, 2001.

[25] C. Chatfield. *The Analysis of Time Series: An Introduction*. Chapman and Hall/CRC, 2003. ISBN 1584883170.

[26] C. Cipollina, M. Vai, D. Porro, and C. Hatzis. Towards understanding of the complex structure of growing yeast populations. *Journal of Biotechnology*, 128(2):393–402, 2007.

[27] Y. Collos. Time-lag algal growth dynamics: biological constraints on primary production in aquatic environments. *Marine Ecology Progress Series*, 33:193–206, 1986.

[28] R. F. Costantino, J. M. Cushing, Brian Dennis, and R. A. Desharnais. Experimentally induced transitions in the dynamic behaviour of insect populations. *Nature*, 375:227–230, 1995.

[29] R. F. Costantino, R. A. Desharnais, J. M. Cushing, and B. Dennis. Chaotic dynamics in an insect population. *Science*, 275(5298): 389–391, 1997.

[30] T. Coulson, E. A. Catchpole, S. D. Albon, B. J. Morgan, J. M. Pemberton, T. H. Clutton-Brock, M. J. Crawley, and B. T. Grenfell. Age, sex, density, winter weather, and population crashes in Soay sheep. *Science*, 292(5521):1528–31, 2001.

[31] T. N. Coulson, F. Guinness, J. Pemberton, and T. H. Clutton-Brock. The Demographic Consequences of Releasing a Population of Red Deer From Culling. *Ecology*, 85(2):411–422, 2004.

[32] K. M. Cuddington and P. Yodzis. Black noise and population persistence. *Proceedings of the Royal Society of London. Series B: Biological Sciences*, 266(1422):969–973, 1999.

[33] J. M. Cushing. Time delays in single species growth models. *Journal of Mathematical Biology*, 4(3):257–264, 1977.

[34] H. Cyr and I. Cyr. Temporal scaling of temperature variability from land to oceans. *Evolutionary Ecology Research*, 5(8):1183–1197, 2003.

[35] J. de la Rocha, B. Doiron, E. Shea-Brown, K. Josić, and A. Reyes. Correlation between neural spike trains increases with firing rate. *Nature*, 448:802–6, 2007.

[36] S. De Monte, F. D'Ovidio, S. Danø, and P. G. Sø rensen. Dynamical quorum sensing: Population density encoded in cellular dynamics. *Proceedings of the National Academy of Sciences of the United States of America*, 104(47):18377–81, 2007.

[37] A. M. De Roos, O. Diekmann, and J. A. J. Metz. Studying the dynamics of structured population models: a versatile technique and its application to Daphnia. *The American Naturalist*, 139(1): 123–147, 1992.

[38] B. Dennis, R. A. Desharnais, J. M. Cushing, S. M. Henson, and R. F. Costantino. Estimating chaos and complex dynamics in an insect population. *Ecological Monographs*, 71(2):277–303, 2001.

[39] Q. Dortch, J. R. Clayton, and S. S. Thoresen. Species differences in accumulation of nitrogen pools in phytoplankton. *Marine Biology*, 250:237–250, 1984.

[40] D. J. Earn, P. Rohani, and B. T. Grenfell. Persistence, chaos and synchrony in ecology and epidemiology. *Proceedings of the Royal Society of London. Series B: Biological Sciences*, 265(1390): 7–10, 1998.

[41] D. J. D. Earn. Coherence and Conservation. *Science*, 290(5495): 1360–1364, 2000.

[42] C. S. Elton. Periodic fluctuations in the numbers of animals: their causes and effects. *British Journal of Experimental Biology*, 2 (1):119–163, 1924.

[43] S. Engen, R. Lande, and B.-E. Saether. The spatial scale of population fluctuations and quasi-extinction risk. *The American Naturalist*, 160(4):439–51, 2002.

[44] Steinar Engen and Bernt-Erik Saether. Generalizations of the Moran effect explaining spatial synchrony in population fluctuations. *The American Naturalist*, 166(5):603–12, 2005.

[45] S. A. Estay, M. Lima, and R. Harrington. Climate mediated exogenous forcing and synchrony in populations of the oak aphid in the UK. *Oikos*, 118(2):175–182, 2009.

[46] C. Fontaine and A. Gonzalez. Population synchrony induced by resource fluctuations and dispersal in an aquatic microcosm. *Ecology*, 86(6):1463–1471, 2005.

[47] M. C. Forchhammer, E. Post, N. C. Stenseth, and D. M. Boertmann. Long-term responses in arctic ungulate dynamics to changes in climatic and trophic processes. *Population Ecology*, 44 (2):113–120, 2002.

[48] K. Fraedrich and R. Blender. Scaling of Atmosphere and Ocean Temperature Correlations in Observations and Climate Models. *Physical Review Letters*, 90(10):13–16, 2003.

[49] G. F. Fussmann, S. P. Ellner, K. W. Shertzer, and N. G. Hairston. Crossing the Hopf bifurcation in a live predator-prey system. *Science*, 290(5495):1358–60, 2000.

[50] K. Goto and C. H. Johnson. Is the cell division cycle gated by a circadian clock? The case of Chlamydomonas reinhardtii. *The Journal of Cell Biology*, 129(4):1061–1069, 1995.

[51] A. R. Gould, N. P. Everett, T. L. Wang, and H. E. Street. Studies on the control of the cell cycle in cultured plant cells – I. Effects of Nutrient Limitation and Nutrient Starvation. *Protoplasma*, 106: 1–13, 1981.

[52] J. V. Greenman and T. G. Benton. The impact of stochasticity on the behaviour of nonlinear population models: synchrony and the Moran effect. *Oikos*, 93:343–351, 2001.

[53] J. V. Greenman and T. G. Benton. The frequency spectrum of structured discrete time population models: its properties and their ecological implications. *Oikos*, 110(2):369–389, 2005.

[54] B. T. Grenfell, K. Wilson, B. F. Finkenstadt, T. N. Coulson, S. Murray, S. D. Albon, J. M. Pemberton, T. H. Clutton-Brock, and M. J. Crawley. Noise and determinism in synchronized sheep dynamics. *Nature*, 394:674–677, 1998.

[55] R. R. L. Guillard and C. J. Lorenzen. Yellow-green algae with chlorophyllide c. *Journal of Phycology*, 8(1):10–14, 1972.

[56] N. M. Haddad, D. Tilman, and J. M. H. Knops. Long-term oscillations in grassland productivity induced by drought. *Ecology Letters*, 5(1):110–120, 2002.

[57] J. Halley. Ecology, evolution and 1/f-noise. *Trends in Ecology & Evolution*, 11(1):33–37, 1996.

[58] S. G. Halterman and D. W. Toetz. Kinetics of nitrate uptake by freshwater algae. *Hydrobiologia*, 114(3):209–214, 1984.

[59] S. Harrison and J.F. Quinn. Correlated environments and the persistence of metapopulations. *Oikos*, 56(3):293–298, 1989.

[60] A. Hastings. Chaos in Ecology: Is Mother Nature a Strange Attractor? *Annual Review of Ecology and Systematics*, 24(1):1–33, 1993.

[61] A. Hastings. Transients: the key to long-term ecological understanding? *Trends in Ecology & Evolution*, 19(1):39–45, 2004.

[62] A. Hastings. Timescales, dynamics, and ecological understanding. *Ecology*, 91(12):3471–3480, 2010.

[63] C. Hatzis and D. Porro. Morphologically-structured models of growing budding yeast populations. *Journal of Biotechnology*, 124 (2):420–38, 2006.

[64] M. Heino. Noise colour, synchrony and extinctions in spatially structured populations. *Oikos*, 83:368–375, 1998.

[65] M. Heino, V. Kaitala, E. Ranta, and J. Lindstrom. Synchronous dynamics and rates of extinction in spatially structured populations. *Proceedings of the Royal Society of London. Series B: Biological Sciences*, 264(1381):481–486, 1997.

[66] S. M. Henson, J. M. Cushing, R. F. Costantino, B. Dennis, and R. A. Desharnais. Phase switching in population cycles. *Proceedings of the Royal Society of London. Series B: Biological Sciences*, 265(1411):2229–2234, 1998.

[67] D. Herbert, R. Elsworth, and R. C. Telling. The continuous culture of bacteria; a theoretical and experimental study. *Journal of General Microbiology*, 14(3):601–22, 1956.

[68] C.-H. Hsieh, C. S. Reiss, J. R. Hunter, J. R. Beddington, R. M. May, and G. Sugihara. Fishing elevates variability in the abundance of exploited species. *Nature*, 443:859–62, 2006.

[69] P. J. Hudson and I. M. Cattadori. The Moran effect: a cause of population synchrony. *Trends in Ecology & Evolution*, 14(1):1–2, 1999.

[70] Bernard Hugueny. Spatial synchrony in population fluctuations: extending the Moran theorem to cope with spatially heterogeneous dynamics. *Oikos*, 115(1):3–14, 2006.

[71] T. Humphrey and G. Brooks. *Cell Cycle Control: Mechanisms and Protocols (Methods in Molecular Biology)*. Humana Press, 2010.

[72] J. A. Hutchings and J. D. Reynolds. Marine Fish Population Collapses: Consequences for Recovery and Extinction Risk. *BioScience*, 54(4):297, 2004.

[73] P. Inchausti and J. Halley. The long-term temporal variability and spectral colour of animal populations. *Evolutionary Ecology Research*, 4:1033–1048, 2002.

[74] S. Jenouvrier, C. Barbraud, and H. Weimerskirch. Long-term contrasted responses to climate of two Antarctic seabird species. *Ecology*, 86(11):2889–2903, 2005.

[75] E. Jeppesen, B. Kronvang, M. Meerhoff, M. Søndergaard, K. M. Hansen, H. E. Andersen, T. L. Lauridsen, L. Liboriussen, M. Beklioglu, A. Ozen, and J. E. Olesen. Climate change effects on

runoff, catchment phosphorus loading and lake ecological state, and potential adaptations. *Journal of Environmental Quality*, 38 (5):1930–41, 2007.

[76] C. M. Jessup, R. Kassen, S. E. Forde, B. Kerr, A. Buckling, P. B. Rainey, and Brendan J. M. Bohannan. Big questions, small worlds: microbial model systems in ecology. *Trends in Ecology & Evolution*, 19(4):189–97, 2004.

[77] J. Jones, Patrick J. Doran, and Richard T. Holmes. Climate and Food Synchronize Regional Forest Bird Abundances. *Ecology*, 84(11):3024–3032, 2003.

[78] K. Jürgens and C. Matz. Predation as a shaping force for the phenotypic and genotypic composition of planktonic bacteria. *Antonie van Leeuwenhoek*, 81(1-4):413–34, 2002.

[79] B. E. Kendall, C. J. Briggs, W. W. Murdoch, and P. Turchin. Why do populations cycle? A synthesis of statistical and mechanistic modeling approaches. *Ecology*, 80(6):1789–1805, 1999.

[80] B. E. Kendall, O. N. Bjørnstad, J. Bascompte, T. H. Keitt, and W. F. Fagan. Dispersal, Environmental Correlation, and Spatial Synchrony in Population Dynamics. *The American Naturalist*, 155(5):628–636, 2000.

[81] T. Klemola, O. Huitu, and K. Ruohomäki. Geographically partitioned spatial synchrony among cyclic moth populations. *Oikos*, 114(2):349–359, 2006.

[82] Y. Kuramoto. Self-entrainment of a population of coupled nonlinear oscillators. *Lecture Notes in Physics*, 39:420–422, 1975.

[83] Y. Kuramoto. *Chemical Oscillations, Waves, and Turbulence*. Springer, Berlin, 1984.

[84] Y. M. Lai, J. Newby, and P. Bressloff. Effects of Demographic Noise on the Synchronization of a Metapopulation in a Fluctuating Environment. *Physical Review Letters*, 107(11):1–5, 2011.

[85] V. Lemesle and J. L. Gouzé. A simple unforced oscillatory growth model in the chemostat. *Bulletin of Mathematical Biology*, 70(2):344–57, 2008.

[86] A. Liebhold, W. D. Koenig, and O. N. Bjørnstad. Spatial synchrony in population dynamics. *Annual Review of Ecology, Evolution, and Systematics*, 35:467–490, 2004.

[87] Z. Liu, M. Gao, Z. Li, and G. Zhu. Synchrony of spatial populations: heterogeneous population dynamics and reddened environmental noise. *Population Ecology*, 51(1):221–226, 2009.

[88] A. Longhurst. The sustainability myth. *Fisheries Research*, 81 (2-3):107–112, 2006.

[89] A. J. Lotka. The growth of mixed populations: two species competing for a common food supply. *Journal of the Washington Academy of Sciences*, 22:461–469, 1932.

[90] Z. F. Mainen and T. J. Sejnowski. Reliability of spike timing in neocortical neurons. *Science*, 268(5216):1503–6, 1995.

[91] J. P. Manderson. The spatial scale of phase synchrony in winter flounder (Pseudopleuronectes americanus) production increased among southern New England nurseries in the 1990s. *Canadian Journal of Fisheries and Aquatic Sciences*, 65(3):340–351, 2008.

[92] E. Martegani, D. Porro, B. M. Ranzi, and L. Alberghina. Involvement of a cell size control mechanism in the induction and maintenance of oscillations in continuous cultures of budding yeast. *Biotechnology and Bioengineering*, 36(5):453–9, 1990.

[93] T. M. Massie, B. Blasius, G. Weithoff, U. Gaedke, and G. F. Fussmann. Cycles, phase synchronization, and entrainment in single-species phytoplankton populations. *Proceedings of the National Academy of Sciences of the United States of America*, 107 (9):4236–41, 2010.

[94] R. M. May. Limit cycles in predator-prey communities. *Science*, 177(4052):900–2, 1972.

[95] R. M. May. Biological Populations with Nonoverlapping Generations: Stable Points, Stable Cycles, and Chaos. *Science*, 186 (4164):645–647, 1974.

[96] R. M. May. Simple mathematical models with very complicated dynamics. *Nature*, 261:459–67, 1976.

[97] R. M. May, G. R. Conway, and M. P. Hassell. Time delays, density-dependence and single-species oscillations. *Journal of Animal Ecology*, 43(3):747–770, 1974.

[98] E. McCauley, W. A. Nelson, and R. M. Nisbet. Small-amplitude cycles emerge from stage-structured interactions in Daphnia-algal systems. *Nature*, 455:1240–3, 2008.

[99] E. Montbrió, J. Kurths, and B. Blasius. Synchronization of two interacting populations of oscillators. *Physical Review E*, 70(5): 1–4, 2004.

[100] P. A. P. Moran. The statistical analysis of the Canadian lynx cycle. II. Synchronization and meteorology. *Australian Journal of Zoology*, 1(3):291–298, 1953.

[101] D. O. Morgan. *The Cell Cycle: Principles of Control (Primers in Biology)*. New Science Press, Ltd., 2007.

[102] L. D. Mueller and A. Joshi. *Stability in Model Populations (Monographs in Population Biology)*. Princeton University Press, Princeton, NJ, 2000.

[103] T. Münch, B. Sonnleitner, and A. Fiechter. The decisive role of the Saccharomyces cerevisiae cell cycle behaviour for dynamic growth characterization. *Journal of Biotechnology*, 22(3):329–51, 1992.

[104] W. W. Murdoch, B. E. Kendall, R. M. Nisbet, C. J. Briggs, E. McCauley, and R. Bolser. Single-species models for many-species food webs. *Nature*, 417:541–3, 2002.

[105] W. W. Murdoch, C. J. Briggs, and R. M. Nisbet. *Consumer-Resource Dynamics*. Princeton University Press, Princeton, NJ, 2003.

[106] J. H. Myers. Synchrony in outbreaks of forest Lepidoptera: a possible example of the Moran effect. *Ecology*, 79(3):1111–1117, 1998.

[107] Z. Néda, E. Ravasz, Y. Brechet, T. Vicsek, and A. L. Barabási. The sound of many hands clapping – tumultuous applause can transform itself into waves of synchronized clapping. *Nature*, 403:849–50, 2000.

[108] A. Novick and L. Szilard. Description of the chemostat. *Science*, 112(1946):715–716, 1950.

[109] R. J. Olson and S. W. Chisholm. Effects of Light and Nitrogen Limitation on the Cell-Cycle of the Dinoflagellate Amphidinium-Carteri. *Journal of Plankton Research*, 8(4):785–793, 1986.

[110] R. J. Olson, D. Vaulot, and S. W. Chisholm. Effects of environmental stresses on the cell cycle of two marine phytoplankton species. *Plant Physiology*, 80(4):918–25, 1986.

[111] C. Parmesan and G. Yohe. A globally coherent fingerprint of climate change impacts across natural systems. *Nature*, 421: 37–42, 2003.

[112] M.s Pascual and H. Caswell. From the cell cycle to population cycles in phytoplankton-nutrient interactions. *Ecology*, 78(3): 897–912, 1997.

[113] M. Peltonen, A.M. Liebhold, O.N. Bjø rnstad, and D.W. Williams. Spatial synchrony in forest insect outbreaks: roles of regional stochasticity and dispersal. *Ecology*, 83(11):3120–3129, 2002.

[114] O. L. Petchey. Environmental colour affects aspects of single-species population dynamics. *Proceedings of the Royal Society of London. Series B: Biological Sciences*, 267(1445):747–54, 2000.

[115] O. L. Petchey, A. Gonzalez, and H. B. Wilson. Effects on population persistence: the interaction between environmental noise colour, intraspecific competition and space. *Proceedings of the Royal Society of London. Series B: Biological Sciences*, 264(1389): 1841–1847, 1997.

[116] J. M. Pickett. Growth of Chlorella in a Nitrate-limited Chemostat. *Plant Physiology*, 55(2):223–225, 1975.

[117] A. Pikovsky, M. Rosenblum, and J. Kurths. *Synchronization: A Universal Concept in Nonlinear Sciences (Cambridge Nonlinear Science Series)*. Cambridge University Press, 2003.

[118] S. L. Pimm and A. Redfearn. The variability of population densities. *Nature*, 334:613–614, 1988.

[119] M. C. Post, E.and Forchhammer. Synchronization of animal population dynamics by large-scale climate. *Nature*, 420:168–71, 2002.

[120] W. C. Quayle, L. S. Peck, H. Peat, J. C. Ellis-Evans, and P. R. Harrigan. Extreme responses to climate change in Antarctic lakes. *Science*, 295(5555):645, 2002.

[121] E. Ranta, V. Kaitala, J. Lindström, and H. Lindén. Synchrony in population dynamics. *Proceedings of the Royal Society of London. Series B: Biological Sciences*, 262:113–118, 1995.

[122] E. Ranta, V. Kaitala, J. Lindström, and E. Helle. The Moran effect and synchrony in population dynamics. *Oikos*, 78(1):136–142, 1997.

[123] G. Y. Rhee. Effects of N: P atomic ratios and nitrate limitation on algal growth, cell composition, and nitrate uptake. *Limnology and Oceanography*, 23(1), 1978.

[124] J. Ripa. Analysing the Moran effect and dispersal: their significance and interaction in synchronous population dynamics. *Oikos*, 89(1):175–187, 2000.

[125] J. Ripa. Food web dynamics in correlated and autocorrelated environments. *Theoretical Population Biology*, 64(3):369–384, 2003.

[126] J. Ripa and M. Heino. Linear analysis solves two puzzles in population dynamics: the route to extinction and extinction in coloured environments. *Ecology Letters*, 2:219–222, 1999.

[127] J. Ripa and P. Lundberg. Noise Colour and the Risk of Population Extinctions. *Proceedings of the Royal Society of London. Series B: Biological Sciences*, 263:1751–1753, 1996.

[128] J. Ripa and E. Ranta. Biological filtering of correlated environments: towards a generalised Moran theorem. *Oikos*, 116: 783–792, 2007.

[129] M. L. Rosenzweig and R. H. MacArthur. Graphical representation and stability conditions of predator-prey interactions. *American Naturalist*, 97(895):209–223, 1963.

[130] T. Royama. *Analytical Population Dynamics (Population and Community Biology Series)*. Chapman & Hall, 1992.

[131] T. Royama. Moran effect on nonlinear population processes. *Ecological Monographs*, 75(2):277–293, 2005.

[132] R. H. Schloemer and R. H. Garrett. Partial purification of the NADH-nitrate reductase complex from Chlorella pyrenoidosa. *Plant Physiology*, 51(3):591, 1973.

[133] J. H. Steele. A comparison of terrestrial and marine ecological systems. *Nature*, 313:355–358, 1985.

[134] R. Storn and K. Price. Differential evolution–a simple and efficient heuristic for global optimization over continuous spaces. *Journal of Global Optimization*, 11(4):341–359, 1997.

[135] S. H. Strogatz. From Kuramoto to Crawford: exploring the onset of synchronization in populations of coupled oscillators. *Physica D: Nonlinear Phenomena*, 143(1-4):1–20, 2000.

[136] S. H. Strogatz. *Sync: How Order Emerges From Chaos In the Universe, Nature, and Daily Life*. Hyperion, New York, 2004.

[137] S. H. Strogatz, R. E. Mirollo, and P. C. Matthews. Coupled nonlinear oscillators below the synchronization threshold: relaxation by generalized Landau damping. *Physical Review Letters*, 68(18): 2730–2733, 1992.

[138] A. F. Taylor, M. R. Tinsley, F. Wang, Z. Huang, and K. Showalter. Dynamical quorum sensing and synchronization in large populations of chemical oscillators. *Science*, 323(5914):614, 2009.

[139] D. Tilman. Tests of resource competition theory using four species of Lake Michigan algae. *Ecology*, 62(3):802–815, 1981.

[140] S. Tuljapurkar and H. Caswell. *Structured-Population Models in Marine, Terrestrial, and Freshwater Systems (Population and Community Biology Series)*. Springer, 1997.

[141] P. Turchin. *Complex Population Dynamics: A Theoretical/Empirical Synthesis*. Princeton University Press, Princeton, NJ, 2003.

[142] D. A. Vasseur. Environmental colour intensifies the Moran effect when population dynamics are spatially heterogeneous. *Oikos*, 116:1726–1736, 2007.

[143] D. A. Vasseur and J. W. Fox. Phase-locking and environmental fluctuations generate synchrony in a predator-prey community. *Nature*, 460:1007–10, 2009.

[144] D. A. Vasseur and P. Yodzis. The color of environmental noise. *Ecology*, 85(4):1146–1152, 2004.

[145] D. Vaulot, R. J. Olson, S. Merkel, and S. W. Chisholm. Cell-cycle response to nutrient starvation in two phytoplankton species, Thalassiosira weissflogii and Hymenomonas carterae. *Marine Biology*, 95(4):625–630, 1987.

[146] P. F. Verhulst. Notice sur la loi que la population suit dans son accroissement. correspondance mathematique et physique publiee par a. *Quetelet*, 10:113–121, 1838.

[147] J. O. Vik, N. C. Stenseth, G. Tavecchia, and A. Mysterud. Living in synchrony on Greenland coasts? Peer reviewed article. *Nature*, 427:697–698, 2004.

[148] D. G. Wallen and L. D. Cartier. Molybdenum dependence, nitrate uptake and photosynthesis of freshwater plankton algae. *Journal of Phycology*, 11(3):345–349, 1975.

[149] G.-R. Walther, E. Post, P. Convey, A. Menzel, C. Parmesan, T. J. C. Beebee, J.-M. Fromentin, O. Hoegh-Guldberg, and F. Bairlein. Ecological responses to recent climate change. *Nature*, 416:389–395, 2002.

[150] N. Walz, T. Hintze, and R. Rusche. Algae and rotifer turbidostats: studies on stability of live feed cultures. *Hydrobiologia*, 358:127–132, 1997.

[151] M. C. Wichmann, K. Johst, M. Schwager, B. Blasius, and F. Jeltsch. Extinction risk, coloured noise and the scaling of variance. *Theoretical Population Biology*, 68(1):29–40, 2005.

[152] A. T. Winfree. *The Geometry of Biological Time*. Springer, New York, 2001.

DECLARATION

Ich versichere, dass ich die vorliegende Arbeit selbständig angefertigt und keine anderen als die angegebenen Hilfsmittel und Quellen verwendet habe. Die Arbeit wurde bisher an keiner weiteren Hochschule im In- oder Ausland vorgelegt. Die geltende Promotionsordnung der Mathematisch-Naturwissenschaftlichen Fakultät der Universität Potsdam ist mir bekannt.

Potsdam, November 2011

Thomas M. Massie